CHANNEL CHARACTERIZATION AND OBJECT CLASSIFICATION IN NON-STATIONARY AND UNCERTAIN ENVIRONMENTS

by

Vikram Thiruneermalai Gomatam

B.E. in Electronics and Communication Engineering,

Visvesvaraya Technological University, 2007

M.S. in Electrical Engineering, Swanson School of Engineering, 2012

Submitted to the Graduate Faculty of

the Swanson School of Engineering in partial fulfillment

of the requirements for the degree of

Doctor of Philosophy

University of Pittsburgh

2015

UNIVERSITY OF PITTSBURGH

SWANSON SCHOOL OF ENGINEERING

This dissertation was presented

by

Vikram Thiruneermalai Gomatam

It was defended on

January 9, 2015

and approved by

Patrick Loughlin, Ph.D., Professor, Department of Bioengineering

Amro El-Jaroudi, Ph.D., Professor, Deptartment of Electrical and Computer Engineering

Zhi-Hong Mao, Ph.D., Professor, Department of Electrical and Computer Engineering

Ervin Sejdic, Ph.D., Professor, Deptartment of Electrical and Computer Engineering

Leon Cohen, Ph.D., Professor, Deptartment of Physics, CUNY

Dissertation Director: Patrick Loughlin, Ph.D., Professor, Department of Bioengineering

CHANNEL CHARACTERIZATION AND OBJECT CLASSIFICATION IN NON-STATIONARY AND UNCERTAIN ENVIRONMENTS

Vikram Thiruneermalai Gomatam, PhD

University of Pittsburgh, 2015

Classification of SONAR targets in underwater environments has long been a challenging problem. These are mainly due to the presence of undesirable effects like dispersion, attenuation and self-noise. Furthermore, we also have to contend with range dependent environments, like the continental shelf/littoral regions, where most of the human and aquatic life's activities occur.

Our work consists of analyzing the propagation in these environments from a pulse-evolution perspective. We look at cases where characterizing wave propagation using conventional Fourier-spectral analysis is infeasible for practical applications and instead resort to a phase-space approximation for it. We derive the phase-space approximations for a variety of propagating waves and limiting boundary conditions.

We continue our past work on invariant features to enhance classification performance; we simulate the derived features for waves with cylindrical spreading. Another area of our work includes looking at the equation governing the wave propagation from a phase space perspective. It has been shown before that reformulating the classical wave equation in the phase-space provides interesting insights to the solution of the equation. It has been posited that this would be especially useful for non-stationary functions, like the ones governing SONAR propagation underwater.

We perform classification of real world SONAR data measured by the JRP (DRDC-Atlantic, NURC, ARL-PSU, NRL) program. We use a 'classic' MPE classifier on the given non-stationary and contrast its performance with an MPE classifier augmented by a Linear

Time Varying (LTV) filter, to assess the impact of adding a time-varying pre-filter to a classifier (MPE) deemed optimal for stationary additive white Gaussian noise. We show that the addition of the time-varying pre-filter to augment the standard MPE classifier does increase the performance of the classifier.

Finally, we look at the self-noise problem that is commonly present in the littoral regions of the ocean, which also happens to be the region where most of shallow water sound propagation occurs. We look at phase-space approach to the stochastic models that simulate the effect of signal dependent noise reverberations and attempt to design time-varying estimators that would mitigate the problem at hand. We perform simulations that corroborate our premise. Further directions in the aforementioned areas are also presented.

TABLE OF CONTENTS

LIST OF TABLES

LIST OF FIGURES

PREFACE

Dedicated to my parents Kunnavakkam Vinjimur Lakshmi and Thiruneermalai Gomatam Kannan.

First, I'd like to express my profound gratitude to my Academic Advisor Dr. Patrick J. Loughlin for his continued support and direction through all these years. I'd also like to thank the dissertation committee: Dr. El-Jaroudi, Dr. Mao, Dr. Cohen and Dr. Sejdic for their guidance and feedback on my research and dissertation. I should also thank Dr. Mao for being my interim advisor during my early days as a grad student and Dr. Cohen for inviting me to work with him at CUNY.

Additionally, I'd like to thank my teachers, mentors, family and friends for helping me intellectually, morally, spiritually, financially and psychologically through all these lonely years as a grad student.

And finally I'd like to thank all well wishers and strangers with all the aforementioned people for being a part of this non-linear, non-stationary and time-varying process that I'd like to call "my life".

1.0 INVARIANT FEATURES FOR RANGE-DEPENDENT ENVIRONMENTS

1.1 INTRODUCTION

The propagation of sound in the ocean can be significantly affected by the environment. Common propagation effects include multi-path, dispersion and frequency-depedent attenuation (absorption). The problem of dispersion can be especially pronounced with low-frequency broadband sonar in shallow water, where the channel induces geometric, or structural, dispersion owing to the waveguide-like nature of the channel [54]. These environmental effects cause the sonar signal to change as it propagates, such that the backscatter from identical objects can appear different to observers at different locations. Such propagation-induced variability can be detrimental to automatic classification of underwater objects from their sonar backscatter.

At least two approaches can be taken to address these issues: 1) the use of inverse channel models to annul the propagation effects on the received signal [32, 3], and 2) the extraction of features from the signal that are invariant to the propagation effects [48, 46, 47, 49]. The former approach requires accurate knowledge of the channel, while the latter does not, although the invariance of the features obtained typically holds under specific channel characteristics; in particular, the "absorption- and dispersion-invariant moments" (ADIMs) were derived for linear dispersive wave propagation in range-independent environments [49].

Many ocean environments, especially littoral zones, exhibit range dependence. We have shown [25] earlier that the propagation invariant features like the ADIMs performan ce degrades with increasing wedge angle. We later developed features that remained invariant for wave propagating in a wedge which outperformed the earlier features [24]. However all

the features derived were under the assumption that propagating wave is planar. However, in many real world applications, it is imperative to assume that the propagating waves are cylindrical in nature with the associated spreading loss. This chapter simulates the previously derived features from [24] for cylindrical waves to assess the feasiblity of extending the derived feature with added spreading loss. As expected the cylindrical loss did have an impact on the classification performance of the features, with the RDIMS [24] being more robust among the considered features.

1.2   BACKGROUND: FEATURES INVARIANT TO DISPERSION AND ABSORPTION

As in Okopal et al.[49], we consider linear wave propagation in Cartesian coordinates in a range-independent homogenous isovelocity channel (e.g. a parallel plate waveguide), for which the solution to the wave equation is separable in depth z and range x. For a fixed source-receiver depth, we can focus on the propagation effects in range x. Thus, given an initial wave $u(0, t)$ at $x = 0$, the wave $u(x, t)$ at some other position x is given for each mode by [54, 55]

$$u(x, t) = \frac{1}{\sqrt{2\pi}} \int F(0, \omega) e^{jk_x(\omega)x} e^{-j\omega t} d\omega \tag{1.1}$$

where $F(0, \omega)$ is the spectrum (Fourier transform) of the initial wave,

$$F(0, \omega) = \frac{1}{\sqrt{2\pi}} \int u(0, t) e^{j\omega t} dt \tag{1.2}$$

and $k_x(\omega)$ is the horizontal wavenumber, and defines the dispersion relation for each mode of the channel, which represents the propagation effects (i.e. dispersion and absorption). In general, $k_x(\omega)$ can be complex,

$$k_x(\omega) = k_R(\omega) + j\, k_I(\omega) \tag{1.3}$$

The real part of the dispersion relation corresponds to the (generally frequency-dependent) velocity of propagation, and in particular, the group velocity is given by

$$v(\omega) = \left(\frac{dk_R(\omega)}{d\omega} \right)^{-1} \tag{1.4}$$

The imaginary part of the dispersion relation corresponds to frequency-dependent attenuation, or absorption. For a parallel plate waveguide with perfectly reflecting boundaries, the dispersion relation is

$$k_x = \sqrt{\left(\frac{\omega}{c}\right)^2 - \left(\frac{m\pi}{D}\right)^2} \tag{1.5}$$

1.2.1 Attenuation and Dispersion Invariant Moments (ADIMs)

By the results above, the spectrum of the signal can be expressed in terms of its amplitude and phase

$$F(x,\omega) = B(x,\omega)e^{j\psi(x,\omega)} \tag{1.6}$$

with

$$B(x,\omega) = B(0,\omega)e^{-k_I(\omega)x} \tag{1.7}$$

$$\psi(x,\omega) = \psi(0,\omega) + k_R(\omega)x \tag{1.8}$$

where $B(0,\omega)$ and $\psi(0,\omega)$ are the magnitude and phase spectrum of the initial signal.

For complex dispersion which yields exponential spectral attenuation, i.e. $k_I(\omega) = \beta\omega$, features that are invariant to dispersion and absorption can be obtained by the following feature extraction process:[48, 46, 49]

$$Z(x,\omega) = \frac{\partial}{\partial\omega}\ln B(x,\omega) \tag{1.9}$$

$$Z_0(x,\omega) = Z(x,\omega) - mean_\omega\{Z(x,\omega)\} \tag{1.10}$$

As shown by Okopal et al.[49], the spectral function $Z_0(x,\omega)$ is independent of propagation distance – i.e., $Z_0(x,\omega) = Z_0(0,\omega)$ – and hence features extracted from this function are unaffected by propagation. To obtain invariant temporal moments, Okopal et al. [49] compute

$$T_n(x) = \int t^n |v(x,t)|^2 dt \tag{1.11}$$

where

$$v(x,t) = \frac{1}{\sqrt{2\pi}}\int \exp(Z_0(x,\omega))e^{-j\omega t}d\omega \tag{1.12}$$

3

1.2.2 Cepstral Moments

Cepstral moments that are invariant to dispersion can also be obtained, via [49]

$$M_c(x; n) = \int t^n \left| c_u(x, t) \right|^2 dt \tag{1.13}$$

where $c_u(x, t)$ is the cepstrum of $u(x, t)$,

$$c_u(x, t) = \frac{1}{\sqrt{2\pi}} \int \ln B(x, \omega) e^{-j\omega t} d\omega \tag{1.14}$$

1.3 RANGE DEPENDENT PROPAGATION

Underwater sound propagation in littoral regions such as the continental shelf can be modeled as a wedge waveguide, which is range-dependent in nature since the boundaries change with propagation range. There are many methods to solve the range-dependent propagation using the framework of the standard modal solution format, such as the coupled mode, the adiabatic mode and the intrinsic mode solutions [34, 52].

In this work we use the adiabatic approximation, whereby the solution is derived under the assumption that there is no coupling between modes (i.e. the modes are "adiabatic" in nature [52]). Moreover, the variation of depth is small compared to the variation of range; such environments are often referred to as weakly-range-dependent. This results in a feature extraction process that is similar (although not identical) to previous work for the range-independent case [47, 49].

We consider 2-D propagation in the range-depth $(x - z)$ plane, for which the Helmholtz equation in rectangular co-ordinates is [34]

$$\frac{\partial^2 \Phi}{\partial x^2} + \frac{\partial^2 \Phi}{\partial z^2} = \frac{1}{c^2} \frac{\partial^2 \Phi}{\partial t^2} \tag{1.15}$$

The solution Φ has exponential dependence on time as well; writing this explicitly as $\Phi(x, z, t) = p(x, z)e^{-j\omega t}$ and substituting into the equation above yields

$$\frac{\partial^2 p}{\partial x^2} + \frac{\partial^2 p}{\partial z^2} = -\frac{\omega^2}{c^2} \tag{1.16}$$

Equations of this form are solved by separating variables; substituting a solution of the form $p(x, z) = \varphi(x)\psi(z)$ into the above equation yields

$$\frac{d^2\varphi(x)}{dx^2}\psi(z) + \frac{d^2\psi(z)}{dz^2}\varphi(x) + \frac{\omega^2}{c^2}\varphi(x)\psi(z) = 0 \tag{1.17}$$

Separating the individual variables we have

$$\frac{d^2\psi(z)}{dz^2} + k_z^2\psi(z) = 0 \tag{1.18}$$

and

$$\frac{d^2\varphi(x)}{dx^2} + k_x^2\varphi(x) = 0 \tag{1.19}$$

where

$$k_x = \sqrt{\frac{\omega^2}{c^2} - k_z^2} \tag{1.20}$$

The solution to the depth co-ordinate Eq. (1.18) is

$$\psi(z) = A\sin(k_z z) \tag{1.21}$$

Now, the vanishing boundary condition $\psi(z) = 0$ at the range-dependent bottom depth $z = z_{bottom} = f(x)$ requires [52],

$$k_z = \frac{m\pi}{f(x)} \tag{1.22}$$

Substituting this into Eq. (1.20) yields a range-dependent dispersion-like expression,

$$k_x(x) = \sqrt{\left(\frac{\omega}{c}\right)^2 - \left(\frac{m\pi}{f(x)}\right)^2}. \tag{1.23}$$

Substituting this into (1.19) yields

$$\frac{d^2\varphi(x)}{dx^2} + \left(\left(\frac{\omega}{c}\right)^2 - \left(\frac{m\pi}{f(x)}\right)^2\right)\varphi(x) = 0. \tag{1.24}$$

Now, to solve this more complicated differential equation, we assume a solution with a range dependent amplitude and a range dependent phase,

$$\varphi(x) = A(x)e^{j\phi(x)}. \tag{1.25}$$

Plugging this into Eq. (1.24), and using (1.23) to simplify notation, yields

$$A''(x)e^{j\phi(x)} + 2jA'(x)\phi'(x)e^{j\phi(x)} + jA(x)\phi''(x)e^{j\phi(x)} - A(x)\phi'^2(x)e^{j\phi(x)} + k_x^2(x)A(x)e^{j\phi(x)} = 0. \tag{1.26}$$

Eliminating the common $e^{j\phi(x)}$ term and then separating the equation into real and imaginary parts yields the following two equations:

$$A''(x) + A(x)\left[k_x^2(x) - \phi'^2(x)\right] = 0 \tag{1.27}$$

and

$$2A'(x)\phi'(x) + A(x)\phi''(x) = 0 \tag{1.28}$$

Applying the WKB approximation [54] to Eq. (1.27) (by which $A''(x) \approx 0$, consistent with the 'weak' range dependence condition), we obtain

$$\pm k_x(x) = \phi'(x), \tag{1.29}$$

by which the phase is

$$\phi(x) = \pm \int_{x_S}^{x_R} k_x(x)dx, \tag{1.30}$$

where x_S and x_R denote the location of source and receiver, respectively. Plugging this result for $\varphi(x)$ into Eq. (1.28) yields

$$A(x) = \frac{A}{\sqrt{k_x(x)}}. \tag{1.31}$$

where A is a constant (which we can take to be 1 in what follows, without loss of generality). Hence, the total solution at x_R works out to,

$$\varphi(x_R; x_S) = \frac{A}{\sqrt{k_x(x_R)}}e^{\pm j\int_{x_S}^{x_R} k_x(x')dx'}, \tag{1.32}$$

This, then, is the approximate transfer function for a weakly range dependent environment.

1.4 DISPERSION-INVARIANT MOMENTS FOR RANGE-DEPENDENT PROPAGATION

Let $F(x_S, \omega)$ be the initial sonar backscatter spectrum from an object and $F(x_R, \omega)$ be the propagated backscatter response. Then, by the Fourier synthesis approach for linear propagation [34] coupled with the approximate transfer function above, the propagated backscatter response is given by

$$F(x_R, \omega) = \frac{F(x_S, \omega)}{\sqrt{k_x(x_R, \omega)}} e^{\pm j \int_{x_S}^{x_R} k_x(x', \omega) dx'} \tag{1.33}$$

Similar to the range-independent ADIMs processing [49], we take the absolute value on both sides, to eliminate the propagation effects induced by the complex exponential term (note: we implicitly assume k_x is real). For mathematical convenience, we then raise the result to the 4th power, to obtain

$$G(x_R, \omega) = \frac{G(x_S, \omega)}{k_x^2(x_R, \omega)} \tag{1.34}$$

where $G(.) = |F(.)|^4$. Substuiting from Eq. (1.23) for the dispersion relation $k_x(x_R, \omega)$ and re-arranging, Eq. (1.34) is re-written as,

$$\left(\left(\frac{\omega}{c} \right)^2 - \left(\frac{\pi}{f(x_R)} \right)^2 \right) = \frac{G(x_S, \omega)}{G(x_R, \omega)}, \tag{1.35}$$

Subtracting the mean (with respect to ω) from each side eliminates the propagation effects due to $f(x_R)$, yielding

$$\left(\left(\frac{\omega}{c} \right)^2 - \overline{\left(\frac{\omega}{c} \right)^2} \right) = \frac{G(x_S, \omega)}{G(x_R, \omega)} - \overline{\left(\frac{G(x_S, \omega)}{G(x_R, \omega)} \right)}, \tag{1.36}$$

where

$$\overline{Q(\omega)} = \frac{1}{W} \int_W Q(\omega) d\omega, \tag{1.37}$$

and W is the bandwidth of interest.

Now, let $\widehat{G}(x_S, \omega)$ be the estimate of the source feature we are trying to recover. Rearranging Eq. (1.36) we obtain,

$$\widehat{G}(x_S, \omega) = \left[\left(\left(\frac{\omega}{c} \right)^2 - \overline{\left(\frac{\omega}{c} \right)^2} \right) + \overline{\left(\frac{G(x_S, \omega)}{G(x_R, \omega)} \right)} \right] G(x_R, \omega) \tag{1.38}$$

This processed received spectral function, $\widehat{G}(x_S, \omega)$, serves as our propagation-invariant function from which to extract invariant features for classification. Note that the information needed to perform the feature extraction is: $G(x_R, \omega)$ (computed from the received pulse) and the mean of $\frac{G(x_S, \omega)}{G(x_R, \omega)}$. This latter quantity can be computed if one has a known set of expected target responses $G(x_S, \omega)$. If this latter quantity can not be computed because $G(x_S, \omega)$ is not known, an option is to replace $\overline{\left(\frac{G(x_S, \omega)}{G(x_R, \omega)}\right)}$ with $\overline{\left(\frac{1}{G(x_R, \omega)}\right)}$ in (1.38). We used this option in the simulation results reported in the next section, and found that the performance was nearly identical to using the full target source information for this case.

To obtain invariant temporal moments, we first take take the inverse Fourier transform of $\widehat{G}(x_S, \omega)$

$$\widehat{g}(x, t) = \frac{1}{\sqrt{2\pi}} \int \widehat{G}(x_S, \omega) e^{-j\omega t} d\omega. \tag{1.39}$$

The temporal feature $\widehat{g}(x, t)$ can now be used to compute range-insenstive dispersion invariant moments (RDIMs)

$$T_{\widehat{g}}(x; n) = \int t^n \left|\widehat{g}(x, t)\right|^2 dt. \tag{1.40}$$

1.5   PAST RESULTS

1.5.1   Simulation Setup

In order to evaluate the performance of the RDIMs, we ran a numerical simulation of the propagation of the backscatter from two cylinders in an ideal 2-plate wedge waveguide, for which the range-dependent bottom depth is given by

$$z_{bottom} = f(x) = x \tan\theta, \tag{1.41}$$

where θ is the angle of the wedge at its apex. The dispersion relation is therefore

$$k_x(x) = \sqrt{\left(\frac{\omega}{c}\right)^2 - \left(\frac{m\pi}{x \tan\theta}\right)^2} \tag{1.42}$$

Relevant simulation parameters are given in Tables. 1, 2. The cylinder backscatters were propagated up to 4500 m in increments of 50 m, and various features were computed at each

distance. These features were the RDIMs as described above, and the ordinary central temporal moments (MOMs),cepstral moments (CMOMs), and the absorption- and dispersion-invariant moments (ADIMs), as described in [49].

Three wedge angles were investigated: 0.0625, 0.125 and 0.25 degrees. For each wedge, the depth of the target source and the bottom depth of the waveguide at the target source were kept constant at 10m and 25m, respectively, by moving the target from the apex, as illustrated in Fig. 1. This was done to ensure that the frequencies propagating from the source were the same in each case, since the cut off frequency is a function of bottom depth. Also, although the RDIMs were derived under the assumption of a purely real dispersion relation, we included frequency dependent exponential absorption in the simulation, as in the range-independent parallel plate waveguide simulations in [49], with an attenuation coefficient of $10^{-8}m^{-1}Hz^{-1}$, typical of ocean water [4].

Table 1: Geometry of shells

	Inner radius (m)	Outer radius (m)	h
Cylinder 1	1.19	1.20	0.83%
Cylinder 2	1.43	1.45	1.4%

Table 2: Parameters of the Propagating environment

	Water	Air	Steel
Density	$1000 \frac{kg}{m^2}$	$1.2 \frac{kg}{m^2}$	$7800 \frac{kg}{m^2}$
Speed of sound waves	$1500 \frac{m}{s}$	$340 \frac{m}{s}$	$5880 \text{ (dilatational)} \frac{m}{s}$ $3140 \text{ (Shear)} \frac{m}{s}$

1.5.2 Classification Performance

Fig. 2 shows spectrograms of the backscatter from the two cylinders, at three different propagation distances (initial backscatter, backscatter at 2250 m, and at 4500 m) in a wedge
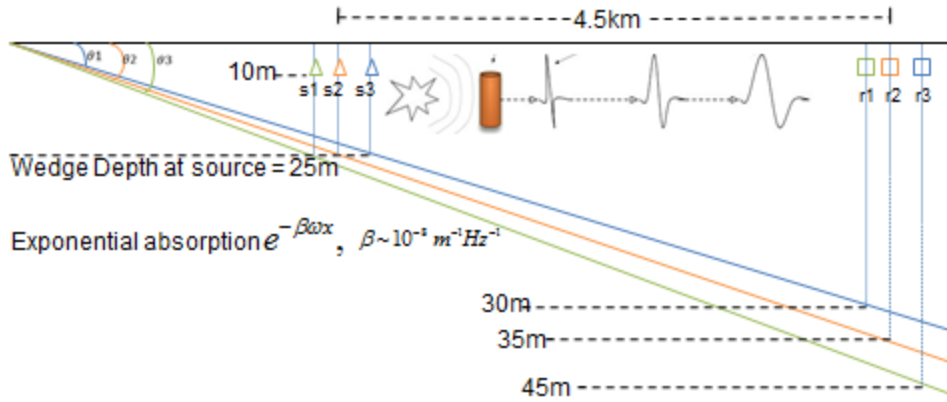
Figure 1: Wedge waveguide simulation setup

with apex angle of 0.25 deg. The wedge depth at the source was 25 m.
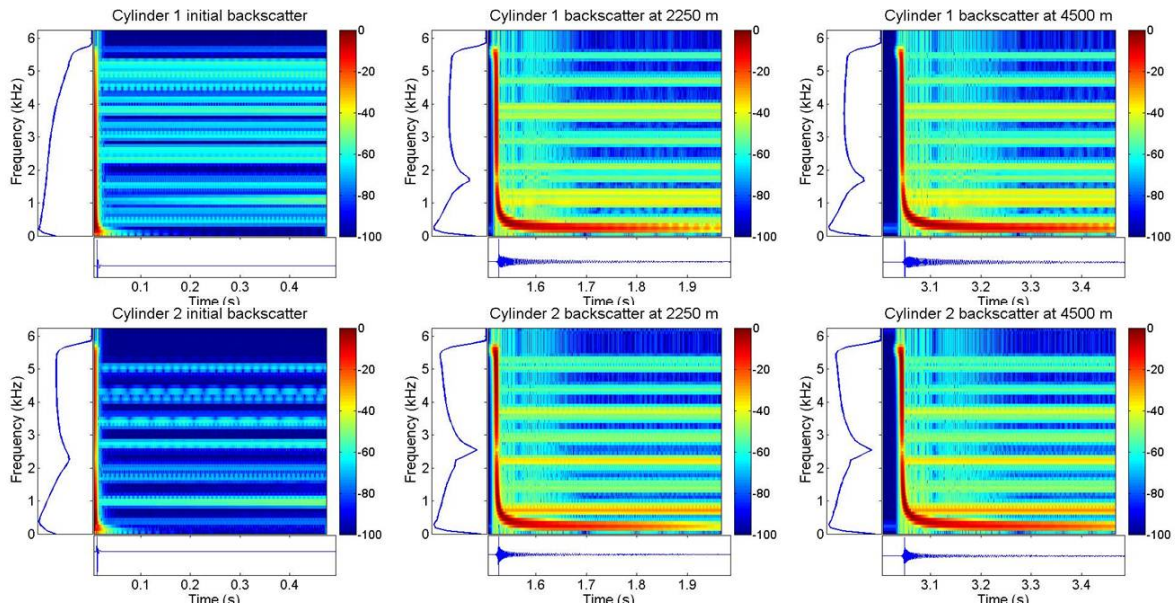
Figure 2: Backscatter plots for cylinder 1 (TOP ROW) and cylinder 2 (BOTTOM ROW) at (LEFT) target source location, (MIDDLE) propagated 2250 m from target, (RIGHT) propagated 4500 m from target. Main color panel shows spectrogram of the backscatter time series, shown in the bottom panel. Side panel shows the spectral density.

10

To compare the performance of RDIMs vs. the other invariant features [49], we computed the features at each distance, and then for each feature we formed a histogram of the feature values for cylinder 1 and a histogram for cylinder 2. We then swept out a ROC curve for each feature from the two histograms. Figs. 3, 4 and 5 show the ROC curves comparing the classification utility of ADIMs, CMOMs and MOMs with RDIMs. A ROC curve that hugs the upper left corner of the plot is indicative of greater classification utility of that feature (i.e. greater separation of the feature histograms from the two cylinders). It is evident from the ROC curves that as the wedge angle increases (environment changes from a nearly parallel two-plate to a more range-dependent form), the range-independent moments degrade, while the RDIMs offer robust performance despite the change.

Figure 3: ROC curves of various moment features for wedge angle = .0625 degrees. Left-to-right: Moment order is second, third, fourth.

Figure 4: ROC curves of various moment features for wedge angle = .125 degrees. Left-to-right: Moment order is second, third, fourth.

Figure 5: ROC curves of various moment features for wedge angle = .25 degrees. Left-to-right: Moment order is second, third, fourth.

1.6 CYLINDRICAL WAVES

The solution to the wave equation in cartesian coordinates provides us with "Planar Waves". This is called so because the wave displacement function Φ in Eq. (1.15) is constant in the plane perpendicular to the axis of propagation for a fixed time $'t'$.

While Planar-wave propagation is adequately expressed by cartesian coordinates, guided wave propagation excited by point sources are generally curvilinear in nature, and are best represented by other coordinate systems [34] . Specifically, the cylindrical coordinates. Naturally several scenarios arise with this type of propagation and we intend to detail them here on a case-by-case basis.

The standard Helmholtz equation in cylindrical coordinates is derived to be

$$\frac{1}{r}\frac{\partial}{\partial r}\left(r\frac{\partial p}{\partial r}\right) + \frac{1}{r^2}\frac{\partial^2 p}{\partial \theta^2} + \frac{\partial^2 p}{\partial z^2} = -\frac{\omega^2}{c^2}p. \tag{1.43}$$

This is the wave equation for a point source in cylindrical geometry. The starting point from which various scenarios commonly encountered in sonar propagation can be explored.

1.6.0.1 Point source in cylindrical coordinates with range-dependent boundaries

The point source in cylindrical coordinates is one of the most widely used scenario in acoustic wave propagation. In this case we assume a point source whose resulting waves

are bounded along the z-axis and has a radiation condition along the r-axis. This condition also makes the field constant along the θ axis, thereby reducing Eq. (1.43) to

$$\frac{1}{r}\frac{\partial}{\partial r}\left(r\frac{\partial p}{\partial r}\right) + \frac{\partial^2 p}{\partial z^2} = -\frac{\omega^2}{c^2}p \tag{1.44}$$

The Normal-mode solution to Eq. (1.44) with fixed boundaries was derived in [34]

$$\text{H}_0{}^{(1)}(kr) = j\sqrt{\frac{2}{\pi k_r r}}\exp\left(i\left(k_r r - \frac{\pi}{4}\right)\right) \tag{1.45}$$

However, in this work we seek a normal-mode solution when the boundaries are a function of range, i.e. range-dependent boundaries. In order to achieve this, we go back to Eq. (1.44). Separating the variables $p(r,z) = R(r)Z(z)$ and representing the first and second order differentials as $R'(r), Z'(z)$ and $R''(r), Z''(z)$ we get

$$R''(r)Z(z) + \frac{1}{r}R'(r)Z(z) + R(r)Z''(z) = -\frac{\omega^2}{c^2}R(r)Z(z), \tag{1.46}$$

$$\frac{R''(r)}{R(r)} + \frac{1}{r}\frac{R'(r)}{R(r)} + \frac{Z''(z)}{Z(z)} = -\frac{\omega^2}{c^2}, \tag{1.47}$$

separating the equation along its variables

$$\frac{R''(r)}{R(r)} + \frac{1}{r}\frac{R'(r)}{R(r)} + k_r^2 = 0, \tag{1.48}$$

$$\frac{Z'(z)}{Z(z)} + k_z^2 = 0, \tag{1.49}$$

where $k_r^2 = \left(\frac{\omega}{c}\right)^2 - k_z^2$.

Solving for Eq. (1.49) we get

$$Z(z) = \text{A}cos(k_z z) + \text{B}sin(k_z z) \tag{1.50}$$

As we mentioned before, the boundaries are range dependent and the field vanishes at $z = 0$ and $z = f(r)$ respectively. Where the former would be the air/water interface and the latter

would be the bottom that varies with horizontal range. Applying the conditions to Eq. (1.50) k_z works out to be

$$k_z = \frac{m\pi}{f(r)}. \tag{1.51}$$

It has to be mentioned that k_z is a function of range r as evidenced by Eq. (1.51), which implies that Eq. (1.47) is not separable. However, in order to separate Eq. (1.47), it is imperative to assume that the boundaries are locally invariant.

The $k_r(r)$ (often termed the dispersion relation) is evaluated to be

$$k_r(r) = \sqrt{\left(\frac{\omega}{c}\right)^2 - \left(\frac{m\pi}{f(r)}\right)^2}. \tag{1.52}$$

Now, the solution for Eq. (1.48) follows a similar procedure outlined in Section 3, starting from Eq. (1.25)

$$\frac{d^2R(r)}{dr^2} + \left(\left(\frac{\omega}{c}\right)^2 - \left(\frac{m\pi}{f(r)}\right)^2\right) R(r) = 0, \tag{1.53}$$

to solve this more complicated differential equation, we assume a solution with a rapidly varying phase component and a slowly varying amplitude

$$R(r) = A(r)e^{j\phi(r)}. \tag{1.54}$$

Plugging this into Eq. (1.53), and using Eq. (1.52) to simplify notation, yields

$$A''(r)e^{j\phi(r)} + 2jA'(r)\phi'(r)e^{j\phi(r)} + jA(r)\phi''(r)e^{j\phi(r)} - A(r)\phi'^2(r)e^{j\phi(r)} + k_r^2(r)A(r)e^{j\phi(r)} = 0. \tag{1.55}$$

Eliminating the common $e^{j\phi(r)}$ term and then separating the equation into real and imaginary parts yields the following two equations:

$$A''(r) + A(r)\left[k_r^2(r) - \phi'^2(r)\right] = 0 \tag{1.56}$$

and

$$2A'(r)\phi'(r) + A(r)\phi''(r) = 0. \tag{1.57}$$

14

Applying the WKB approximation [54] to Eq. (1.56) (by which $A''(r) \approx 0$, consistent with the 'weak' range dependence condition), we obtain

$$\pm k_r(r) = \phi'(r), \tag{1.58}$$

by which the phase is

$$\phi(r) = \pm \int_{r_S}^{r_R} k_r(r)dr, \tag{1.59}$$

where r_S and r_R denote the location of source and receiver, respectively. Plugging this result for $\varphi(r)$ into Eq. (1.57) yields

$$A(r) = \frac{A}{\sqrt{k_r(r)}}, \tag{1.60}$$

and A is a constant whose value is obtained from the range independent solution is as given in Eq. (1.45). Hence, the total solution at r_R works out to be

$$R(r_R; r_S) = \frac{A}{\sqrt{k_r(r_R)}} e^{\pm j \int_{r_S}^{r_R} k_r(r')dr'}, \tag{1.61}$$

the constant A should satisfy Eq. (1.44)is obtained from the range independent solution

$$R(r_R; r_S) = j e^{-j\pi/4} \sqrt{\frac{2}{\pi (r_R - r_S) k_r(r_R)}} e^{\pm j \int_{r_S}^{r_R} k_r(r')dr'}. \tag{1.62}$$

1.7   CLASSIFICATION PERFORMANCE FOR CYLINDRICAL WAVES

In this section we evaluate the classifiction performance using ROC curves using the identical experimental conditions described in Section. 1.5.1. The only difference is that the wedge waveguide now has cylindrical waves propagating as described in Eq. (1.62). Figs. 6, 7 and 8 shows the resulting ROC curves from the simulations.
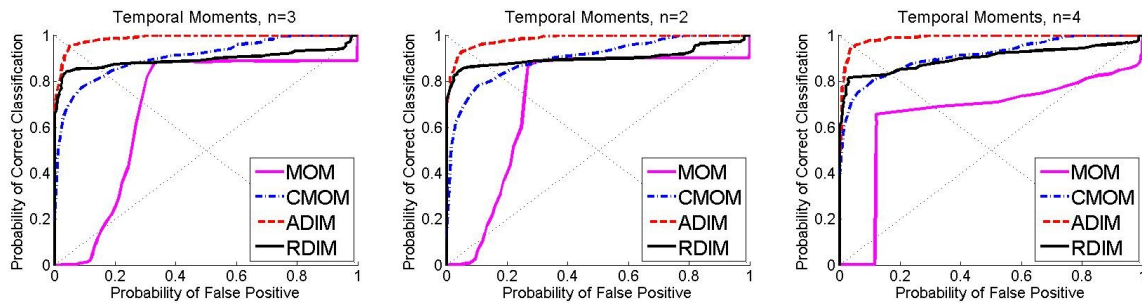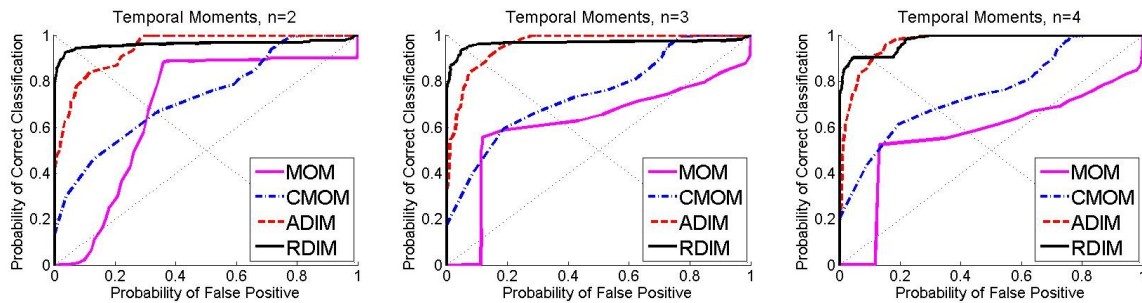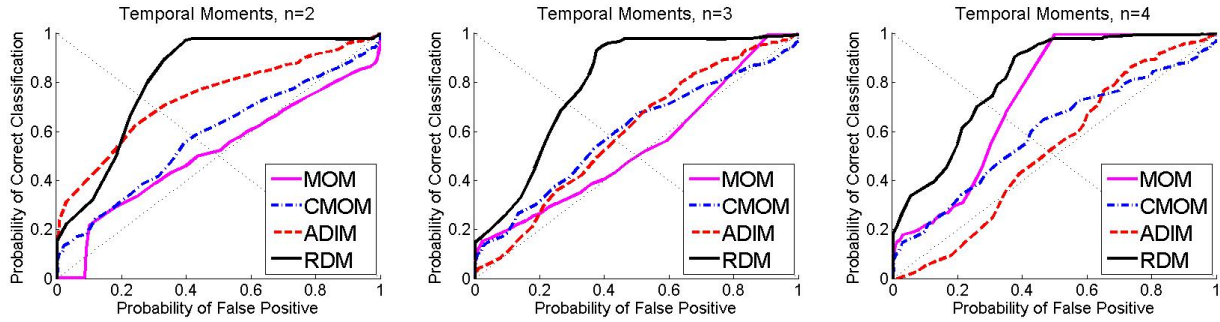
Figure 6: ROC curves of various moment features for wedge angle = .0625 degrees. Left-to-right: Moment order is second, third, fourth.
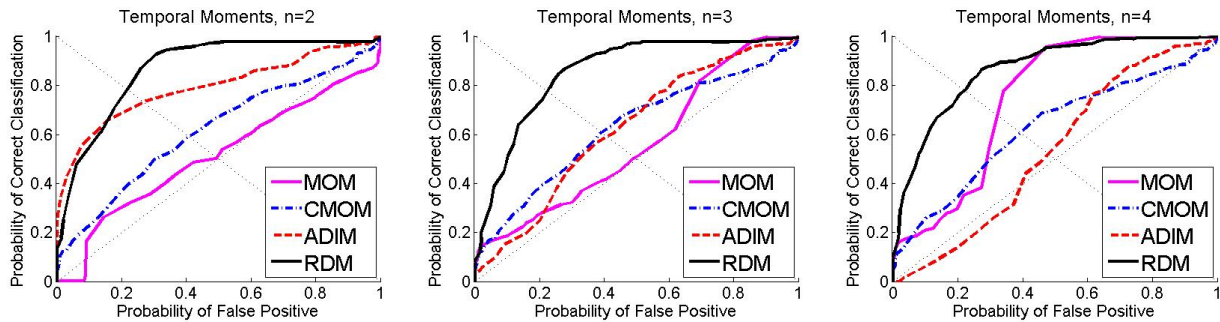
Figure 7: ROC curves of various moment features for wedge angle = .125 degrees. Left-to-right: Moment order is second, third, fourth.

1.8   CONCLUSION

Our simulations show that there is a definite degradation of performance in the features due to cyilndrical spreading. However, the RDIMS still perform equivalent to or better than other moments. The Cepstral and the ADIMS appear to be sensitive to spreading losses while being robust against attenuation in range-independent cases [49]. It can also be seen that application of RDIMS for classification of SONAR bacscatter, travelling in a cyilndrical wavefront would be a worthwhile exercise.
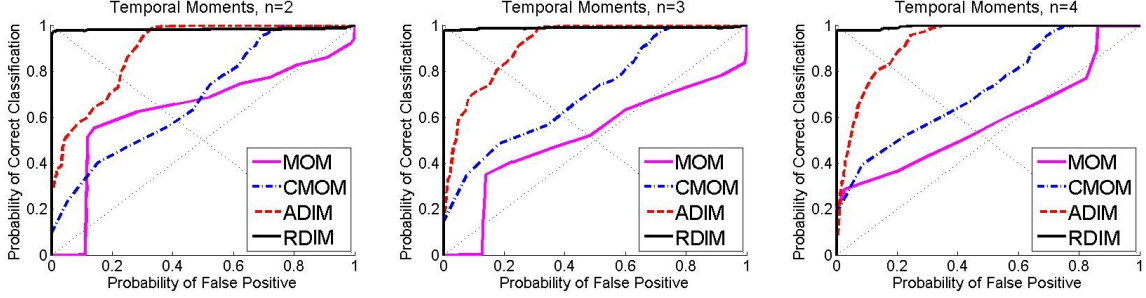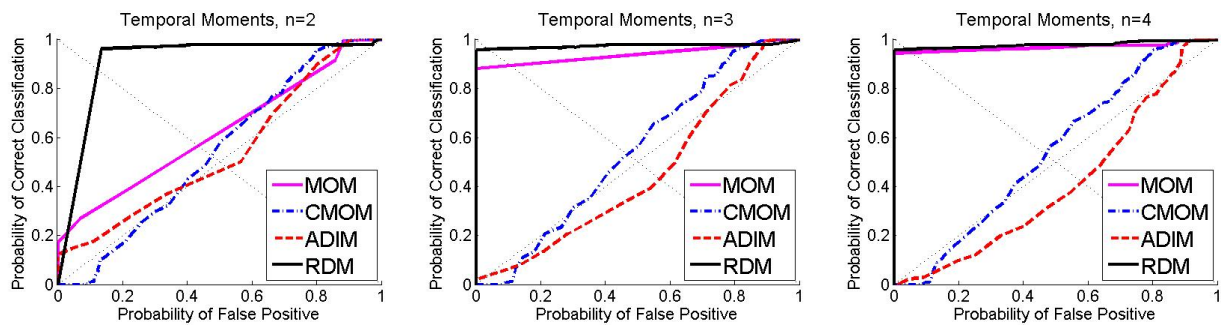
Figure 8: ROC curves of various moment features for wedge angle = .25 degrees. Left-to-right: Moment order is second, third, fourth.

2.0 SONAR SIGNAL FEATURE EXTRACTION FOR RANGE-DEPENDENT PARABOLIC MODEL

2.1 INTRODUCTION

Classifying objects from their sonar backscatter in dispersive and attenuating media is a challenging task because the backscatter changes with propagation, such that the same object can appear to have different "signatures" at different receiver locations. One approach to ameliorate this difficulty is to process the received signal in order to reduce (or ideally eliminate) propagation effects. Past works on deriving dispersion and attenuation invariant moments have concentrated on range-independent [47, 49, 44] or weakly range dependent propagating media [25, 23].

This paper considers feature extraction that can be applied to a variety of environments. Our work here takes the parabolic equation as the basis upon which we extract propagation invariant features. The parabolic equation can be used to model a wide variety of environments, with high accuracy [36]. From the solution to the parabolic equation for range-dependent propagation, we propose a feature extraction algorithm that yields features from the received signal that are invariant to dispersion and attenuation.

2.2 THE PARABOLIC EQUATION(PE) MODEL

Sonar operations in littoral regions are challenged by environmental factors due to interactions of the sonar signal with the ocean surface and bottom, which tend to attenuate and disperse the signal. The littoral or the continental shelf regions have multiple layers of sedi-

ment of varying density at the bottom, making it difficult to model the exact environmental constraints without resorting to approximations. In this work we use the parabolic approximation to the wave equation, or the PE propagation model, first introduced into acoustics by Hardin and Tappert [27]. These authors also proposed a novel iterative solution to solve the wave propagation problem.

2.2.1 The PE as derived by Hardin and Tappert[27]

The starting point for the PE is the Helmholtz equation in cylindrical (r, φ, z) co-ordinates. Assuming cylindrical (azimuthal) symmetry in φ, the equation is

$$\frac{\partial^2 p}{\partial r^2} + \frac{1}{r}\frac{\partial p}{\partial r} + \frac{\partial^2 p}{\partial z^2} + k_0^2 n^2 p = 0, \tag{2.1}$$

Tappert[53] proposed a solution consisting of two components: a propagating component $H_0^{(1)}(k_0 r; \omega)$ and a range-dependent envelope $\psi(r, z; \omega)$,

$$p(r, z; \omega) = \psi(r, z; \omega) H_0^{(1)}(k_0 r; \omega), \tag{2.2}$$

where $k_0 = \omega/c_0$ is the reference wavenumber in air media, r is range, z is depth and $n = \frac{c_0}{c(r,z)}$ is the refractive index of the media, where $c(r, z)$ is the depth-dependent sound speed profile at range r. We omit ω in the succeeding equations since it is the domain that we operate on.

Substituting Eq. (2.2) into Eq. (2.1) and using the property that the Hankel function is a solution to the Bessel differential equation,

$$\frac{\partial^2 H_0^{(1)}(k_0 r)}{\partial r^2} + \frac{1}{r}\frac{\partial H_0^{(1)}(k_0 r)}{\partial r} + k_0^2 H_0^{(1)}(k_0 r) = 0, \tag{2.3}$$

we have that Eq. (2.1) becomes

$$\frac{\partial^2 \psi}{\partial r^2} + \left(\frac{2}{H_0^{(1)}(k_0 r)}\frac{\partial H_0^{(1)}(k_0 r)}{\partial r} + \frac{1}{r}\right)\frac{\partial \psi}{\partial r} + \frac{\partial^2 \psi}{\partial z^2} + k_0^2(n^2 - 1)\psi = 0. \tag{2.4}$$

Applying the far field approximation to the Hankel function

$$H_0^{(1)}(k_0 r) \simeq \sqrt{\frac{2}{\pi k_0 r}} e^{j(k_0 r - \frac{\pi}{4})}, \qquad k_0 r \gg 1 \tag{2.5}$$

19

the above equation simplifies to

$$\frac{\partial^2 \psi}{\partial r^2} + 2ik_0 \frac{\partial \psi}{\partial r} + \frac{\partial^2 \psi}{\partial z^2} + k_0^2(n^2 - 1)\psi = 0 \tag{2.6}$$

Eq. (4.30) is the simplified elliptical wave equation.

This is the juncture at which a variety of approximations are made that would result in a tractable solution for $\psi(r, z; \omega)$. The approximation that Tappert made in [27] (called the *paraxial approximation*) is to neglect the effect of the second order differential $\frac{\partial^2 \psi}{\partial r^2}$ where it is assumed that

$$\frac{\partial^2 \psi}{\partial r^2} \ll 2ik_0 \frac{\partial \psi}{\partial r}, \tag{2.7}$$

for which Eq. (4.30) reduces to

$$2ik_0 \frac{\partial \psi}{\partial r} + \frac{\partial^2 \psi}{\partial z^2} + k_0^2(n^2 - 1)\psi = 0. \tag{2.8}$$

This equation is often referred to as the *Standard Parabolic Equation.*

2.2.2 The Split-Step Fourier Solution

The narrow angle approximation embodied in Eq. (4.31) is convenient for the range-marching solution approach, elaborated in this section, using the Split-Step Fourier (SSPE) method suggested by Tappert et.al in [27]. This stems from Eq. (4.32) where a spatial transfrom in $z \rightarrow k_z$ yields,

$$2ik_0 \frac{\partial \psi(r, k_z)}{\partial r} - k_z^2 \psi(r, k_z) + k_0^2(n^2 - 1)\psi(r, k_z) = 0, \tag{2.9}$$

Rearranging,

$$\frac{\partial \psi(r, k_z)}{\partial r} + \frac{k_0^2(n^2 - 1) - k_z^2}{2ik_0}\psi(r, k_z) = 0, \tag{2.10}$$

whose solution is given by,

$$\psi(r, k_z) = \psi(r_0, k_z)e^{-\frac{k_0^2(n^2-1)-k_z^2}{2ik_0}(r-r_0)}. \tag{2.11}$$

The term $\psi(r_0, k_z)$ is the initial value condition. For the range-marching solution method, $\psi(r_0, k_z)$ is the solution of the previous step and $r - r_0 = \triangle r$ is the range step size.

It must be mentioned here that as this is a recursive process, there needs to be a starter field to initiate the range marching process. The most basic is the Normal-mode starter,

$$\psi(0, z) = \frac{\sqrt{2\pi}}{\rho(z_s)} \frac{\psi(z_s)\psi(z)}{\sqrt{k_r}} \tag{2.12}$$

For more details on the types of starter fields and their relative advantages the reader is referred to Jensen et al. [34]

The split-step Fourier transform is performed by taking Eq. (2.11) and performing an inverse spatial Fourier transform to obtain

$$\psi(r, z) = e^{\frac{ik_0(n^2-1)}{2}(r-r_0)} \int_{-\infty}^{\infty} \psi(r_0, k_z) e^{-\frac{ik_z^2}{2k_0}(r-r_0)} e^{ik_z z} dk_z \tag{2.13}$$

Writing $r - r_0 = \triangle r$, the split-step solution is finally written as,

$$\psi(r, z) = e^{\frac{ik_0(n^2-1)}{2}\triangle r} F^{-1}\left\{ e^{-\frac{ik_z^2}{2k_0}\triangle r} F\left\{\psi(r_0, z)\right\} \right\} \tag{2.14}$$

It should be noted that even though the refractive index n is both range and depth dependent, it is treated as a constant w.r.t each range step while computing Fourier transforms as the media is assumed to be constant within a range step. It has been shown that the error is small (i.e. on the order of the step-size) [27].

2.3 GENERALIZED RANGE-DEPENDENT INVARIANT MOMENTS

The objective of feature extraction process is to negate the propagation effects induced by the channel from the received sonar backscatter. In the parabolic model it amounts to reducing the impact of the range-dependent component $\psi(r,z)$. Inspection of Eq. (2.11) reveals that it is the exponent that introduces the channel characteristics into the solution.

Referring back to the total solution for the Helmholtz equation, Eq. (2.2) with Eq. (2.5), and rewriting Eq. (2.11) for each step $r - r_0$ we have

$$p(r, k_z) = \psi(r_0, k_z) e^{i\left[\frac{k_0\left(\left(\frac{c_0}{c}\right)^2-1\right)}{2} - \frac{k_z^2}{2k_0}\right](r-r_0)} e^{-k_0\left(\left(\frac{c_0}{c}\right)^2\left[\frac{\alpha c}{\omega}\right]\right)(r-r_0)} \sqrt{\frac{2}{\pi k_0 r}} e^{j(\frac{\omega}{c_0}r - \frac{\pi}{4})} \qquad (2.15)$$

where $\alpha = \beta\omega$ represents frequency-dependent attenuation due to the media, often accounted for by introducing a complex term to the refractive index, i.e. $n^2 \sim \left(\frac{c_0}{c}\right)^2 \left[1 + i\frac{2\alpha c}{\omega}\right]$ [34]. Assuming uniform media (i.e. at each range step the medium properties and the boundaries are identical) let the number of steps be N from the source at 0 to the receiver at r i.e. $\triangle r = (r - 0) = r/N$. Now,

$$p(r, k_z) = \psi(0, k_z) e^{i\left[\frac{k_0\left(\left(\frac{c_0}{c}\right)^2-1\right)}{2} - \frac{k_z^2}{2k_0}\right]\triangle r N} e^{-k_0\left(\left(\frac{c_0}{c}\right)^2\left[\frac{\alpha c}{\omega}\right]\right)\triangle r N} \sqrt{\frac{2}{\pi k_0 r}} e^{j(\frac{\omega}{c_0}r - \frac{\pi}{4})} \qquad (2.16)$$

With little modification, the above equation holds for nonuniform and complex media (i.e. for varying c and α at each interval $\triangle r$) as N in the exponent will be replaced by a summation of N intervals representing N segments from the source to the receiver, *i.e.*

$$p(r, k_z) = \psi(0, k_z) e^{i\left\{\sum_{i=1}^{N}\left[\frac{k_0\left(\left(\frac{c_0}{c_i}\right)^2-1\right)}{2} - \frac{k_z^2}{2k_0}\right]\right\}\triangle r} e^{-k_0\left\{\sum_{i=1}^{N}\left(\left(\frac{c_0}{c_i}\right)^2\left[\frac{\alpha_i c_i}{\omega}\right]\right)\right\}\triangle r} \sqrt{\frac{2}{\pi k_0 r}} e^{j(\frac{\omega}{c_0}r - \frac{\pi}{4})}$$
$$(2.17)$$

where α_i and c_i represent the attenuation factor and the sound speed profile, respectively, at step i. From here on we shall use Eq.(2.16) as reference for the feature extraction algorithm. However, the process itself can be applied to any generic environment given by Eq. (2.17).

In order to remove both exponential terms (which introduce the channel effects) the following needs to be done. First, we take the absolute value of Eq. (2.17) to eliminate the complex exponent,

$$|p(r, k_z; \omega)| = \left| \psi(0, k_z; \omega) e^{-k_0 \left(\left(\frac{c_0}{c} \right)^2 \left[\frac{\alpha c}{\omega} \right] \right) \triangle rN} \sqrt{\frac{2c_0}{\pi \omega r}} \right| \tag{2.18}$$

or with $\alpha = \beta \omega$ and $k_0 = \omega/c_0$,

$$|p(r, k_z; \omega)| = \left| \psi(0, k_z; \omega) e^{-\frac{c_0}{c} \beta \omega \triangle rN} \sqrt{\frac{2c_0}{\pi \omega r}} \right| \tag{2.19}$$

Multiplying both sides by $\sqrt{\omega}$ and taking a natural log yields,

$$\ln \left| \sqrt{\omega} p(r, k_z; \omega) \right| = \ln |\psi(0, k_z; \omega)| - \frac{c_0}{c} \beta \omega \triangle rN + \frac{1}{2} \left(\ln(2c_0) - \ln(\pi r) \right) \tag{2.20}$$

As the last two terms are independent of frequency, differentiation w.r.t. ω gives,

$$\frac{\partial}{\partial \omega} \ln \left| \sqrt{\omega} p(r, k_z; \omega) \right| = \frac{\partial}{\partial \omega} \ln |\psi(0, k_z; \omega)| - \frac{c_0}{c} \beta \triangle rN \tag{2.21}$$

The propagation effects of the last term, which corresponds to a constant level shift, can be eliminated by subtracting the mean over ω; specifically, defining

$$Z(r, k_z; \omega) = \frac{\partial}{\partial \omega} \ln \left| \sqrt{\omega} p(r, k_z; \omega) \right| \tag{2.22}$$

and

$$\overline{Z(x, k_z; \omega)} = \frac{1}{W} \int_W Z(x, k_z; \omega) d\omega \tag{2.23}$$

where W is the bandwidth of interest, then the processed received sonar signal given by

$$Z_0(r, k_z; \omega) = Z(r, k_z; \omega) - \overline{Z(x, k_z; \omega)} \tag{2.24}$$

is independent of propagation effects embodied in the exponential terms of Eq.(2.16). One can then extract various features (e.g., moments) from this processed signal to obtain invariant features for classification.

23

2.4 CONCLUSION

Building on past work for range-independent and weakly range-dependent sonar propagation, we have presented a feature extraction method based on the parabolic approximation for range dependent sonar propagation, to obtain features that are invariant to dispersion and attenuation.

3.0 PHASE-SPACE ANALYSIS FOR RANGE-DEPENDENT PROPAGATION

3.1 INTRODUCTION

Time-frequency analysis has been effectively applied to linear wave propagation, such as underwater sound propagation (i.e. sonar), because often there are time-varying spectral changes due to dispersive characteristics of the medium and target [18, 19, 20, 21, 33, 43, 50, 56]. Recently a phase space approximation for linear dispersive propagation was developed, based on the time-frequency (or position-wavenumber) Wigner distribution [38, 7]. This approximation was shown to be more accurate than the stationary phase approximation for dispersive propagation [8], and also lead to the development of dispersion-invariant features for target classification [47, 49]. The approximation was developed based on the normal mode solution to dispersive propagation, for range-independent channels. In this paper, we derive a Wigner approximation for range *dependent* propagation described by adiabatic mode theory. Analogies are drawn between the range-dependent approximation derived here and the previously derived range-independent case.

3.2 BACKGROUND: LINEAR DISPERSIVE PROPAGATION AND WIGNER APPROXIMATION

3.2.1 Linear Dispersive Propagation

In this section, we review the Wigner approximation for range-independent propagation [38, 7]. Let $u(x, t)$ denote the wave at some distance x from the source. Then, for linear dispersive propagation, the wave is given by [54, 55],

$$u(x, t) = \frac{1}{\sqrt{2\pi}} \int F(0, \omega) e^{jk(\omega)x} e^{-j\omega t} d\omega \qquad (3.1)$$

per mode, where $F(0, \omega)$ is the Fourier spectrum of the initial wave,

$$F(0, \omega) = \frac{1}{\sqrt{2\pi}} \int u(0, t) e^{j\omega t} dt \qquad (3.2)$$

and $k(\omega)$ is the dispersion relation coupling radial (ω) and spatial (k) frequencies. The spectrum of the wave at position x is given by

$$F(x, \omega) = \frac{1}{\sqrt{2\pi}} \int u(x, t) e^{j\omega t} dt. \qquad (3.3)$$

and therefore Eq. (3.1) can be written as

$$u(x, t) = \frac{1}{\sqrt{2\pi}} \int F(x, \omega) e^{-j\omega t} d\omega \qquad (3.4)$$

where

$$F(x, \omega) = F(0, \omega) e^{jk(\omega)x} \qquad (3.5)$$

Thus, by Eq. (3.5), we see that dispersive propagation can be viewed as a filtering of the wave by a linear, time-invariant but spatially-dependent filter with frequency response $H(\omega; x) = e^{jk(\omega)x}$. This can be written in terms of a convolution integral as

$$u(x, t) = \int u(0, t - \tau) h(\tau; x) d\tau \qquad (3.6)$$

where $h(t; x)$ is the impulse response of the propagation channel or medium at location x,

$$h(t; x) = \frac{1}{\sqrt{2\pi}} \int e^{jk(\omega)x - j\omega t} d\omega \qquad (3.7)$$

3.2.2 Wigner approximation

Because linear dispersive propagation can be formulated as a filtering operation, we consider the Wigner approximation for a filtered signal[37], and then apply it to pulse propagation.

Let $y(t)$ denote a filtered version of the signal $s(t)$,

$$y(t) = \int s(\tau)\, h(t - \tau)\, d\tau \tag{3.8}$$

where $h(t)$ is the impulse response of the filter, the Fourier transform of which gives the frequency response $H(\omega)$, which we express in terms of amplitude and phase as

$$H(\omega) = B_H(\omega)\, e^{j\psi_H(\omega)} = e^{\beta_H(\omega) + j\psi_H(\omega)} \tag{3.9}$$

The Wigner distribution of $y(t)$ is given by[6]

$$W_y(t,\omega) = \frac{1}{2\pi} \int y\left(t + \frac{\tau}{2}\right) y^*\left(t - \frac{\tau}{2}\right) e^{-j\omega\tau} d\tau \tag{3.10}$$

$$= \frac{1}{2\pi} \int Y^*\left(\omega + \frac{\theta}{2}\right) Y\left(\omega - \frac{\theta}{2}\right) e^{-j\theta t} d\theta \tag{3.11}$$

where $Y(\omega)$ is the Fourier transform of $y(t)$,

$$Y(\omega) = \frac{1}{\sqrt{2\pi}} \int y(t)\, e^{-j\omega t} d\omega \tag{3.12}$$

Plugging Eq. (3.8) into Eq. (3.10), one can express the Wigner distribution $y(t)$ in terms of the Wigner distributions of $s(t)$ and $h(t)$, respectively, as [39, 6]

$$W_y(t,\omega) = \int W_s(\tau,\omega)\, W_h(t - \tau,\omega)\, d\tau \tag{3.13}$$

By Eqs. (3.9) and (3.11) the Wigner distribution of $h(t)$ can be written as

$$W_h(t,\omega) = \frac{1}{2\pi} \int e^{\beta_H\left(\omega + \frac{\theta}{2}\right) + \beta_H\left(\omega - \frac{\theta}{2}\right) + j\left(\psi_H\left(\omega - \frac{\theta}{2}\right) - \psi_H\left(\omega + \frac{\theta}{2}\right) - \theta t\right)} d\theta \tag{3.14}$$

Approximations of this expression can be obtained by applying the series expansion

$$g(\omega \pm \theta/2) = \sum_{n=0}^{\infty} \frac{1}{n!} \left(\pm \frac{\theta}{2}\right)^n g^{(n)}(\omega) \tag{3.15}$$

27

to the exponentiated terms in Eq. (3.14), where $g^{(n)}(\omega)$ denotes the nth derivative. For convenience we explicitly write out the particular forms of the expansion that we make use of here:

$$\beta(\omega + \frac{\theta}{2}) + \beta(\omega - \frac{\theta}{2}) = \sum_{n=0}^{\infty} \frac{\beta^{(2n)}(\omega)}{(2n)!} \frac{\theta^{2n}}{2^{2n-1}} = 2\beta(\omega) + \frac{1}{4}\theta^2 \beta''(\omega) + \dots \quad (3.16)$$

$$\psi(\omega - \frac{\theta}{2}) - \psi(\omega + \frac{\theta}{2}) = \sum_{n=0}^{\infty} \frac{-\psi^{(2n+1)}(\omega)}{(2n+1)!} \frac{\theta^{2n+1}}{2^{2n}} = -\theta\psi'(\omega) - \frac{1}{24}\theta^3 \psi'''(\omega) + \dots. \quad (3.17)$$

Applying these expansions to $W_h(t,\omega)$ and keeping the first term of each yields the approximation [37],

$$W_h(t,\omega) \approx \frac{1}{2\pi} \int e^{2\beta_H(\omega) - j(\theta\psi'_H(\omega) + \theta t)} \, d\theta = B_H^2(\omega)\,\delta(t + \psi'_H(\omega)) \quad (3.18)$$

$$= |H(\omega)|^2 \, \delta(t + \psi'_H(\omega)) \quad (3.19)$$

Substituting this result into Eq. (3.13) yields an approximation for the Wigner distribution of the filtered signal [37],

$$W_y(t,\omega) \approx |H(\omega)|^2 \, W_s(t + \psi'_H(\omega), \omega) \quad (3.20)$$

It follows that for linear wave propagation, as given by Eqs. (3.5) and (3.6), we can approximate the Wigner distribution of the wave at x in terms of the Wigner distribution of the initial wave. First, however, we re-write Eq. (3.5) slightly in terms of an initial source location $x = x_S$ and receiver $x = x_R$, and write the dispersion relation in terms of its real and imaginary parts,

$$k_x(\omega) = k_x^{\Re}(\omega) + j\,k_x^{\Im}(\omega) \quad (3.21)$$

Accordingly, the Fourier spectrum at the receiver is

$$F(x_R, \omega) = F(x_S, \omega)e^{-k_x^{\Im}(\omega)(x_R - x_S)}\,e^{jk_x^{\Re}(\omega)(x_R - x_S)} \quad (3.22)$$

where $F(x_S, \omega)$ is the spectrum of the pulse at the source and the channel frequency response is

$$H(\omega; x_R - x_S) = e^{-k_x^{\Im}(\omega)(x_R - x_S)}\,e^{jk_x^{\Re}(\omega)(x_R - x_S)} \quad (3.23)$$

Thus, it follows from the Wigner approximation for filtered signals that the Wigner distribution of the wave at the receiver $x = x_R$ can be approximated in terms of the Wigner distribution of the wave at the source $x = x_S$ by he

$$W(x_R, t, \omega) \approx e^{-2k_x^{\Im}(\omega)(x_R - x_S)} W(x_S, t - k_x^{\Re'}(\omega)(x_R - x_S), \omega) \qquad (3.24)$$

which is the Wigner approximation for (range-independent) dispersive propagation [38, 7].

3.3   WIGNER APPROXIMATION FOR RANGE DEPENDENT PROPAGATION

In this section we derive the Wigner approximation for a wave propagating in a range dependent environment. We use the adiabatic approximation of the normal-mode solution as the range dependent model[34, 52]. In order to determine the impulse response of the channel we need to solve the Helmholtz equation with varying boundaries.

3.3.1   Adiabatic mode theory

We consider 2-D propagation in the range-depth $(x - z)$ plane, for which the Helmholtz equation in rectangular co-ordinates is [34]

$$\frac{\partial^2 \Phi}{\partial x^2} + \frac{\partial^2 \Phi}{\partial z^2} = \frac{1}{c^2} \frac{\partial^2 \Phi}{\partial t^2} \qquad (3.25)$$

The solution Φ has exponential dependence on time as well; writing this explicitly as $\Phi(x, z, t) = p(x, z)e^{-j\omega t}$ and substituting into the equation above yields

$$\frac{\partial^2 p}{\partial x^2} + \frac{\partial^2 p}{\partial z^2} = -\frac{\omega^2}{c^2} p \qquad (3.26)$$

Equations of this form are solved by separating variables; substituting a solution of the form $p(x, z) = \varphi(x)\psi(z)$ into the above equation yields[34]

$$\frac{d^2\varphi(x)}{dx^2}\psi(z) + \frac{d^2\psi(z)}{dz^2}\varphi(x) + \frac{\omega^2}{c^2}\varphi(x)\psi(z) = 0 \qquad (3.27)$$

Re-arranging and letting $\psi''(z) = \frac{d^2\psi(z)}{dz^2}$ and $\varphi'' = \frac{d^2\varphi(x)}{dx^2}$, we have

$$\frac{\psi''(z)}{\psi(z)} + \frac{\varphi''(x)}{\varphi(x)} = -\frac{\omega^2}{c^2} \qquad (3.28)$$

It follows that the two terms on the left must each equal a constant, which is denoted explicitly by

$$\frac{\psi''(z)}{\psi(z)} = -k_z^2 \qquad (3.29)$$

$$\frac{\varphi''(x)}{\varphi(x)} = -k_x^2 \qquad (3.30)$$

Accordingly, the following two equations are obtained:

$$\frac{d^2\psi(z)}{dz^2} + k_z^2\psi(z) = 0 \qquad (3.31)$$

and

$$\frac{d^2\varphi(x)}{dx^2} + k_x^2\varphi(x) = 0 \qquad (3.32)$$

where

$$k_x = \sqrt{\frac{\omega^2}{c^2} - k_z^2} \qquad (3.33)$$

The solution to the depth co-ordinate (Eq. (3.31)) is

$$\psi(z) = A\sin(k_z z) \qquad (3.34)$$

Now, the vanishing boundary condition $\psi(z) = 0$ at the range-dependent bottom depth $z = z_{bottom} = f(x)$ requires [52],

$$k_z = \frac{m\pi}{f(x)} \qquad (3.35)$$

Substituting this into Eq. (3.33) yields a range-dependent dispersion-like expression,

$$k_x(x) = \sqrt{\left(\frac{\omega}{c}\right)^2 - \left(\frac{m\pi}{f(x)}\right)^2} \qquad (3.36)$$

Substituting this into Eq. (3.32) yields

$$\frac{d^2\varphi(x)}{dx^2} + \left(\left(\frac{\omega}{c}\right)^2 - \left(\frac{m\pi}{f(x)}\right)^2\right)\varphi(x) = 0 \qquad (3.37)$$

Now, to solve this more complicated differential equation, we assume a solution with a range dependent amplitude and a range dependent phase,

$$\varphi(x) = A(x)e^{j\phi(x)} \tag{3.38}$$

Plugging this into Eq. (3.37), and using Eq. (3.36) to simplify notation, yields

$$A''(x)e^{j\phi(x)} + 2jA'(x)\phi'(x)e^{j\phi(x)} + jA(x)\phi''(x)e^{j\phi(x)} - A(x)\phi'^2(x)e^{j\phi(x)} + k_x^2(x)A(x)e^{j\phi(x)} = 0 \tag{3.39}$$

Eliminating the common $e^{j\phi(x)}$ term and then separating the equation into real and imaginary parts yields the following two equations:

$$A''(x) + A(x)\left[k_x^2(x) - \phi'^2(x)\right] = 0 \tag{3.40}$$

and

$$2A'(x)\phi'(x) + A(x)\phi''(x) = 0 \tag{3.41}$$

Applying the WKB approximation [54] to Eq. (3.40) (by which $A''(x) \approx 0$, consistent with the 'weak' range dependence condition), we obtain

$$\pm k_x(x) = \phi'(x) \tag{3.42}$$

by which the phase is

$$\phi(x) = \pm \int_{x_S}^{x_R} k_x(x)dx \tag{3.43}$$

where x_S and x_R denote the location of source and receiver, respectively. Plugging this result for $\varphi(x)$ into Eq. (3.41) yields

$$A(x) = \frac{A}{\sqrt{k_x(x)}} \tag{3.44}$$

where A is a constant (which we can take to be 1 in what follows, without loss of generality). Hence, the total solution at x_R works out to,

$$\varphi(x_R; x_S) = \frac{A}{\sqrt{k_x(x_R)}}e^{\pm j \int_{x_S}^{x_R} k_x(x')dx'} \tag{3.45}$$

This, then, is the approximate transfer function for a weakly range dependent environment.

By the Fourier synthesis approach for linear propagation [34] coupled with the approximate transfer function above, the propagated backscatter response is given by

$$F(x_R, \omega) = F(x_S, \omega) \frac{1}{\sqrt{k_x(x_R)}} e^{j \int_{x_S}^{x_R} k_x(x') dx'} \qquad (3.46)$$

where $F(x_S, \omega)$ is the Fourier transform of the pulse at source 's' and we use the positive exponent for forward propagating wave.

3.3.2 Non-Planar wave propagation

The solution to the wave equation in cartesian coordinates provides us with "Plane Waves". This is called so because the wave displacement function Φ in Eq. (3.25) is constant in the plane perpendicular to the axis of propagation for a fixed time $'t'$.

While Planar-wave propagation is adequately expressed by cartesian coordinates, guided wave propagations are generally curvilinear in nature and are best represented by other coordinate systems [34] . Specifically, the cylindrical coordinates. Naturally several scenarios arise with this type of propagation and we intend to detail them here on a case-by-case basis.

The standard Helmholtz equation in cylindrical coordinates is derived to be

$$\frac{1}{r} \frac{\partial}{\partial r} \left(r \frac{\partial p}{\partial r} \right) + \frac{1}{r^2} \frac{\partial^2 p}{\partial \theta^2} + \frac{\partial^2 p}{\partial z^2} = -\frac{\omega^2}{c^2} p \qquad (3.47)$$

This is the wave equation for a point source in cylindrical geometry. The starting point from which explore various scenarios commonly encountered in sonar propagation.

3.3.2.1 Case1: Infinite line source in cylindrical coordinates
Here, the assumption made is that the source is an infinite line. This is often useful while attempting to analyze wave propagation in a two dimensional wedge with perfectly reflecting boundaries. It is convenient to assume the source to be along the z-axis or prallel to it, thereby making the field p constant along the axis. This reduces Eq. (3.47) to [11, 45, 52]

$$\frac{1}{r} \frac{\partial}{\partial r} \left(r \frac{\partial p}{\partial r} \right) + \frac{1}{r^2} \frac{\partial^2 p}{\partial \theta^2} = -\frac{\omega^2}{c^2} p \qquad (3.48)$$

this is viewed as a **point source in polar coordinates** generating circular waves along the wedge. Writing the field as a product of two independent variables $p(r, \theta) = R(r)\Theta(\theta)$ and representing the first and second order differentials as $R'(r), \Theta'(\theta)$ and $R''(r), \Theta''(\theta)$ we rewrite Eq. (3.48) as

$$R''(r)\Theta(\theta) + \frac{1}{r}R'(r)\Theta(\theta) + \frac{1}{r^2}R(r)\Theta''(\theta) = -\frac{\omega^2}{c^2}R(r)\Theta(\theta) \tag{3.49}$$

$$r^2\frac{R''(r)}{R(r)} + r\frac{R'(r)}{R(r)} + \frac{\Theta''(\theta)}{\Theta(\theta)} = -\frac{\omega^2}{c^2}r^2 \tag{3.50}$$

separating the equation along its independent variables

$$r^2\frac{R''(r)}{R(r)} + r\frac{R'(r)}{R(r)} + r^2k^2 - m^2 = 0 \tag{3.51}$$

$$\frac{\Theta''(\theta)}{\Theta(\theta)} + k_\theta^2 = 0 \tag{3.52}$$

Solving Eq. (3.52)

$$\Theta(\theta) = \mathrm{A}cos(k_\theta\theta) + \mathrm{B}sin(k_\theta\theta) \tag{3.53}$$

and applying the vanishing boundaries at $\theta = 0$ and $\theta = \alpha$ we get

$$k_\theta = \frac{m\pi}{\alpha} \tag{3.54}$$

this is the standard modal solution to the boundary value problem.

Now, Eq. (3.51) is a standard Bessel's equation whose solution is given by

$$R(r) = \mathrm{H}_{k_\theta}^{(1)}(kr) \tag{3.55}$$

[1]we are showing only the forward propagating solution. The asymptotic approximation of the Hankel function is

$$\mathrm{H}_{k_{m\theta}}^{(1)}(kr) = \sqrt{\frac{2}{\pi kr}}\exp\left(i\left(kr - \frac{\pi}{4} - k_\theta\frac{\pi}{2}\right)\right) \tag{3.56}$$

---

[1]The derivation carried out in[45] has a slight error while separating the variables which we have rectified here

For an impulse source placed at (r_S, θ_S) the propagating field at (r_R, θ_R) is the one dimensional Green's function. Hence Eq. (3.56) is rewritten as

$$R\left(r_R; r_S\right) = \sqrt{\frac{2}{\pi k(r_R - r_S)}} \exp\left(i\left(k(r_R - r_S) - \frac{\pi}{4} - k_\theta \frac{\pi}{2}\right)\right) \tag{3.57}$$

3.3.2.2   Case2: Point source in cylindrical coordinates (Range independent boundary)   This is the most widely used scenario in acoustic wave propagation. In this case we assume a point source whose resulting waves are bounded along the z-axis and has a radiation condition along the r-axis. This condition also makes the field constant along the θ axis, thereby reducing Eq. (3.47) to

$$\frac{1}{r}\frac{\partial}{\partial r}\left(r\frac{\partial p}{\partial r}\right) + \frac{\partial^2 p}{\partial z^2} = -\frac{\omega^2}{c^2}p \tag{3.58}$$

Separating variables $p(r, z) = R(r)Z(z)$ and representing the first and second order differentials as $R'(r), Z'(z)$ and $R''(r), Z''(z)$ we get

$$R''(r)Z(z) + \frac{1}{r}R'(r)Z(z) + R(r)Z''(z) = -\frac{\omega^2}{c^2}R(r)Z(z) \tag{3.59}$$

$$\frac{R''(r)}{R(r)} + \frac{1}{r}\frac{R'(r)}{R(r)} + \frac{Z''(z)}{Z(z)} = -\frac{\omega^2}{c^2} \tag{3.60}$$

separating along the independent variables

$$\frac{R''(r)}{R(r)} + \frac{1}{r}\frac{R'(r)}{R(r)} + k_r^2 = 0 \tag{3.61}$$

$$\frac{Z'(z)}{Z(z)} + k_z^2 = 0 \tag{3.62}$$

where $k_r^2 = \left(\frac{\omega}{c}\right)^2 - k_z^2$.

Solving for Eq. (3.62)

$$Z(z) = \text{A}cos(k_z z) + \text{B}sin(k_z z) \tag{3.63}$$

34

the modal solution is obtained by applying the vanishing boundaries at $z = 0$ and $z = D$

$$k_z = \frac{m\pi}{D} \tag{3.64}$$

Now, Eq. (3.61) is the modified Bessel's equation whose solution is the Hankel function

$$R(r) = \frac{j}{4}\mathrm{H}_0^{(1)}(k_r r) \tag{3.65}$$

whose asymptotic approximation is

$$\mathrm{H}_0^{(1)}(kr) = j\sqrt{\frac{2}{\pi k_r r}}\exp\left(i\left(k_r r - \frac{\pi}{4}\right)\right) \tag{3.66}$$

The Green's function at (r_R, z_R) for an impulse source placed at (r_S, z_S) is written as

$$R(r_R; r_S) = j\sqrt{\frac{2}{\pi(r_R - r_S)k_r}}\exp\left(i\left(k_r(r_R - r_S) - \frac{\pi}{4}\right)\right) \tag{3.67}$$

3.3.2.3 Case3: Point source in cylindrical coordinates (Range dependent boundaries)

Normal mode theory could be extended to range dependent boundaries provided, there is no "coupling" between the modes (i.e. Modes are Adiabatic). We start with a point source and with conditions identical to Eq. (3.58)

$$\frac{1}{r}\frac{\partial}{\partial r}\left(r\frac{\partial p}{\partial r}\right) + \frac{\partial^2 p}{\partial z^2} = -\frac{\omega^2}{c^2}p \tag{3.68}$$

Separating the variables $p(r, z) = R(r)Z(z)$ and representing the first and second order differentials as $R'(r), Z'(z)$ and $R''(r), Z''(z)$ we get

$$R''(r)Z(z) + \frac{1}{r}R'(r)Z(z) + R(r)Z''(z) = -\frac{\omega^2}{c^2}R(r)Z(z) \tag{3.69}$$

$$\frac{R''(r)}{R(r)} + \frac{1}{r}\frac{R'(r)}{R(r)} + \frac{Z''(z)}{Z(z)} = -\frac{\omega^2}{c^2} \tag{3.70}$$

separating the equation along its variables

$$\frac{R''(r)}{R(r)} + \frac{1}{r}\frac{R'(r)}{R(r)} + k_r^2 = 0 \tag{3.71}$$

$$\frac{Z'(z)}{Z(z)} + k_z^2 = 0 \tag{3.72}$$

where $k_r^2 = \left(\frac{\omega}{c}\right)^2 - k_z^2$.

Solving for Eq. (3.72) we get

$$Z(z) = \mathrm{A}cos(k_z z) + \mathrm{B}sin(k_z z) \tag{3.73}$$

As we mentioned before, the boundaries are range dependent and the field vanishes at $z = 0$ and $z = f(r)$ respectively. Where the former would be the air/water interface and the latter would be the bottom that varies with horizontal range. Applying the conditions to Eq. (3.73) k_z works out to be

$$k_z = \frac{m\pi}{f(r)} \tag{3.74}$$

It has to be mentioned that k_z is a function of range r as evidenced by Eq. (3.74), which implies that Eq. (3.70) is not separable. However, in order to separate Eq. (3.70), it is imperative to assume that the boundaries are locally invariant.

The $k_r(r)$ (often termed the dispersion relation) is evaluated to be

$$k_r(r) = \sqrt{\left(\frac{\omega}{c}\right)^2 - \left(\frac{m\pi}{f(r)}\right)^2} \tag{3.75}$$

Now, the solution for Eq. (3.71) follows a similar procedure outlined in Section 3, starting from Eq. (3.38)

$$\frac{d^2 R(r)}{dr^2} + \left(\left(\frac{\omega}{c}\right)^2 - \left(\frac{m\pi}{f(r)}\right)^2\right) R(r) = 0 \tag{3.76}$$

to solve this more complicated differential equation, we assume a solution with a rapidly varying phase component and a slowly varying amplitude

$$R(r) = A(r)e^{j\phi(r)} \tag{3.77}$$

Plugging this into Eq. (3.76), and using Eq. (3.75) to simplify notation, yields

$$A''(r)e^{j\phi(r)} + 2jA'(r)\phi'(r)e^{j\phi(r)} + jA(r)\phi''(r)e^{j\phi(r)} - A(r)\phi'^2(r)e^{j\phi(r)} + k_r^2(r)A(r)e^{j\phi(r)} = 0 \tag{3.78}$$

Eliminating the common $e^{j\phi(r)}$ term and then separating the equation into real and imaginary parts yields the following two equations:

$$A''(r) + A(r)\left[k_r^2(r) - \phi'^2(r)\right] = 0 \tag{3.79}$$

and

$$2A'(r)\phi'(r) + A(r)\phi''(r) = 0 \tag{3.80}$$

Applying the WKB approximation [54] to Eq. (3.79) (by which $A''(r) \approx 0$, consistent with the 'weak' range dependence condition), we obtain

$$\pm k_r(r) = \phi'(r) \tag{3.81}$$

by which the phase is

$$\phi(r) = \pm \int\limits_{r_S}^{r_R} k_r(r)dr \tag{3.82}$$

where r_S and r_R denote the location of source and receiver, respectively. Plugging this result for $\varphi(r)$ into Eq. (3.80) yields

$$A(r) = \frac{A}{\sqrt{k_r(r)}} \tag{3.83}$$

and A is a constant whose value is obtained from the range independent solution derived in Eq. (3.66). Hence, the total solution at r_R works out to be

$$R(r_R; r_S) = \frac{A}{\sqrt{k_r(r_R)}} e^{\pm j \int_{r_S}^{r_R} k_r(r')dr'} \tag{3.84}$$

the constant A should satisfy Eq. (3.68)is obtained from the range independent solution

$$R(r_R; r_S) = je^{-j\pi/4}\sqrt{\frac{2}{\pi(r_R - r_S)k_r(r_R)}} e^{\pm j \int_{r_S}^{r_R} k_r(r')dr'} \tag{3.85}$$

3.3.2.4   Total solutions   It has to be mentioned here that Eqns. (3.56, 3.67 and 3.85) are one-dimensional Green's function for an impulsive source. However, the total solution to the wave equation defined in Eqns. (3.58, 3.48 and 3.25) should contain both the bounded and propagating solutions [45, 44, 52, 11].

The forced Helmholtz equation for an infinite line source in cylindrical coordinates is modified from Eq. (3.48)

$$\frac{1}{r}\frac{\partial}{\partial r}\left(r\frac{\partial p}{\partial r}\right) + \frac{1}{r^2}\frac{\partial^2 p}{\partial \theta^2} + \frac{\omega^2}{c^2}p = \frac{\delta\left(r - r_S\right)\delta\left(\theta - \theta_S\right)}{2\pi r} \tag{3.86}$$

whose solution works out to be

$$p(r, \theta) = \sum_{m=1}^{N} sin\left(\frac{m\pi}{f(r_S)}\theta_S\right) sin\left(\frac{m\pi}{f(r)}\theta\right)\frac{i}{\sqrt{8\pi(r - r_S)k_m}}\exp\left(i\left((r - r_S)k_m - \frac{\pi}{4} - k_\theta\frac{\pi}{2}\right)\right) \tag{3.87}$$

Similarly the forced Helmholtz equation for plane waves is written from Eq. (3.25) as

$$\frac{\partial^2 p}{\partial x^2} + \frac{\partial^2 p}{\partial z^2} + \frac{\omega^2}{c^2}p = \delta\left(x - x_S\right)\delta\left(z - z_S\right) \tag{3.88}$$

and teh corresponding solution is

$$p(x, z) = \sum_{m=1}^{N} sin\left(\frac{m\pi}{f(x_S)}z_S\right) sin\left(\frac{m\pi}{f(x)}z\right)\frac{1}{\sqrt{k_{xm}(x)}}\exp\left(i\left(\int_{x_S}^{x} k_{xm}\left(x'\right)dx'\right)\right) \tag{3.89}$$

The forced Helmholtz equation for a point source with cylindrical symmetry is

$$\frac{1}{r}\frac{\partial}{\partial r}\left(r\frac{\partial p}{\partial r}\right) + \frac{\partial^2 p}{\partial z^2} - \frac{\omega^2}{c^2}p = \frac{\delta\left(r - r_S\right)\delta\left(z - z_S\right)}{2\pi r} \tag{3.90}$$

and range independent boundary is written as

$$p(r, z) = \sum_{m=1}^{N} sin\left(\frac{m\pi}{D}z_S\right) sin\left(\frac{m\pi}{D}z\right)\frac{i}{\sqrt{8\pi(r - r_S)k_{rm}}}\exp\left(i\left((r - r_S)k_{rm} - \frac{\pi}{4}\right)\right) \tag{3.91}$$

38

and the range dependent boundary problem of Eq. (3.68) is written as

$$p(r,z) = \sum_{m=1}^{N} sin\left(\frac{m\pi}{f(r_S)}z_S\right) sin\left(\frac{m\pi}{f(r)}z\right) \frac{i}{\sqrt{8\pi(r-r_S)k_{rm}(r)}} \exp\left(i\left(\int_{r_S}^{r} k_{rm}(r')dr' - \frac{\pi}{4}\right)\right)$$
(3.92)

3.3.3 A Range Dependent Wigner Approximation

The Wigner distribution of $F(x_R, \omega)$ is given by [6],

$$W(x_R, t, \omega) = \frac{1}{2\pi} \int F^*(x_R, \omega + \frac{\lambda}{2}) F(x_R, \omega - \frac{\lambda}{2}) e^{jt\lambda} d\lambda$$
(3.93)

By Fourier inversion we have,

$$F^*(x_R, \omega + \frac{\lambda}{2}) F(x_R, \omega - \frac{\lambda}{2}) = \frac{1}{2\pi} \int W(x_R, t, \omega) e^{-jt\lambda} d\lambda$$
(3.94)

Using this identity, we write the Wigner distribution of the propagated pulse in terms of the Wigner of the pulse at the source, from Eq. (3.46)

$$W(x_R, t, \omega) = \frac{1}{2\pi} \int F(x_S, \omega - \frac{\lambda}{2}) F^*(x_S, \omega + \frac{\lambda}{2}) \frac{1}{\sqrt{k_x^*(x_R, \omega + \frac{\lambda}{2})k_x(x_R, \omega - \frac{\lambda}{2})}}$$
(3.95)

$$e^{-j\int_{x_S}^{x_R} k_x^*(x', \omega + \frac{\lambda}{2})dx'} e^{+j\int_{x_S}^{x_R} k_x(x', \omega - \frac{\lambda}{2})dx'}$$
(3.96)

Writing $\int_{x_S}^{x_R} k_x(x')dx'$ (which is a function of frequency ω) as $K_x(x_R, \omega) - K_x(x_S, \omega)$, and expressing this in terms of its real and imaginary parts,

$$K_x(x, \omega) = K_x^{\Re}(x, \omega) + jK_x^{\Im}(x, \omega)$$
(3.97)

and following similar steps as in the range-independent approximation (see Appendix 1), we obtain

$$W(x_R, t, \omega) \approx \frac{\exp\left(-2(K_x^{\Im}(x_S, \omega) - K_x^{\Im}(x_R, \omega))\right)}{|k_x(x_R, \omega)|} W\left(x_S, t - \left(K_x^{\Re'}(x_R, \omega) - K_x^{\Re'}(x_S, \omega)\right), \omega\right)$$
(3.98)

39

3.3.4 Wigner approximations in Cylindrical Coordinates

While the major objective of the Wigner approximation is to provide us with insight about the propagating wave, it can also be used to bypass computation of the dispersion relation which can often be tedious. In the following sections we use the Wigner approximation for both applications.

3.3.4.1 Wigner approximation for an infinite line source in cylindrical coordinates

Eq. (3.57) doesn't have a dispersion relation and cosequently evaluation of its integrals is a trivial problem. However, the Wigner approximation will still provide us with information regarding the behaviour of the wave.

The Wigner distribution for $F(r_R, \omega)$ as given in [6] is,

$$W(r_R, t, \omega) = \frac{1}{2\pi} \int F^*(r_R, \omega + \frac{\lambda}{2}) F(r_R, \omega - \frac{\lambda}{2}) e^{jt\lambda} d\lambda \tag{3.99}$$

By Fourier inversion we have,

$$F^*(r_R, \omega + \frac{\lambda}{2}) F(r_R, \omega - \frac{\lambda}{2}) = \frac{1}{2\pi} \int W(r_R, t, \omega) e^{-jt\lambda} d\lambda \tag{3.100}$$

Expressing the fourier spectrum at the receiver in terms of the source we get

$$F(r_R, \omega) = F(r_S, \omega) \sqrt{\frac{2}{\pi k (r_R - r_S)}} \exp\left(j \left(k (r_R - r_S) - \frac{\pi}{4} - k_\theta \frac{\pi}{2} \right) \right) \tag{3.101}$$

where $k_\theta = \frac{m\pi}{\alpha}$ and $k = \frac{\omega}{c} + jk^\Im$ where $k^\Im$ is the frequency dependent attenuating factor.

$$
\begin{aligned}
W(r_R, t, \omega) =\ & \frac{1}{2\pi} \int F(r_S, \omega - \frac{\lambda}{2}) F^*(r_S, \omega + \frac{\lambda}{2}) \\
& \sqrt{\frac{2}{\pi \left(\frac{\omega}{c} - \frac{\lambda}{2c} + jk^\Im \left(\omega - \frac{\lambda}{2} \right) \right) (r_R - r_S)}} \sqrt{\frac{2}{\pi \left(\frac{\omega}{c} + \frac{\lambda}{2c} - jk^\Im \left(\omega + \frac{\lambda}{2} \right) \right) (r_R - r_S)}} \\
& \exp\left(j \left(\left(\frac{\omega}{c} - \frac{\lambda}{2c} + jk^\Im \left(\omega - \frac{\lambda}{2} \right) \right) (r_R - r_S) - \frac{\pi}{4} - k_\theta \frac{\pi}{2} \right) \right) \\
& \exp\left(-j \left(\left(\frac{\omega}{c} + \frac{\lambda}{2c} - jk^\Im \left(\omega + \frac{\lambda}{2} \right) \right) (r_R - r_S) - \frac{\pi}{4} - k_\theta \frac{\pi}{2} \right) \right) e^{jt\lambda} d\lambda
\end{aligned} \tag{3.102}
$$

expressing in terms of the Wigner distribution at the source

$$W(r_R, t, \omega) = \frac{1}{2\pi} \int \int W(r_S, t', \omega) \times$$

$$\sqrt{\frac{2}{\pi \left(\frac{\omega}{c} - \frac{\lambda}{2c} + jk^\Im \left(\omega - \frac{\lambda}{2}\right)\right) (r_R - r_S)}} \sqrt{\frac{2}{\pi \left(\frac{\omega}{c} + \frac{\lambda}{2c} - jk^\Im \left(\omega + \frac{\lambda}{2}\right)\right) (r_R - r_S)}}$$

$$\exp\left(j\left(\left(\frac{\omega}{c} - \frac{\lambda}{2c} + jk^\Im \left(\omega - \frac{\lambda}{2}\right)\right)(r_R - r_S) - \frac{\pi}{4} - k_\theta \frac{\pi}{2}\right)\right)$$

$$\exp\left(-j\left(\left(\frac{\omega}{c} + \frac{\lambda}{2c} - jk^\Im \left(\omega + \frac{\lambda}{2}\right)\right)(r_R - r_S) - \frac{\pi}{4} - k_\theta \frac{\pi}{2}\right)\right)$$

$$e^{j\lambda(t-t')} d\lambda dt' \tag{3.103}$$

Considering only the first order terms (from binomial expansions), we write the Wigner distribution of the propagated pulse in terms of the Wigner of the pulse at the source (shown in Appendix 2),

$$W(r_R, t, \omega) = \frac{2 \exp\left(-2k^\Im(\omega)(r_R - r_S)\right)}{\pi (r_R - r_S) |k(\omega)|} W\left(r_S, t - \frac{1}{c}(r_R - r_S), \omega\right) \tag{3.104}$$

where $|k(\omega)| = \sqrt{(k^\Re(\omega))^2 + (k^\Im(\omega))^2}$.

It has to be mentioned here that the first order approximations are applied only for the attenauation multipliers and the imaginary part of the exponential. The Wigner distribution itself is exact, but the attenuating multipliers are accurate upto the first order.

3.3.4.2 Wigner approximation in Cylindrical Coordinates for Range-independent boundaries

The adiabatic-mode solution also holds its validity for point sources with azimuthal symmetry in cylindrical co-ordinates, which allows one to derive a Wigner approximation for this case as well. The Wigner distribution of $F(r_R, \omega)$ as given in [6],

$$W(r_R, t, \omega) = \frac{1}{2\pi} \int F^*(r_R, \omega + \frac{\lambda}{2}) F(r_R, \omega - \frac{\lambda}{2}) e^{jt\lambda} d\lambda \tag{3.105}$$

By Fourier inversion we have,

$$F^*(r_R, \omega + \frac{\lambda}{2}) F(r_R, \omega - \frac{\lambda}{2}) = \frac{1}{2\pi} \int W(r_R, t, \omega) e^{-jt\lambda} d\lambda \tag{3.106}$$

Using this identity, we write the Wigner distribution of the propagated pulse in terms of the Wigner of the pulse at the source using the solution from Eq. (3.67),

$$W(r_R, t, \omega) = \frac{1}{2\pi} \int F(r_S, \omega - \frac{\lambda}{2}) F^*(r_S, \omega + \frac{\lambda}{2}) \frac{2}{\pi (r_R - r_S) \sqrt{k_r^*(\omega + \frac{\lambda}{2}) k_r(\omega - \frac{\lambda}{2})}}$$

$$e^{-jk_r^*(\omega + \frac{\lambda}{2})(r_R - r_S)} e^{+jk_r(\omega - \frac{\lambda}{2})(r_R - r_S)} \tag{3.107}$$

We observe that the solution is similar to the previous case except for the $r^{\frac{1}{2}}$ term which is due to cylindrical spreading of the waves. The adiabatic approximate solution also turns out to be similar in structure. Proceeding in the same vein as the previous section we obtain for the Wigner approximation (Appendix 3),

$$W(x_R, t, \omega) \approx \frac{2\exp\left(-2(r_R - r_S)k_r^{\Im}(\omega)\right)}{\pi(r_R - r_S) |k_r(r_R, \omega)|} W(r_S, t - (r_R - r_S)k_r^{\Re'}(\omega), \omega) \tag{3.108}$$

3.3.4.3 Wigner approximation in Cylindrical Coordinates for Range-dependent boundaries
The adiabatic-mode solution also holds its validity for point sources with azimuthal symmetry in cylindrical co-ordinates, which allows one to derive a Wigner approximation for this case as well.Starting with the Helmholtz equation in cylindrical co-ordinates we have:

The Wigner distribution for $F(r_R, \omega)$ as given in [6],

$$W(r_R, t, \omega) = \frac{1}{2\pi} \int F^*(r_R, \omega + \frac{\lambda}{2}) F(r_R, \omega - \frac{\lambda}{2}) e^{jt\lambda} d\lambda \tag{3.109}$$

By Fourier inversion we have,

$$F^*(r_R, \omega + \frac{\lambda}{2}) F(r_R, \omega - \frac{\lambda}{2}) = \frac{1}{2\pi} \int W(r_R, t, \omega) e^{-jt\lambda} d\lambda \tag{3.110}$$

Using this identity, we write the Wigner distribution of the propagated pulse in terms of the Wigner of the pulse at the source,

$$W(r_R, t, \omega) = \frac{1}{2\pi} \int F(r_S, \omega - \frac{\lambda}{2}) F^*(r_S, \omega + \frac{\lambda}{2}) \frac{2}{\pi \sqrt{k_r^*(r_R, \omega + \frac{\lambda}{2}) k_r(r_R, \omega - \frac{\lambda}{2})}}$$

$$e^{-j \int_{r_S}^{r_R} k_r^*(r', \omega + \frac{\lambda}{2}) dr'} e^{+j \int_{r_S}^{r_R} k_r(r', \omega - \frac{\lambda}{2}) dr'} \tag{3.111}$$

42

Writing $\int_{r_S}^{r_R} k_r(r')dr'$ (which is a function of frequency ω) as $K_r(r_R, \omega) - K_r(r_S, \omega)$, and expressing this in terms of its real and imaginary parts,

$$K_r(r, \omega) = K_r^{\Re}(r, \omega) + jK_r^{\Im}(r, \omega) \tag{3.112}$$

We observe that the solution is similar to the previous case except for the $r^{\frac{1}{2}}$ term which is due to cylindrical spreading of the waves. The adiabatic approximate solution also turns out to be similar in structure. Proceeding in the same vein as the previous section we obtain for the Wigner approximation (Appendix 4),

$$W(x_R, t, \omega) \approx \frac{2\exp\left(2(K_r^{\Im}(r_S, \omega) - K_r^{\Im}(r_R, \omega))\right)}{\pi(r_R - r_S)\,|k_r(r_R, \omega)|} W\left(r_S, t - \left[K_r^{\Re'}(r_R, \omega) - K_r^{\Re'}(r_S, \omega)\right], \omega\right) \tag{3.113}$$

3.4   SIMULATION

Our simulations are carried out for a broadband pulse of 1KHz of duration 0.5 seconds. The source depth is kept at 25 meters and the propagated distance is 2500 meters with an attenuation coefficient of $10^{-8}m^{-1}Hz^{-1}$,. For the wedge waveguide the angle of the wedge at the apex is kept at 2 degrees thereby making the receiver depth to be 113 meters, the source and the receiver are kept at 15 meters from the air-water interface.

The exact and approximate Wigner distribution for a range-independent parallel plate waveguide is shown in Fig. 9, wedge waveguide with planar wave propagation is shown in Fig. 10, a parallel plate (range-independent) waveguide with a point source generating cylindrical waves is shown in Fig. 11 and finally, a wedge waveguide with cylindrical wave propagation is shown in Fig. 12. Fig. 9 shows us that -barring the crossterms- the approximate Wigner distribution is almost exactly the same as the exact Wigner of the propagated pulse, in the case of a planar wave propagating in a parallel plate waveguide. Fig. 10 shows that the dispersion curve has been well modeled by the approximate Wigner distribution though not as accurate as the parallel plate waveguide. Comparing Fig. 11 with Fig. 10 shows that the approximation for the point source in a range-independent environment the planar

43

wave in a wedge waveguide behave similarly as the attentuating terms are similar. Finally, Fig. 12 shows a considerable degree of attenuation we see that the approximation has more attenuation than the acutal Wigner distribution. This could partially be attributed the frequency-dependent attenuation and cylindrical spreading shown in Eq. (3.113). Despite these minor shortcommings, Leading us to the conclusion that the approximate phase-space representation is accurate enough to be used as an analysis tool.
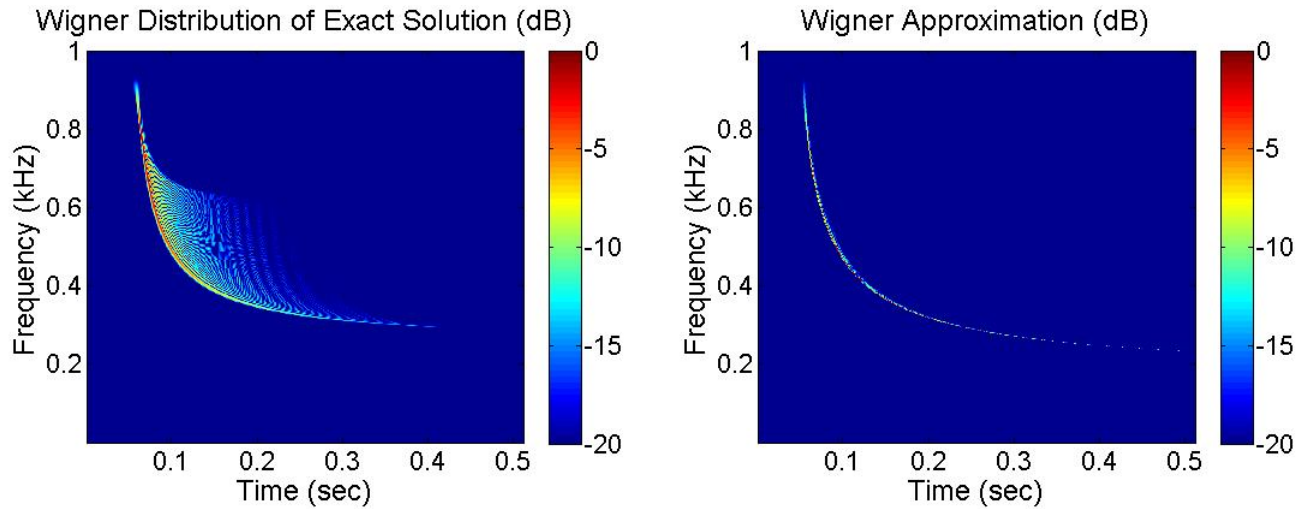
Figure 9: Comparison of actual Wigner distribution and approximate Wigner distribution for parallel plate waveguide with planar wave propagation
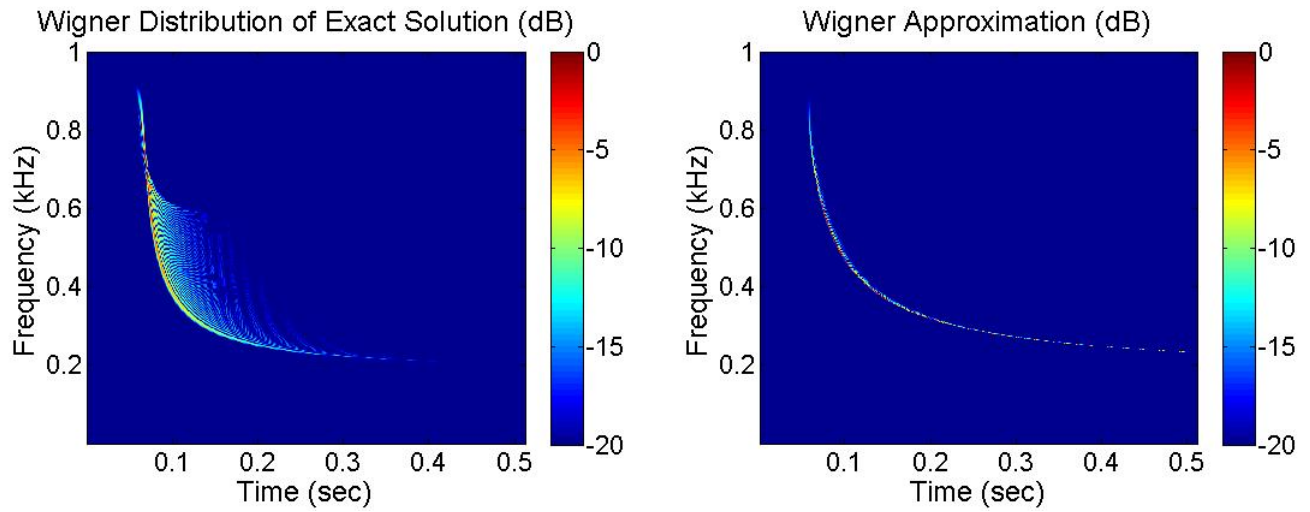
Figure 10: Comparison of actual Wigner distribution and approximate Wigner distribution for a wedge waveguide with planar wave wave propagation.
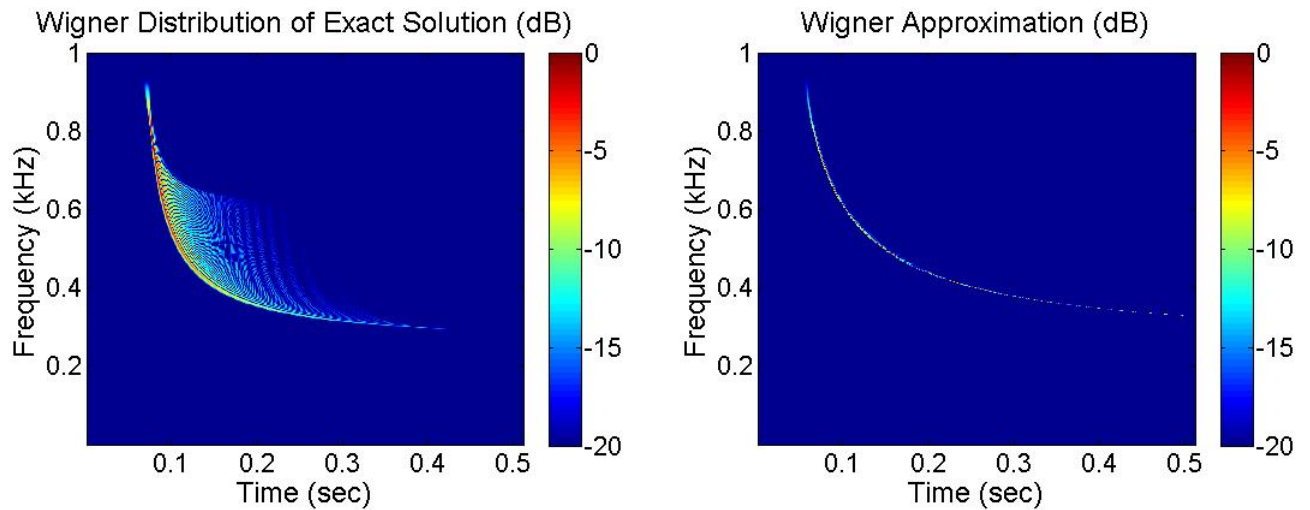
Figure 11: Comparison of actual Wigner distribution and approximate Wigner distribution for a parallel plate waveguide with cylindrical waves.
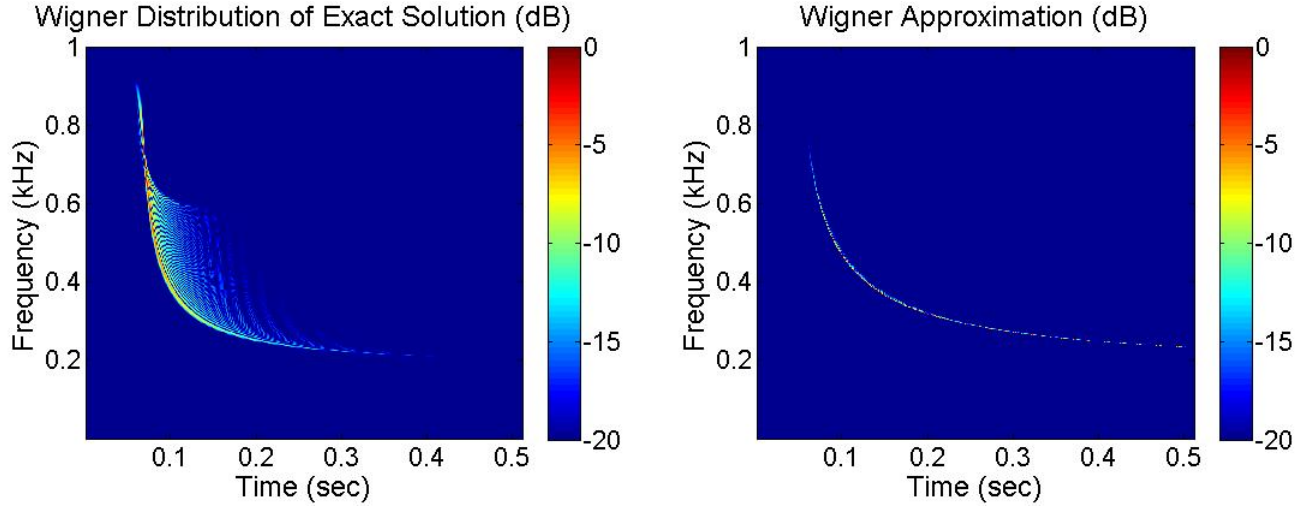
Figure 12: Comparison of actual Wigner distribution and approximate Wigner distribution for a wedge waveguide with cylindrical waves.

3.5   CONCLUSION

In this work we derived Wigner approximations to various propagation scenarios; building upon the works by [8, 7] to include a wider array of waves and boundaries commonly encountered in sonar and radar problems. The results are similar to each other in that the propagating components are exponential in nature. We also see that the approximate solutions for range dependent boundaries converge to range-independent solutions upto a constant factor.

Our simulations show that planar waves with range-independent boundaries tend to have more accurate approximations while range dependent boundaries and cylindrical spreading do result in reduction of accuracy. Cylindrical spreading function is a major cause for error as the spreading factor and media dependent attentuation is squared by the Wigner approximation expression.

4.0 OPERATOR APPROACH TO PARABOLIC EQUATION

4.1 INTRODUCTION

The classical method of studying systems governing differential equations involved finding functions either numerically or analytically that satisfied the requirements of the given equation. However, Cohen and Galleani [17, 16, 14] proposed a method where the given dynamical system is reformulated for a two dimensional function. This formulation, if solveable, has been shown to provide additional information about the system that a simple 2-D transform of a 1-D solution wouldn't as shown in [17, 16, 14]. In this chapter we formulate the parabolic model PE model in terms of a 2-D dynamical system and subsequenty explore possible avenues for solving them which would hopefully provide more insight into the pulse evolution of sonar targets.

4.2 BACKGROUND

It is a well known fact that a number of physical systems including the acoustic wave propagation discussed in the previous chapter are represented by linear differential equations. A general form is often written as

$$a_n \frac{d^n x}{dt^n} + a_{n-1} \frac{d^{n-1} x}{dt^{n-1}} \ldots + a_1 \frac{dx}{dt} + a_0 x = f(t) \tag{4.1}$$

where $f(t)$ is the forcing variable and $x(t)$ is the state variable. So, basically $f(t)$ generates the output $x(t)$ when passed through the system defined by Eq. (4.1). This can be rewritten

in polynomial form

$$P_n(D)\,x(t) = f(t). \tag{4.2}$$

Where

$$P_n(D) = a_n \frac{d^n x}{dt^n} + a_{n-1} \frac{d^{n-1} x}{dt^{n-1}} \ldots + a_1 \frac{dx}{dt} + a_0 x \tag{4.3}$$

and $D = \frac{d}{dt}$ the differential operator.

Now, before we attempt to reformulate Eq. (4.1) in terms of the Wigner distribution of the function, we need to introduce several operators and identities that would facilitate our objective. The Wigner of two signals is given by

$$W_{x,y}(t,\omega) = \frac{1}{2\pi} \int x^* \left(t - \frac{\tau}{2} \right) y \left(t + \frac{\tau}{2} \right) e^{-j\tau\omega} d\tau, \tag{4.4}$$

also called the cross Wigner distribution of two signals. If $x(t)$ and $y(t)$ are the same, then the above equation is called the auto-wigner of the signal.

$$W_{x,x}(t,\omega) = \frac{1}{2\pi} \int x^* \left(t - \frac{\tau}{2} \right) x \left(t + \frac{\tau}{2} \right) e^{-j\tau\omega} d\tau. \tag{4.5}$$

Let

$$\dot{g}(t) = \frac{dg(t)}{dt}; \qquad g^{(n)}(t) = \frac{d^n g(t)}{dt^n}. \tag{4.6}$$

The above expressions are used generate certain identities that will prove useful while reformulating the differntial equations.

$$W_{x,y}(t,\omega) = \frac{1}{2\pi} \int x^* \left(t - \frac{\tau}{2} \right) y \left(t + \frac{\tau}{2} \right) e^{-j\tau\omega} d\tau, \tag{4.7}$$

equivalently this can be written in the frequency domain as

$$W_{x,y}(t,\omega) = \frac{1}{2\pi} \int X^* \left(\omega + \frac{\theta}{2} \right) Y \left(\omega - \frac{\theta}{2} \right) e^{j\theta t} d\theta. \tag{4.8}$$

Now the Wigner distribution of a differentiated function can be written as follows

$$W_{\dot{x},y}(t,\omega) = \frac{1}{2\pi} \int \frac{dx^* \left(t - \frac{\tau}{2} \right)}{dt} y \left(t + \frac{\tau}{2} \right) e^{-j\tau\omega} d\tau, \tag{4.9}$$

or equivalently in the frequency domain as

$$W_{\dot{x},y}(t,\omega) = -\frac{j}{2\pi} \int \left(\omega + \frac{\theta}{2} \right) X^* \left(\omega + \frac{\theta}{2} \right) Y \left(\omega - \frac{\theta}{2} \right) e^{j\theta t} d\theta, \tag{4.10}$$

this holds as differential of a function in time domain would result in multiplication of the variable in the Fourier domain. Rearranging the above equation

$$W_{\dot{x},y}\left(t,\omega\right) = -\frac{j}{2\pi}\left\{\int \omega X^*\left(\omega+\frac{\theta}{2}\right)Y\left(\omega-\frac{\theta}{2}\right)e^{j\theta t}d\theta + \int\frac{\theta}{2}X^*\left(\omega+\frac{\theta}{2}\right)Y\left(\omega-\frac{\theta}{2}\right)e^{j\theta t}d\theta,\right\}$$
(4.11)

$$W_{\dot{x},y}\left(t,\omega\right) = -j\omega W_{x,y}\left(t,\omega\right) + \frac{1}{4\pi}\left(\int\frac{d}{dt}X^*\left(\omega+\frac{\theta}{2}\right)Y\left(\omega-\frac{\theta}{2}\right)e^{j\theta t}d\theta\right),$$
(4.12)

as θ and t are Fourier duals of each other in this equation. This results in

$$W_{\dot{x},y}\left(t,\omega\right) = -j\omega W_{x,y}\left(t,\omega\right) + \frac{1}{2}\frac{d}{dt}W_{x,y}\left(t,\omega\right),$$
(4.13)

now, this can be rewritten as a single operator variable

$$W_{\dot{x},y}\left(t,\omega\right) = \left(-j\omega + \frac{1}{2}\frac{d}{dt}\right)W_{x,y}\left(t,\omega\right), \qquad W_{\dot{x},y}\left(t,\omega\right) = AW_{x,y}\left(t,\omega\right).$$
(4.14)

Using a similar argument we can derive

$$W_{x,\dot{y}} = \left(\frac{1}{2}\frac{\partial}{\partial t} + j\omega\right)W_{x,y} = BW_{x,y},$$
(4.15)

where $\dot{x}(t) = \frac{dx(t)}{dt}$ and $\dot{y}(t) = \frac{dy(t)}{dt}$ as mentioned before.

Now, going back to Eq. (4.2), let us attempt to derive a cross Wigner between a function f and $P(D)x$

$$W_{f,P(D)x} = \sum_{i=1}^{n}a_i W_{f,x^{(i)}},$$
(4.16)

using the summation property in Eq. (4.10) and $x^{(i)}$ is the ith derivative of x. Now, $W_{f,x^{(i)}}$ similar to Eq. (4.15) and hence our Eq. (4.16) becomes

$$W_{f,P(D)x} = \sum_{i=1}^{n}a_i B^n W_{f,x}, \quad W_{f,P(D)x} = P_n\left(B\right)W_{f,x}.$$
(4.17)

49

Now we have an equivalent Wigner representation for the polynomial operator. Extending this to the whole Eq. (4.2) (i.e. taking the Wigner w.r.t f on both sides of the equation)

$$P_n(B) W_{f,x} = W_{f,f}. \tag{4.18}$$

Applying cross Wigner w.r.t. x gives us

$$P_n^*(A) W_{x,f} = W_{f,f}. \tag{4.19}$$

Combining Eqns. (4.18, 4.19) we get

$$P_n^*(A) P_n(B) W_{x,x} = W_{f,f}. \tag{4.20}$$

Wigner of product of functions [13]

$$W_{fx,x} = f^*(\varepsilon_x) W_{x,x} = \left[\frac{1}{2j} \frac{\partial}{\partial p} + x \right] W_{x,x}. \tag{4.21}$$

Starting from

$$W_{fx,y} = \frac{1}{2\pi} \int f^*\left(t - \frac{\tau}{2} \right) x^*\left(t - \frac{\tau}{2} \right) y\left(t + \frac{\tau}{2} \right) e^{-j\tau\omega} d\tau, \tag{4.22}$$

where $f(t)$'s Fourier dual is written as

$$f(t) = \int F(\omega) e^{j\omega t} \tag{4.23}$$

making Eq. (4.22)

$$W_{fx,y} = \frac{1}{2\pi} \iint F^*(\omega') e^{-j\omega'\left(t - \frac{\tau}{2} \right)} x^*\left(t - \frac{\tau}{2} \right) y\left(t + \frac{\tau}{2} \right) e^{-j\tau\omega} d\omega' d\tau, \tag{4.24}$$

$$W_{fx,y} = \frac{1}{2\pi} \iint F^*(\omega') e^{-j\omega' t} x^*\left(t - \frac{\tau}{2} \right) y\left(t + \frac{\tau}{2} \right) e^{-i\tau\left(\omega - \frac{\omega'}{2} \right)} d\omega' d\tau, \tag{4.25}$$

which becomes

$$W_{fx,y} = \frac{1}{2\pi} \int F^*(\omega') e^{-j\omega' t} W\left(t, \omega - \frac{\omega'}{2} \right) d\omega', \tag{4.26}$$

$$W_{fx,y} = \frac{1}{2\pi} \int F^*(\omega') e^{-j\omega' t - \frac{\omega'}{2} D_\omega} W(t, \omega) d\omega', \tag{4.27}$$

50

hence

$$W_{fx,y} = f^*\left(\varepsilon_x\right) W_{x,x} = f^*\left(t + \frac{1}{2j}\frac{d}{d\omega}\right) W_{x,x}, \tag{4.28}$$

$$W_{x,gx} = g\left(\mathcal{F}_x\right) W_{x,x} = \left[-\frac{1}{2j}\frac{d}{d\omega} + t\right] W_{x,x}, \tag{4.29}$$

where $f = f(t)$ and $g = g(t)$ are functions.

In the next section, we shall use these identities to reformulate the parabolic equation (PE) model.

4.3   CURRENT WORK

Our intention here is to compute the Wigner distribution for the non-separable wave equations. Specifically the range-dependent elliptic wave equation which is approximated to a parabolic equation. [34, 28, 27]

The starting point is the cylindrical Helmholtz equation, [34]

$$\frac{\partial^2\psi}{\partial r^2} + 2jk_0\frac{\partial\psi}{\partial r} + \frac{\partial^2\psi}{\partial z^2} + k_0^2(n^2 - 1)\psi = 0. \tag{4.30}$$

This is often termed as the elliptical wave equation and n is the refractive index of the media. Making the paraxial approximation

$$\frac{\partial^2\psi}{\partial r^2} \ll 2jk_0\frac{\partial\psi}{\partial r}, \tag{4.31}$$

reduces Eq. (4.30) to

$$2jk_0\frac{\partial\psi}{\partial r} + \frac{\partial^2\psi}{\partial z^2} + k_0^2(n^2 - 1)\psi = 0. \tag{4.32}$$

This is the simplest approximation yielding the parabolic equation. Other approximations can be made using operators shown below [34].

Define the operators

$$P = \frac{\partial}{\partial r}, \qquad Q = \sqrt{n^2 + \frac{1}{k_0^2}\frac{\partial^2}{\partial z^2}}, \tag{4.33}$$

51

applying Eq. (4.33) to Eq. (4.30) yields [34]

$$\left[P^2 + 2jk_0P + k_0^2\left(Q^2 - 1\right)\right]\psi = 0. \tag{4.34}$$

Factoring Eq. (4.34) into two propagating wave components, an outgoing and incoming wave gives [34],

$$\left(P + jk_0 - jk_0Q\right)\left(P + jk_0 + jk_0Q\right)\psi - jk_0\left[P, Q\right]\psi = 0, \tag{4.35}$$

where $[P, Q]\psi = (PQ - QP)\psi$ is a commutator term. For range-independent media, the commutator term is zero since $PQ = QP$, in that case Eq. (4.35) is exact for any $[P, Q]$.

Now, to apply Cohen-Galleani operator method to solve Eq. (4.35), we need to introduce a 4-d Wigner-type distribution [14],

$$K_{\psi,\psi}(r, k_r, z, k_z) = \int\int \psi(r + \frac{\tau}{2}, z + \frac{\nu}{2})\psi^*(r - \frac{\tau}{2}, z - \frac{\nu}{2})e^{-j\tau k_r}e^{-j\nu k_z}d\tau d\nu. \tag{4.36}$$

Defining the operators

$$A_r = \frac{1}{2}\frac{\partial}{\partial r} - jk_r; \qquad B_r = \frac{1}{2}\frac{\partial}{\partial r} + jk_r \tag{4.37}$$

$$A_z = \frac{1}{2}\frac{\partial}{\partial z} - jk_z; \qquad B_z = \frac{1}{2}\frac{\partial}{\partial z} + jk_z. \tag{4.38}$$

the following relations for the 4-D Wigner distribution are obtained (see [17, 16, 14, 13] for details)

$$K_{\frac{\partial\psi}{\partial r},\psi} = A_rK_{\psi,\psi} = \left[\frac{1}{2}\frac{\partial}{\partial r} - jk_r\right]K_{\psi,\psi} \tag{4.39}$$

$$K_{\psi,\frac{\partial\psi}{\partial r}} = B_rK_{\psi,\psi} = \left[\frac{1}{2}\frac{\partial}{\partial r} + jk_r\right]K_{\psi,\psi} \tag{4.40}$$

$$K_{\frac{\partial\psi}{\partial z},\psi} = A_zK_{\psi,\psi} = \left[\frac{1}{2}\frac{\partial}{\partial z} - jk_z\right]K_{\psi,\psi} \tag{4.41}$$

$$K_{\psi,\frac{\partial\psi}{\partial z}} = B_zK_{\psi,\psi} = \left[\frac{1}{2}\frac{\partial}{\partial z} + jk_z\right]K_{\psi,\psi} \tag{4.42}$$

We now apply this method to transform the elliptical wave equation from Eq.(4.30) to phase space.

4.3.1 Case1: n is a constant (Range-Independent Media)

Repeating the elliptical wave equation here for convenience,

$$\frac{\partial^2 \psi}{\partial r^2} + 2jk_0 \frac{\partial \psi}{\partial r} + \frac{\partial^2 \psi}{\partial z^2} + k_0^2(n^2 - 1)\psi = 0. \tag{4.43}$$

To obtain the equivalent phase-space equation in terms of the 4-D Wigner distribution K, we evaluate the cross Wigner of Eq.(4.43) w.r.t $\psi(r, z; \omega)$ and conversely, the cross wigner of $\psi(r, z; \omega)$ w.r.t Eq.(4.43). Doing so yields

$$K_{\frac{\partial^2 \psi}{\partial r^2}, \psi} + K_{2ik_0 \frac{\partial \psi}{\partial r}, \psi} + K_{\frac{\partial^2 \psi}{\partial z^2}, \psi} + K_{k_0^2(n^2-1)\psi, \psi} = 0, \tag{4.44}$$

and

$$K_{\psi, \frac{\partial^2 \psi}{\partial r^2}} + K_{\psi, 2jk_0 \frac{\partial \psi}{\partial r}} + K_{\psi, \frac{\partial^2 \psi}{\partial z^2}} + K_{\psi, k_0^2(n^2-1)\psi} = 0. \tag{4.45}$$

Applying the operator from Eqns.(4.39 and 4.40) on the terms with second and first order differentials (i.e. $K_{\frac{\partial^2 \psi}{\partial r^2}, \psi}$, $K_{\psi, \frac{\partial^2 \psi}{\partial r^2}}$ and $K_{2jk_0 \frac{\partial \psi}{\partial r}, \psi}$, $K_{\psi, 2jk_0 \frac{\partial \psi}{\partial r}}$ respectively), and then applying the operator from Eq. (4.41 and 4.42) to $K_{\frac{\partial^2 \psi}{\partial z^2}, \psi}$ and $K_{\psi, \frac{\partial^2 \psi}{\partial z^2}}$, we obtain the following simplifications

$$A_r^2 K_{\psi, \psi} - 2jk_0 A_r K_{\psi, \psi} + A_z^2 K_{\psi, \psi} + k_0^2(n^2 - 1)K_{\psi, \psi} = 0 \tag{4.46}$$

and

$$B_r^2 K_{\psi, \psi} + 2jk_0 B_r K_{\psi, \psi} + B_z^2 K_{\psi, \psi} + k_0^2(n^2 - 1)K_{\psi, \psi} = 0. \tag{4.47}$$

Subtracting Eq. (4.46) from Eq. (4.47) yields

$$\left(A_r^2 - B_r^2\right) K_{\psi, \psi} - 2jk_0 \left(A_r + B_r\right) K_{\psi, \psi} + \left(A_z^2 - B_z^2\right) K_{\psi, \psi} = 0. \tag{4.48}$$

Re-arranging the terms gives

$$-\left(A_r^2 - B_r^2\right) K_{\psi, \psi} + 2jk_0 \left(A_r + B_r\right) K_{\psi, \psi} = \left(A_z^2 - B_z^2\right) K_{\psi, \psi} \tag{4.49}$$

which simplifies to

$$2jk_r \frac{\partial K_{\psi, \psi}}{\partial r} + 2jk_0 \frac{\partial K_{\psi, \psi}}{\partial r} = -2jk_z \frac{\partial K_{\psi, \psi}}{\partial z}. \tag{4.50}$$

or

$$(k_r + k_0) \frac{\partial K_{\psi,\psi}}{\partial r} + k_z \frac{\partial K_{\psi,\psi}}{\partial z} = 0. \tag{4.51}$$

which is the 4-D Wigner phase space form of the elliptical wave equation. Whether solutions or approximations to this equation are more readily obtained than for Eq. 4.43 remains to be seen.

4.3.2 Case2: Refractive index n is a function of range and depth $n(r, z)$

For this case we add a couple more operators for multiplicative functions [15]

$$W_{fx,y} = f^*(\varepsilon)W_{x,y} \tag{4.52}$$

$$W_{x,fy} = f(\mathcal{F})W_{x,y} \tag{4.53}$$

where

$$\varepsilon = \frac{1}{2j} \frac{\partial}{\partial \omega} + t \tag{4.54}$$

$$\mathcal{F} = -\frac{1}{2j} \frac{\partial}{\partial \omega} + t. \tag{4.55}$$

Extending this to the variables in the parabolic equation

$$\varepsilon_r = \frac{1}{2j} \frac{\partial}{\partial k_r} + r, \qquad \mathcal{F}_r = -\frac{1}{2j} \frac{\partial}{\partial k_r} + r, \tag{4.56}$$

$$\varepsilon_z = \frac{1}{2j} \frac{\partial}{\partial k_z} + z, \qquad \mathcal{F}_z = -\frac{1}{2j} \frac{\partial}{\partial k_z} + z. \tag{4.57}$$

Repeating Eqns. (4.44 and 4.45) for range/depth dependent refractive indices we get

$$K_{\frac{\partial^2 \psi}{\partial r^2},\psi} + K_{2jk_0 \frac{\partial \psi}{\partial r},\psi} + K_{\frac{\partial^2 \psi}{\partial z^2},\psi} + K_{k_0^2(n^2(r,z)-1)\psi,\psi} = 0, \tag{4.58}$$

$$K_{\psi,\frac{\partial^2 \psi}{\partial r^2}} + K_{\psi,2jk_0 \frac{\partial \psi}{\partial r}} + K_{\psi,\frac{\partial^2 \psi}{\partial z^2}} + K_{\psi,k_0^2(n^2(r,z)-1)\psi} = 0, \tag{4.59}$$

54

and applying operators defined in Eqns. (4.56 and 4.57) along with Eqns. (4.37 and 4.38) we get

$$A_r^2 K_{\psi,\psi} - 2jk_0 A_r K_{\psi,\psi} + A_z^2 K_{\psi,\psi} + k_0^2(n^{*2}(\varepsilon_r, \varepsilon_z) - 1)K_{\psi,\psi} = 0 \tag{4.60}$$

$$B_r^2 K_{\psi,\psi} + 2jk_0 B_r K_{\psi,\psi} + B_z^2 K_{\psi,\psi} + k_0^2(n^2(\mathcal{F}_r, \mathcal{F}_z) - 1)K_{\psi,\psi} = 0. \tag{4.61}$$

Subtracting Eqns. (4.60 and 4.61) yields

$$\left(A_r^2 - B_r^2\right) K_{\psi,\psi} - 2jk_0\left(A_r - B_r\right) K_{\psi,\psi} + \left(A_z^2 - B_z^2\right) K_{\psi,\psi} + k_0^2(n^{*2}(\varepsilon_r, \varepsilon_z) - n^2(\mathcal{F}_r, \mathcal{F}_z))K_{\psi,\psi} = 0. \tag{4.62}$$

which evaluates to

$$-2jk_r \frac{\partial K_{\psi,\psi}}{\partial r} - 2jk_0 \frac{\partial K_{\psi,\psi}}{\partial r} - 2jk_z \frac{\partial K_{\psi,\psi}}{\partial z} + k_0^2(n^{*2}(\varepsilon_r, \varepsilon_z) - n^2(\mathcal{F}_r, \mathcal{F}_z))K_{\psi,\psi} = 0 \tag{4.63}$$

or

$$(k_r + k_0) \frac{\partial K_{\psi,\psi}}{\partial r} + k_z \frac{\partial K_{\psi,\psi}}{\partial z} + \frac{j}{2}k_0^2(n^{*2}(\varepsilon_r, \varepsilon_z) - n^2(\mathcal{F}_r, \mathcal{F}_z))K_{\psi,\psi} = 0. \tag{4.64}$$

Solving this equation is clearly more involved than the range-independent case, Eq. (4.51).

4.3.3   Further Work

Looking at Eq. (4.51)

$$(k_r + k_0) \frac{\partial K_{\psi,\psi}}{\partial r} + k_z \frac{\partial K_{\psi,\psi}}{\partial z} = 0, \tag{4.65}$$

there are several approaches that could be pursued to find a solution. A common approach is to assume that the function $K_{\psi\psi}$ is a product of individual variables and Eq. (4.65) can be re-written as

$$(k_r + k_0) \frac{\partial R(r)Z(z)\Bbbk_r(k_r)\Bbbk_z(k_z)}{\partial r} + k_z \frac{\partial R(r)Z(z)\Bbbk_r(k_r)\Bbbk_z(k_z)}{\partial z} = 0. \tag{4.66}$$

It is completely possible that the function $K_{\psi\psi}$ is not merely a product of function of individual variables and a more complicated relation exists. In which case our intention is to

ascertain the behaviour of a function parameterized by a particular variable, i.e. by assuming that either $\frac{\partial}{\partial r}$ or $\frac{\partial}{\partial z}$ is zero and then attempt to solve the resulting equation. Another method would involve trying to numerically solve the equation using a solver and see how the time-varying nature of solution manifests itself in the 4-d Wigner distribution.

Once we find a solution to Eq. (4.65), we can use that knowledge to solve Eq. (4.64), a more complicated form of the range independent equation. One possible way to approach this would be to provide simple range dependencies in the refractive index $n(r, z)$ term and then move on to more complicated and realistic sound speed profiles. However, it has to be mentioned here that solving the range dependent problem would be possible only after finding a solution to the range-independent case. If we are able to find a solution to Eq. (4.64) it wou ld be more accurate as we side step the issue of paraxial or weak range-dependent approximations.

5.0 TIME-FREQUENCY FILTERING FOR CLASSIFYING TARGETS IN NONS-STATIONARY CLUTTER

5.1 INTRODUCTION AND BACKGROUND

Classification of underwater targets from their active sonar backscatter is a challenging task, often complicated by backscatter from other objects that give rise to clutter. This leads to the issue of target classification in the presence of signal dependent or self-noise, which is a more complicated problem than target classification in ambient (i.e. additive independent) noise. We consider a common sum of point-scatterers clutter model,[10] wherein the clutter return consists of multiple echoes of the transmit signal, with random parameters such as propagation distance, time delay and strength. This clutter is nonstationary, as manifest by the time-dependence of its autocorrelation function and its Wigner spectrum.[9] Because the propagation channel can also induce nonstationarities[38] and the target itself can have a time-varying spectrum, it is natural to consider a time-varying, or time-frequency phase space, approach to target classification.

One of the earliest works in the field of time-frequency for signal classification was done by Altes,[1] where the spectrogram of the received signal was correlated with a reference spectrogram. Detectors for different cases of signal complexity are discussed and locally optimum tests are derived for the corresponding detectors.

Detectors based on time-frequency subspaces were explored by Hlawatsch and Kozek,[30] where regions containing signal energy are decomposed into basis vectors and subsequently recovered at the receiver by using time-frequency orthogonal projections. This was implemented as a multi-class target classifier by Chevret [5].

Okopal et al. considered a phase-space based feature extraction method that generates moment features that are invariant to specific propagation effects; in particular, dispersion and frequency-dependent absorption in range-independent channels.[47, 49] Extensions to range-dependent propagation were considered by Gomatam and Loughlin.[23]

The approach of using time-frequency kernels for enhanced target classification was proposed by McLaughlin and Atlas,[2] and Gillespie and Atlas [22]. They analyzed the problem of designing a time-frequency kernel that would maximize the Frobenius norm between any two given class of signals [2]. A modified approach was proposed[22] where the Fisher discriminant ratio of the target class was used to design the kernel that would overcome the limiting factors like small training sample size.

In this chapter, we employ the optimal time-frequency kernel design for nonstationary spectral estimation derived by Sayeedl and Jones,[51] to implement a time-frequency filter bank for distinguishing targets from clutter. This differs from the approach described in [22] in that the kernel is used as two-dimensional filter of the received signal in the ambiguity domain, rather than a specific time-frequency signal representation that would yield the maximum inter-class distance.

In the following section, we review the nonstationary nature of a common clutter model, and then subsequently implement the optimal kernel approach and illustrate its potential to discriminate targets in clutter via simulations.

5.2 CLUTTER MODEL WITH NONSTATIONARY STATISTICS

We consider a common model for clutter[10, 40, 41, 42], by which multiple copies of the transmitted signal are reflected back to the receiver with some random amplitude scaling, a_n,

$$u_C(x,t) = \frac{1}{\sqrt{N}} \sum_{n=1}^{N} a_n u_n(x,t;\varepsilon) \tag{5.1}$$

Here, we take $u_n(x,t;\varepsilon)$ to be the reflected signal from each clutter scatterer, with ε accounting for random aspects, such as the locations of each scattering element.

To provide a quantitative example from which the inherent nonstationary statistics of $u_C(x,t)$ will become evident,[9] let the signal reflected from each clutter scatterer be

$$u_n(x,t) = v(x - x_n, t) \tag{5.2}$$

where $v(x,t)$ is the propagating transmit signal and x_n designates the different locations of the clutter elements. Further, let the different amplitudes a_n and positions x_n be independently Gaussian distributed

$$P(a_n) = \sqrt{\frac{1}{2\pi\sigma_a^2}} e^{-\frac{1}{2\sigma_a^2}(a_n - z_a)^2}; \qquad P(x_n) = \sqrt{\frac{1}{2\pi\sigma_x^2}} e^{-\frac{1}{2\sigma_x^2}(x_n - z_x)^2} \tag{5.3}$$

If the initial pulse $v(x,t)$ at $t = 0$ is a chirp

$$v(x,0) = \left(\frac{\alpha}{\pi}\right)^{1/4} e^{-\frac{\alpha}{2}x^2} e^{j\left(k_0 x + \frac{\beta}{2}x^2\right)} \tag{5.4}$$

where $k_0 = \frac{\omega_0}{c}$, then the time-varying Wigner spectrum of the clutter works out to be[9]

$$\overline{W}(t, \omega; x) = K \exp\left(-\frac{q(\alpha^2 + \beta^2)(z - x + ct)^2 + (\alpha + q)(\omega/c + k_0)^2 - 2\beta q(z - x + ct)(\omega/c + k_0)}{\alpha^2 + \beta^2 + \alpha q}\right) \tag{5.5}$$

where $K = \frac{\sigma_a^2 c}{\pi}\sqrt{\frac{\alpha q}{\alpha^2 + \beta^2 + \alpha q}}$ and $q = \frac{1}{2\sigma_x^2}$. Note that this depends on t and hence the clutter is nonstationary (the Wigner spectrum for a wide-sense stationary process is independent of t and proportional to the power spectrum[6]).

The (symmetric) ambiguity function is the Fourier dual of the Wigner distribution and is given by[6]

$$A(\theta, \tau; x) = \frac{1}{2\pi} \int u^*(x, t - \frac{1}{2}\tau) u(x, t + \frac{1}{2}\tau) \exp(j\theta t)\, dt \tag{5.6}$$

For the clutter model above, the expected ambiguity function $E\{A(\theta, \tau; x)\}$ (inverse 2-D Fourier transform of the Wigner spectrum) is

$$E\{A(\theta, \tau; x)\} = \overline{A}(\theta, \tau; x) = \frac{\sigma_a^2}{4c^2} \frac{1}{4\pi} \exp\left(-\left\{\frac{(\beta c^2 \tau + \theta)^2}{4\alpha c^2} + \frac{\alpha c^2 \tau^2}{4} + \frac{\theta^2}{4c^2 q} + jck_0\tau + j\frac{\theta}{c}(z - x)\right\}\right) \tag{5.7}$$

5.3 OPTIMAL MSE KERNEL DESIGN

The mean squared error estimation is a fundamental approach for classification.[35] We employ this approach here, in terms of the ambiguity function of the received signal, to design optimal time-frequency filters (kernels) for each class.

Let us assume that we know, either from theory or experimental measurements, the expected ambiguity function for each target class, $E\{A_T^{(i)}(\theta, \tau)\} = \overline{A}_T^{(i)}(\theta, \tau)$, and the clutter, $E\{A_C^*(\theta, \tau)\} = \overline{A}_C(\theta, \tau)$. Our objective then is to design a time-frequency filter for each class, denoted by the kernel $\Phi^{(k)}(\theta, \tau)$, that yields the minimum mean squared distance to the correct target class (i.e. when $k = i$). The problem formulation is analogous to the nonstationary spectral estimation problem[51], and is given by

$$\arg \min_{\Phi^{(k)}} E \left\{ \iint \left| \overline{A}_T^{(i)}(\theta, \tau) - \Phi^{(k)}(\theta, \tau) A_r(\theta, \tau) \right|^2 d\theta d\tau \right\} \tag{5.8}$$

where A_r is the ambiguity function of the received signal. The optimal kernel for class (k) is given by[51]

$$\phi_{opt}^{(k)} = \frac{E\left\{A_T^{(k)}\right\} E\left\{A_r^*\right\}}{E\left\{|A_r|^2\right\}} \tag{5.9}$$

Assuming that the SNR is large enough such that ambient noise is not a dominant factor and can be ignored, the received signal is modeled as the sum of target and clutter returns

$$r(t) = T^{(k)}(t) + C(t) \tag{5.10}$$

The ambiguity function of the received signal is

$$A_r(\theta, \tau) = A_{T^{(k)}}(\theta, \tau) + A_C(\theta, \tau) + 2 \, Re\left\{A_{T^{(k)}C}(\theta, \tau)\right\} \tag{5.11}$$

where $A_{T^{(k)}C}(\theta, \tau)$ is the cross-ambiguity function between the target $T^{(k)}$ and clutter C. If the clutter and target returns are independent, then

$$E\left\{A_r^*\right\} = E\left\{A_{T^{(k)}}^*(\theta, \tau)\right\} + E\left\{A_C^*(\theta, \tau)\right\} \tag{5.12}$$

60

The denominator of Eq. (5.9) works out as

$$
\begin{aligned}
E\left\{|A_r|^2\right\} &= E\Big\{|A_{T^{(k)}}(\theta,\tau)|^2 + |A_C(\theta,\tau)|^2 + 4\,Re\left\{A_{T^{(k)}C}(\theta,\tau)\right\}^2 + \\
&\quad A_{T^{(k)}}(\theta,\tau)\,A_C^*(\theta,\tau) + 2A_{T^{(k)}}(\theta,\tau)\,Re\left\{A_{T^{(k)}C}(\theta,\tau)\right\} + A_{T^{(k)}}^*(\theta,\tau)\,A_C(\theta,\tau) + \\
&\quad 2A_C(\theta,\tau)\,Re\left\{A_{T^{(k)}C}(\theta,\tau)\right\} + 2A_{T^{(k)}}^*(\theta,\tau)\,Re\left\{A_{T^{(k)}C}(\theta,\tau)\right\} + \\
&\quad 2A_C^*(\theta,\tau)\,Re\left\{A_{T^{(k)}C}(\theta,\tau)\right\}\Big\} \qquad\qquad\qquad (5.13) \\
&= E\left\{|A_{T^{(k)}}(\theta,\tau)|^2\right\} + E\left\{|A_C(\theta,\tau)|^2\right\} + E\left\{4\,Re\left\{A_{T^{(k)}C}(\theta,\tau)\right\}^2\right\} + \\
&\quad E\left\{A_{T^{(k)}}(\theta,\tau)\,A_C^*(\theta,\tau)\right\} + E\left\{2A_{T^{(k)}}(\theta,\tau)\,Re\left\{A_{T^{(k)}C}(\theta,\tau)\right\}\right\} + \\
&\quad E\left\{A_{T^{(k)}}^*(\theta,\tau)\,A_C(\theta,\tau)\right\} + E\left\{2A_C(\theta,\tau)\,Re\left\{A_{T^{(k)}C}(\theta,\tau)\right\}\right\} + \\
&\quad E\left\{2A_{T^{(k)}}^*(\theta,\tau)\,Re\left\{A_{T^{(k)}C}(\theta,\tau)\right\}\right\} + E\left\{2A_C^*(\theta,\tau)\,Re\left\{A_{T^{(k)}C}(\theta,\tau)\right\}\right\} \quad (5.14)
\end{aligned}
$$

Hence, if the statistics of the target and clutter classes are known such that the calculations above can be done, it is possible to derive a closed form solution for the optimal target specific kernel. Alternately, if sufficient training data can be obtained, the optimal kernel can be computed empirically, as we do in the simulations below.

5.4   SIMULATION RESULTS

We performed classification of multiple targets in the presence of signal-dependent clutter. Four target-specific kernels were designed based on training data, with each target having different statistical characteristics for the parameters x_n from Eq. (5.3). In particular, the standard deviations of the scattering distances (σ_x) for different targets and clutter are summarized in Table 3. The general simulation parameters are shown in Table 4.

The figures show the results (i.e. histograms of the computed MSE for each testing trial) of classifying four targets in the presence of clutter. The targets have the same parameters except for the standard deviation in scattering distances σ_x which become more and more clutter-like with increasing σ_x. Each figure plots the histogram results for a particular target class when classifying with the optimal kernel (left) and when computing the MSE without first applying the optimal kernel (right). As can be seen, when the optimal kernel is used to

Table 3: σ_x for targets and clutter

	Standard Deviation x_n
Target 1	10
Target 2	20
Target 3	30
Target 4	40
Clutter	50

Table 4: General Simulation Parameters

Sampling Frequency	2000 Hz
Pulse Duration	.25 s
c(sound speed)	1500 m/s
ω_0 center frequency in Eq. (5.4)	500 Hz
No. of point target returns N in Eq. (5.1)	10
No. of point clutter returns N in Eq. (5.1)	50
Total Training Samples	100
Total Test Samples	80
Target and Clutter mean for a_n in Eq. (5.1)	1
Target and Clutter Standard Deviation for a_n in Eq. (5.1)	1
Target and Clutter mean for x_n in Eq. (5.3)	0

filter the received signal prior to computing the mean square distance to each target class, the correct target is identified (i.e. the histogram of the correct target lies to the left of the other histograms).

It can also be seen that as σ_x increases for the targets (largest for target class 4), such that it approaches that of the clutter, the corresponding classification performance degrades

Figure 13: Classification results for Target 1 ($\sigma_x = 10$). LEFT: Histogram of MSE values for the four target classes processed via the optimal kernel for Target 1 (*i.e.* Eq. (5.8) with $i = k = 1$). RIGHT: Histogram of MSE values when no kernel is used (i.e. $\Phi^{(k)}(\theta, \tau) = 1$). The correct target is well separated from the other target classes when the optimal kernel is used.

Figs. 13, 14, 15 and 16. This is an intuitive result, i.e. as the target becomes more clutter-like (or vice versa), the classifier finds it harder to effectively separate the classes.

Figure 14: Classification results for Target 2 ($\sigma_x = 20$). LEFT: Histogram of MSE values for the four target classes processed via the optimal kernel for Target 2 (Eq. (5.8) with $i = k = 2$). RIGHT: Histogram of MSE values when no kernel is used (i.e. $\Phi^{(k)}(\theta, \tau) = 1$). The correct target is well separated from the other target classes when the optimal kernel is used.

5.5 CONCLUSION

A time-frequency filtering approach utilizing optimal MSE kernel design was presented for classification of targets in signal dependent clutter. Simulations showed that using target specific kernels improves class separation of the target and the clutter.

One issue that needs to be addressed is that different kernels seem to carry different energies and hence result in MSE values that are on a different scale. This should be able to be remedied via appropriate normalization at the output of the time-frequency filter. Also to be done is application of the approach to experimental sonar data.
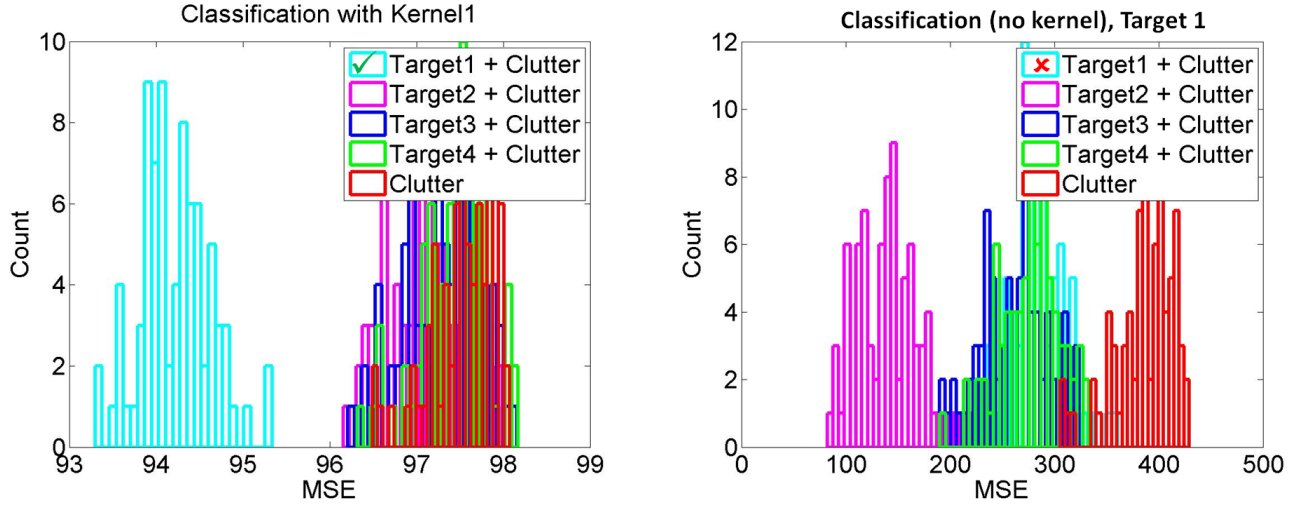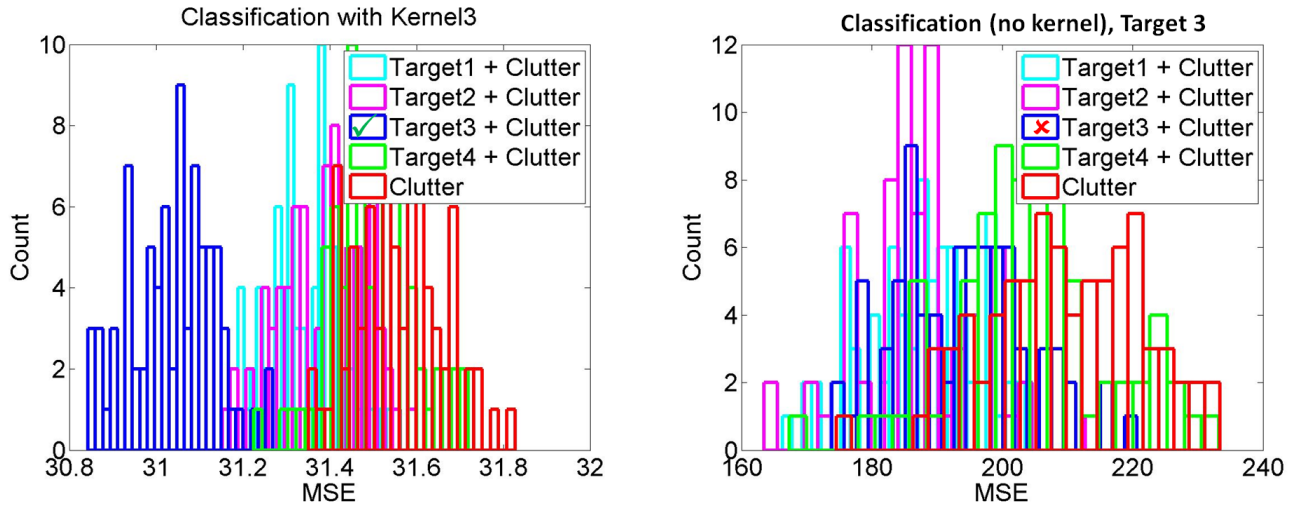
Figure 15: Classification results for Target 3 ($\sigma_x = 30$). LEFT: Histogram of MSE values for the four target classes processed via the optimal kernel for Target 3 (Eq. (5.8) with $i = k = 3$). RIGHT: Histogram of MSE values when no kernel is used (i.e. $\Phi^{(k)}(\theta, \tau) = 1$). The correct target is separated from the other target classes when the optimal kernel is used.
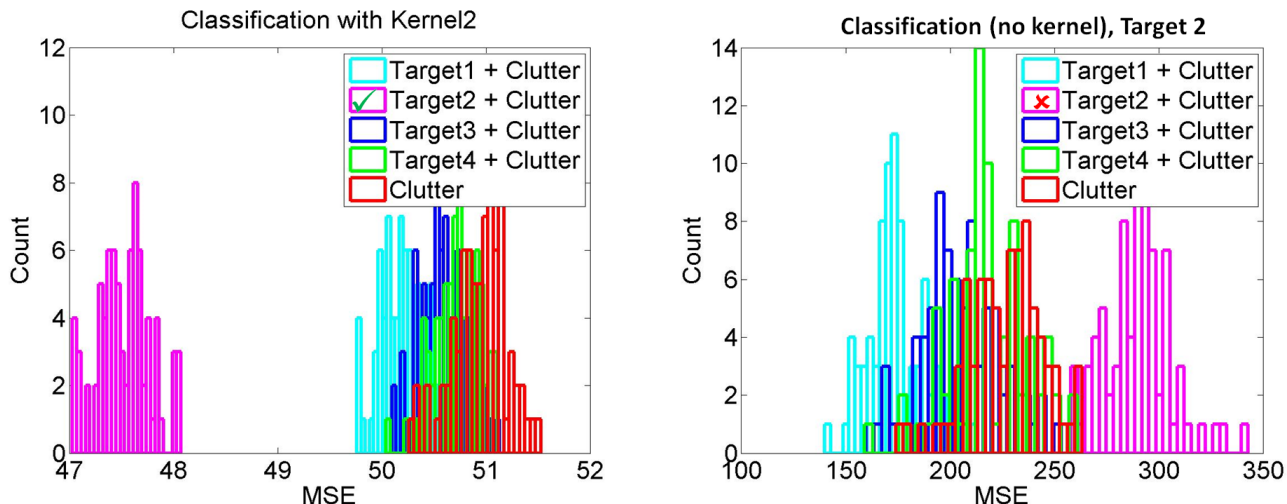
65
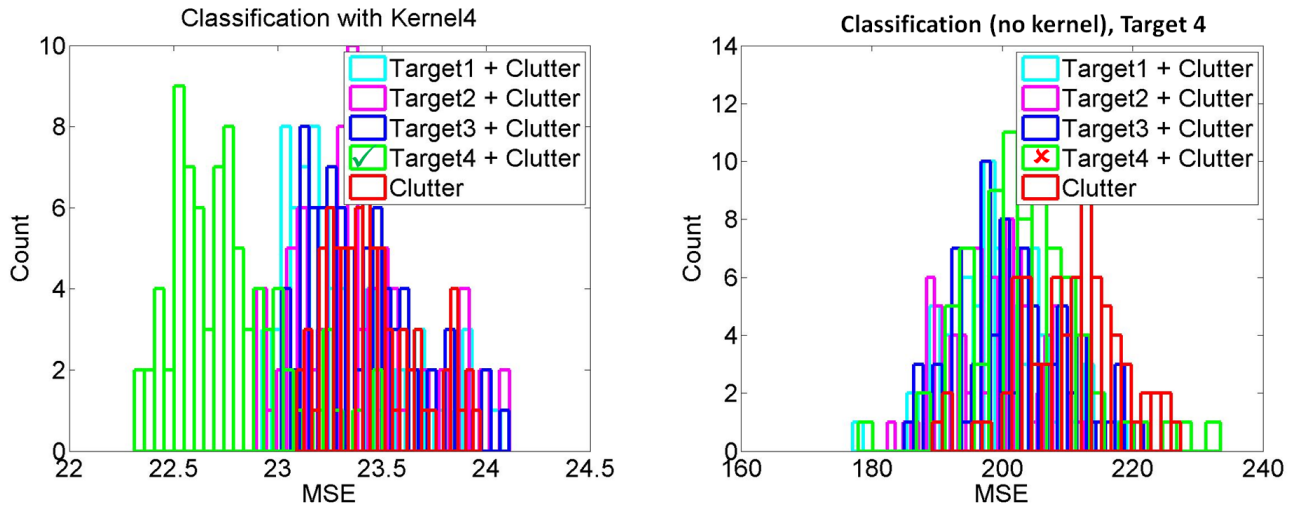
Figure 16: Classification results for Target 4 ($\sigma_x = 40$). LEFT: Histogram of MSE values for the four target classes processed via the optimal kernel for Target 4 (Eq. (5.8) with $i = k = 4$). RIGHT: Histogram of MSE values when no kernel is used (i.e. $\Phi^{(k)}(\theta, \tau) = 1$). The correct target is separated from the other target classes when the optimal kernel is used. As expected for this case, though, the separation distance diminishes as the clutter becomes more target-like.

66

6.0 CLASSIFICATION USING PROJECTION FILTERING

6.1 INTRODUCTION

SONAR targets and clutter are often non-stationary in nature and the oceanic channel is inherently time-varying (both seasonal and intra-day). The detection and classification of targets in the presence of clutter could be improved by applying Linear Time Varying (LTV) filters. In this chapter we apply the LTV filters to classify between target and clutter, the approach used for designing and implementing the LTV filters follow the work of Hlawatsch and Kozek [30, 12]. The classification is performed on the SONAR data measured by the JRP (DRDC-Atlantic, NURC, ARL-PSU, NRL) program. The signals provided are match-filtered and labelled either as target or clutter for a range of SNR's, while another set of data individually identifies the three main targets. In our problem, we perform a two kinds classification: 1. between the target and the clutter class 2. between three target classes.

The receiver architecture used would be an MPE (minimum distance) classifier, the MPE classifier has been shown to be optimal when the targets are corrupted by additive white Gaussian noise. As mentioned earlier the target and clutter is presumed non-stationary and possibly be corrupted by non-stationary and/or non-Gaussian noise. Naturally, the MPE classifier would cease to be optimal under the conditions, this could partially be negated by using the LTV as a pre-filter to augment the MPE classifier by eliminating any non-Gaussian and non-stationary components from the targets and then perform classification.

In this chapter, we provide some background on the signal space representation of time-frequency distribution and the construction of the LTV filter. We then perform classification performance on the acoustic data and compare the results of a standard MPE classifier and the augmented MPE classifier with LTV pre-filter. The comparison of the LTV filter and

the orthogonal projection operation is made and oblique projection operation is suggested as an alternative when two signal spaces have significant overlap. Conclusions from the results and future directions are presented.

6.2 BACKGROUND

The approach to build the LTV filter begins with the Wigner distribution given in [6]

$$W_x(t, f) = \int x \left(t + \frac{\tau}{2} \right) x^* \left(t - \frac{\tau}{2} \right) e^{-j2\pi f \tau} d\tau \tag{6.1}$$

The Wigner distribution is one of the simpler ways in which a signal can be represented in the time-frequency plane.

The concept of time-frequency representation of a signal can be extended to a signal space as well. If the signal space S is linear, then it can be represented as a sum of orthonormal basis vectors $\{u_k(t)\}_{k=1}^{N_S}$ where N_S is the dimension. The Wigner distribution of a signal space is given by

$$W_S(t, f) = \sum_{k=1}^{N_S} W_{u_k}(t, f) \tag{6.2}$$

Analogus to the Wigner distribution of a signal, $W_S(t, f)$ is a representation of the time-frequency regions that could be covered by the linear combination of the elements in the basis set $\{u_k(t)\}_{k=1}^{N_S}$.

The goal is to derive the orthogonal basis signals that spans the space whose energy is contained in the region $\Re$ in the time-frequency plane Fig. 17, where $\Re$ is a time-frequency region of interest (a specific target or a reference signal). In order to effectively implement the LTV filter, two major criteria has to be satisfied; concentration and localization.
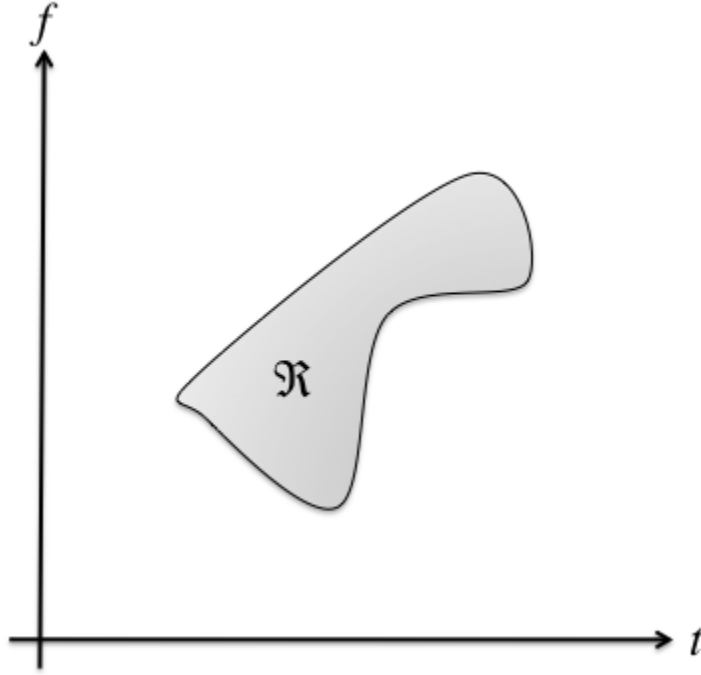
Figure 17: Time-frequency support of an arbitrary region to be passed by an LTV filter. Anything outside of $\Re$ is (ideally) rejected.

6.2.1 Concentration Objective Function

One objective for designing the LTV filter is to be concentrated in the desired time-frequency region $\Re$ as described by Hlawatsch [29, 31, 30]

$$\rho(S, \Re) \triangleq \frac{E_S^{(\Re)}}{N_S} = \frac{\iint W_S(t, f) \, I_\Re(t, f) dt df}{\iint W_S(t, f) \, dt df} \qquad (6.3)$$

where $E_S^{(\Re)}$ is the energy of the signal space S contained in the region $\Re$ and N_S is the dimension and the total energy contained by the signal space S. The region $I_\Re$ is an indicator region defined as

$$I_\Re(t, f) = \begin{cases} 1, \ (t, f) \in \Re & 0, \ (t, f) \notin \Re \end{cases} \qquad (6.4)$$

It could be said that if the dimension of the space is approximately equal to the energy of space contained in $\Re$ or if $\rho(S, \Re) \approx 1$, then good concentration is achieved. This also means

that if more energy is required for the subspace to represent, the greater its dimension will be. Howerver, this is not possible by just maximizing Eq. (6.3) as $E_S^\Re$ is neither positive, nor less than N_S.

6.2.2 Localization Objective Function

The Concentration function explained earlier is useful for determining how well the energy is contained inside the region $\Re$, it is however, not well suited to deriving an optimal subspace S that minimizes the holes or gaps within the region $\Re$. So, a measure that keeps the energy as close to the indicator region $\Re$ as possible is needed, it is defined as follows [30]

$$\varepsilon^2(S, \Re) = \|I_\Re - W_S\|^2 = \iint \left[I_\Re(t, f) - W_S(t, f)\right]^2 dt df \tag{6.5}$$

The relationship between the concentration Eq. (6.3) and the localization metric Eq. (6.5) is derived to be

$$\varepsilon^2(S, \Re) = A_\Re + N_S \left[1 - 2\rho(S, \Re)\right] \tag{6.6}$$

where

$$A_\Re = \iint_{(t,f)\in\Re} dt df = \iint I_\Re(t, f) \, dt df \tag{6.7}$$

is the time-frequency area of interest. Also, it can be shown that Eq. (6.5) is lower bounded by [30]

$$\varepsilon^2(S, \Re) \geqslant \left|\sqrt{N_S} - \sqrt{A_\Re}\right| \tag{6.8}$$

this suggests that good localization is obtained if the dimension of the signal space is approximately equal to the area of the region $\Re$ in the time-frequency plane. Eq. (6.8) also shows that as $A_\Re$ increases, the dimension of the subspace required to adequately cover the region $\Re$ increases thereby increasing the processing time to design the filter.

6.2.3 Optimal Subspace

The two conditions requried to derive the optimal subspace has been described earlier.

$$I_{\Re}(t, f) = \sum_{k=1}^{\infty} \lambda_k W_{u_k}(t, f) \tag{6.9}$$

with $\lambda_k \in \mathbb{R}$. Where the real valued coefficients λ_k and the orthonormal coefficients $u_k(t)$ are solutions to the eigenequation

$$\int H_{\Re}(t_1, t_2) \, u_k(t_2) dt_2 = \lambda_k u_k(t_1) \tag{6.10}$$

and the relationship between the kernel and the indicator function can be written as

$$H_{\Re}(t_1, t_2) = \int I_{\Re} \left(\frac{t_1 + t_2}{2}, f \right) e^{j2\pi(t_1 - t_2)f} df \tag{6.11}$$

$H_{\Re}(t_1, t_2)$ can be obtained by treating $I_{\Re}(t, f)$ as a wigner distribution and applying the inversion formula [6]. The relationship between $I_{\Re}(t, f)$ and eigenvalues and eigenvectors of $H_{\Re}(t_1, t_2)$ will help us in defining the optimal subspace. In order to achieve that, we need to define a relationship between Eqns. (6.3 and 6.5) and the eigenvalues of $H_{\Re}(t_1, t_2)$. For a given subspace dimension $N_{\Re}$ the minimum localization error is given by [30].

$$\varepsilon^2(S, \Re)_{min, N_{\Re}} = \sum_{k=1}^{N_{\Re}} (1 - \lambda_k)^2 + \sum_{k=N_{\Re}+1}^{\infty} \lambda_k^2 \tag{6.12}$$

Secondly, for a given subspace of dimension $N_{\Re}$ the maximum concentration is written as

$$\rho(S, \Re)_{max, N_{\Re}} = \frac{1}{N_{\Re}} \sum_{k=1}^{N_{\Re}} \lambda_k \tag{6.13}$$

If the eigenvalues are arranged in descending order ($\lambda_k > \lambda_{k+1}$), Eq. (6.12) is minimized over all $N_{\Re}$ if we choose $N_{\Re}$ such that the first $N_{\Re}$ eigenvalues are greater than $\frac{1}{2}$. From this we can state that the subspace that minimizes the localization error is the set of eigenvalues that are greater than $\frac{1}{2}$, when this condition is satisfied then Eq. (6.13) would be a monotonically decreasing function with increasing $N_{\Re}$. The subspace that maximizes the concentration has dimension of $N_{\Re} = 1$ and is a constant multiple of the biggest eigenvector. However, this

doesn't guarantee the minimum for Eq. (6.12). To summarize, the basis vectors that yield optimal concentration and localization in the desired time-frequency region is given by

$$S_{\Re}^{(N_\Re)} = \{u_1(t), u_2(t), \ldots\ldots, u_{N_\Re}(t)\} \tag{6.14}$$

for all $\lambda_1 > \lambda_2 > \lambda_3 > \ldots\ldots > \lambda_{N_\Re} > \frac{1}{2}$.

The filter implementation of the above solution can be described as follows. Let $x(t)$ be the received signal possibly corrupted by random and non-stationary noise and distortions. The LTV filtering can be achieved by applying the projecting the signal $x(t)$ onto the vector space defined by Eq. (6.14), mathematically given by

$$y(t) = \sum_{k=1}^{N_\Re} \lambda_k \left\langle x\left(t\right), u_k\left(t\right) \right\rangle u_k\left(t\right) \tag{6.15}$$

where $\left\langle x\left(t\right), u_k\left(t\right) \right\rangle$ is the inner product of the received signal imposed on to the signal space.

6.3   APPLICATION OF LTV FILTERS TO CLASSIFY TARGETS IN THE PRESENCE OF CLUTTER

As mentioned earlier, the filter is tested on the acoustic data provided by the JRP (DRDC-Atlantic, NURC, ARL-PSU, NRL) program. Three separate measurements were made over a span of two years, the pings used were a linear up chirp from 500 to 3500 Hz, each ping is 1 second in duration and is sampled at 12.8 kHz.

For our experiment we consider three targets from the data set. The Oilrig, The Well head and The Hollow Cylinder (Passive Acoustic Target). The signals provided are match filtered and labelled among the three targets.

Any signal that isn't associated with the known targets are labelled clutter. There are fifty examples of "Target" and "Clutter" class provided with Signal-to-Noise Ratios (SNR) in the following ranges: 18-15dB, 15-12dB, 12-9dB, 6-9dB, 3-6dB, 0-3dB, (-3)-0dB and (-6)-(-3)dB.

6.3.1   Experiment Setup

Since each signal example has 12801 samples which is too big to perform complex matrix operations to generate the filter. Instead, we truncated parts of the signal that didn't carry any useful information, leaving only 2200 samples for processing. In our experiment we compare the classification performance provided by the MPE classifier architecture with the MPE classifier augmented by the LTV filter. In order to generate a reference signal we take the spectrograms of 20 example signals from each class and average them. We use the average spectrogram as the prototype to generate the LTV filter.

In order to generate a Matched Filter for the MPE archtitecture we average the spectrogram of 5 signals from the same class. The magnitude and phase of the signal is then recontructed from the spectrogram [6], the time marginal is written as

$$P(t) = \int SP_{avg}(t, \omega) d\omega \approx |s(t)|^2 \tag{6.16}$$

and the instantaneous phase is written as

$$\langle \omega \rangle_t = \frac{1}{P(t)} \int \omega SP_{avg}(t, \omega) d\omega \approx \varphi^{'}(t) \tag{6.17}$$

the time series for the matched filter can be obtained from

$$h_{MF_i}(-t) = \sqrt{P(t)} \cos \left(\int\limits_0^t \varphi^{'}(\tau) \, d\tau \right) \tag{6.18}$$

The "classic" MPE architecture is given in Fig. 18, also known as the minimum distance receiver, the test statistic used in the receiver could be simplified into a replica correlator as shown in Fig. 19 [35] Fig. 20 shows the MPE classifier 'augmented' by the LTV filter for each signal class [26].
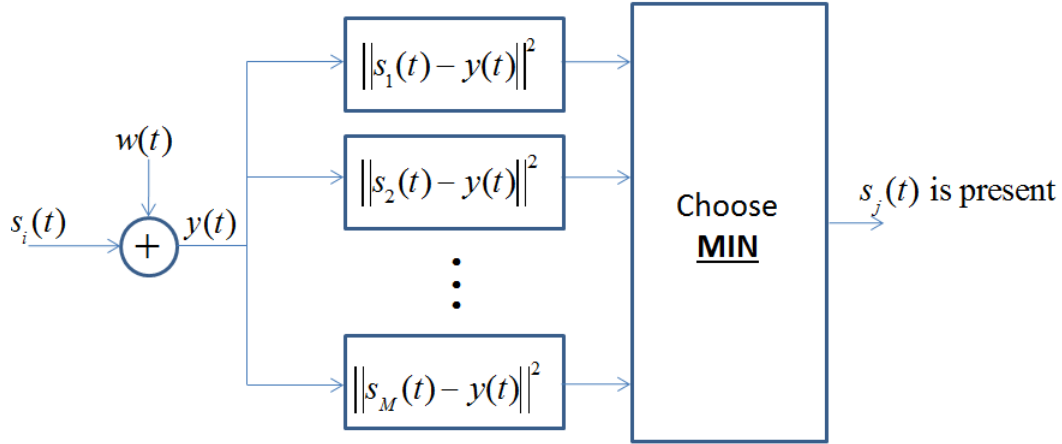
Figure 18: Minimum Distance Receiver

$$E_{s_i} = \int |s_i(t)|^2 \, dt$$
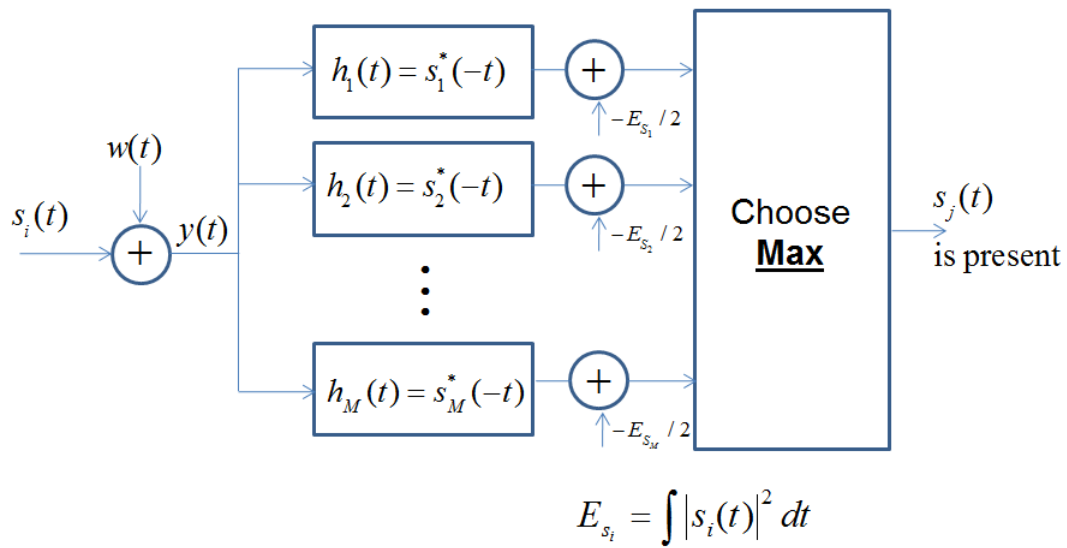
Figure 19: Minimum Probability of Error (MPE) Classifier

6.3.2   Experiment Results

As mentioned before, we performed two types of classification; between the target and clutter classes and between three target classes; the oil rig, the well head and the hollow cylinder (passive acoustic target 1).
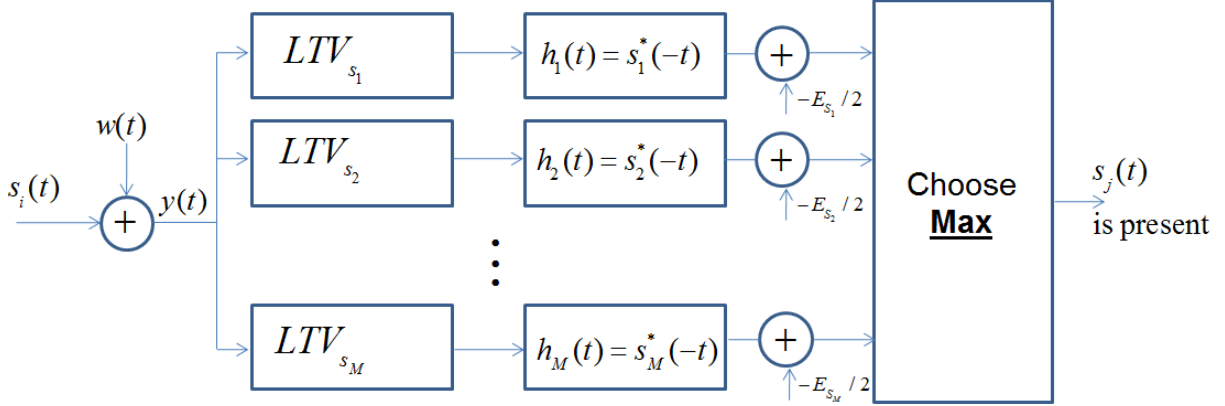
Figure 20: MPE Classifier augmented by the class-specific LTV filter

In the first case we perform classification between the target and the clutter class. To assess the effectiveness of the LTV filter, we design the filter whose indicator functions are thresholded at different energy levels of the prototype spectrogram shown in Fig.21.

Tables. 5, 6, 7, 8, 9 and 10 show the probability of correct classification and the probability of false alarm at different range of SNR's. Each level of SNR have fifty samples of target and clutter signals. Except for the highest SNR level (15-18dB) where 20 signals were used to generate the LTV filter and 5 to generate the matched filter for the receiver, leaving us with 25 test signals on which classification was carried out.

The degradation of the classification performance as a function of SNR is summarized in Fig. 23. Here, the classification performance of the MPE classifier "augmented" by the the LTV filter generated with an indicator region where the energy level was thresholded at 20dB, is compared with the standard MPE classifier.

In the second case, we perform classification between the three target classes, the dataset is not labelled by SNR. The generated LTV filters thresholded at different levels is shown in Fig. 22. Tables 11, 12, and 13 show the classification performance of the augmented MPE classifier with LTV filters generated by thresholding the indicator region at different energy levels.
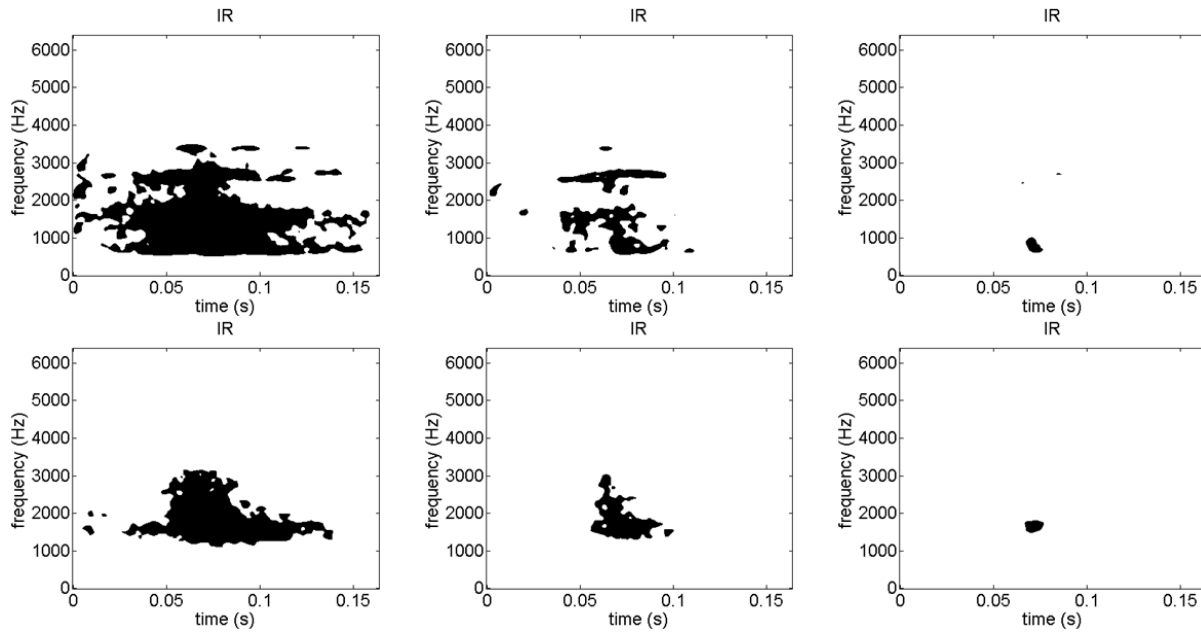
Figure 21: Target and Clutter LTV filter indicator region at 30,20 and 10 dB thresholds

In contrast, the MPE classifier with no LTV filltering's performance shown in Table. 14, under- performs in comparison with the 20dB thresholded augmented LTV classifier.

Table 5: Classification Results: Target v/s Clutter, SNR 15-18 dB

P(Target | Target) Probability of Correct Classification				
LTV filter Thresholds	30dB	20dB	10dB	No LTV
Target	0.72 (18/25)	0.8 (20/25)	0.72 (18/25)	0.76 (19/25)
P(Target | Clutter) Probability of False Alarm				
LTV filter Thresholds	30dB	20dB	10dB	No LTV
Target	0.2 (5/25)	0.12 (3/25)	0.2 (5/25)	0.12 (3/25)

6.4   CONCLUSION AND FUTURE WORKS

As we had seen in the results the MPE classifier augmented by the LTV filter outperforms the un-augmented classifier under most cases. It was also seen that the performance degraded as a function of the SNR, thus showing that ambient white noise is a limiting factor to the performance of classifier. Given the near-linear degradation in the classification performance w.r.t SNR, it could be said that the LTV filter effectively reduces the non-stationarity of target and clutter classes.

Table 6: Classification Results: Target v/s Clutter, SNR 12-15 dB

P(Target | Target) Probability of Correct Classification				
LTV filter Thresholds	30dB	20dB	10dB	No LTV
Target	0.68 (34/50)	0.82 (41/50)	0.74 (37/50)	0.76 (38/50)
P(Target— Clutter) Probability of False Alarm				
LTV filter Thresholds	30dB	20dB	10dB	No LTV
Target	0.18 (9/50)	0.16 (8/50)	0.2 (10/50)	0.14 (7/50)

Table 7: Classification Results: Target v/s Clutter, SNR 9-12 dB

P(Target— Target) Probability of Correct Classification				
LTV filter Thresholds	30dB	20dB	10dB	No LTV
Target	0.66 (33/50)	0.74 (37/50)	0.6 (30/50)	0.66 (33/50)
P(Target— Clutter) Probability of False Alarm				
LTV filter Thresholds	30dB	20dB	10dB	No LTV
Target	0.24 (12/50)	0.2 (10/50)	0.26 (13/50)	0.3 (15/50)

Table 8: Classification Results: Target v/s Clutter, SNR 6-9 dB

P(Target— Target) Probability of Correct Classification				
LTV filter Thresholds	30dB	20dB	10dB	No LTV
Target	0.52 (26/50)	0.58 (29/50)	0.52 (26/50)	0.52 (26/50)
P(Target— Clutter) Probability of False Alarm				
LTV filter Thresholds	30dB	20dB	10dB	No LTV
Target	0.44 (22/50)	0.4 (20/50)	0.42 (21/50)	0.46 (23/50)

Table 9: Classification Results: Target v/s Clutter, SNR 3-6 dB

P(Target— Target) Probability of Correct Classification				
LTV filter Thresholds	30dB	20dB	10dB	No LTV
Target	0.52 (26/50)	0.56 (28/50)	0.48 (24/50)	0.52 (26/50)
P(Target— Clutter) Probability of False Alarm				
LTV filter Thresholds	30dB	20dB	10dB	No LTV
Target	0.52 (26/50)	0.46 (23/50)	0.5 (25/50)	0.46 (23/50)

Table 10: Classification Results: Target v/s Clutter, SNR 0-3 dB

P(Target— Target) Probability of Correct Classification				
LTV filter Thresholds	30dB	20dB	10dB	No LTV
Target	0.48 (24/50)	0.5 (25/50)	0.46 (23/50)	0.44 (22/50)
P(Target— Clutter) Probability of False Alarm				
LTV filter Thresholds	30dB	20dB	10dB	No LTV
Target	0.54 (27/50)	0.52 (26/50)	0.5 (25/50)	0.48 (24/50)
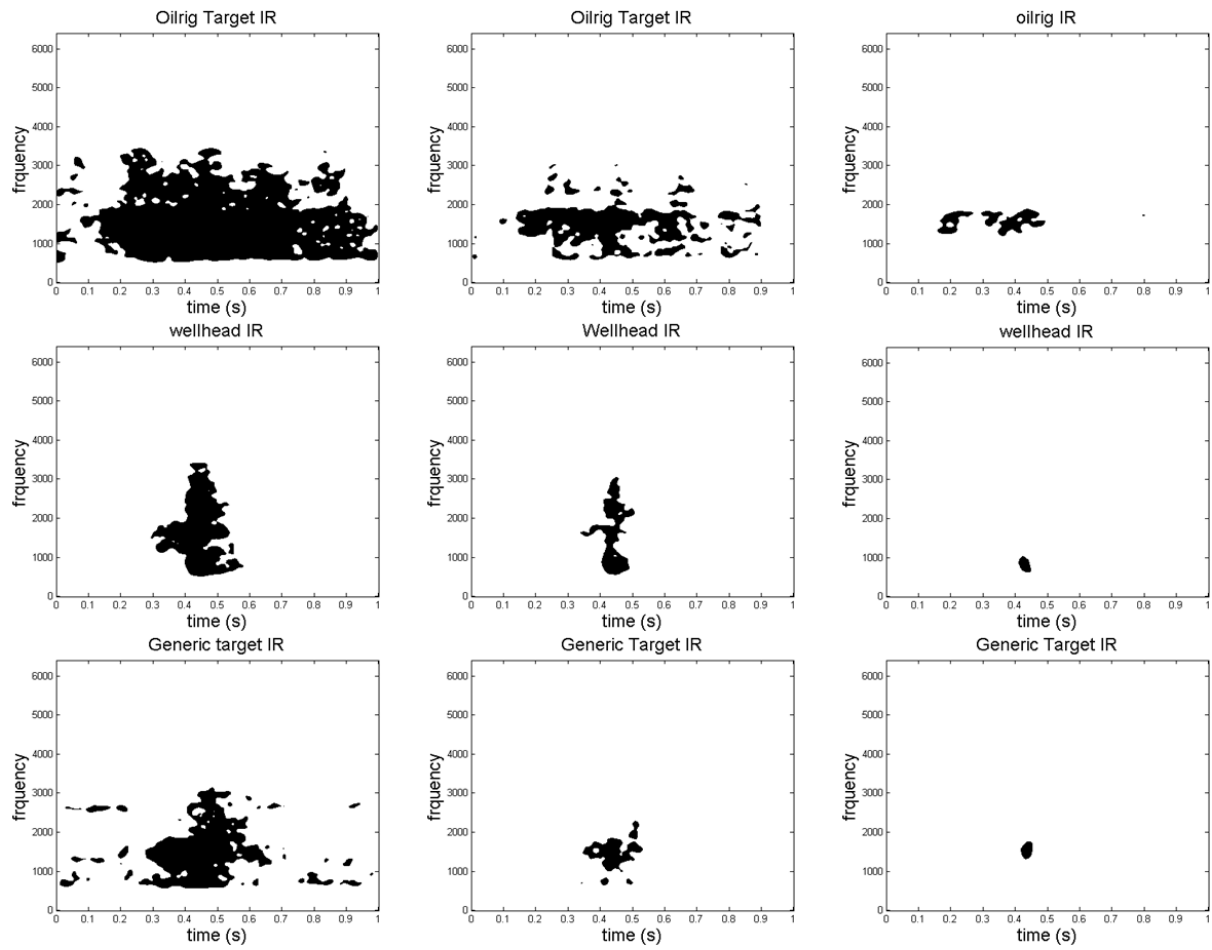
Figure 22: Target and Clutter LTV filter indicator region at 30,20 and 10 dB thresholds
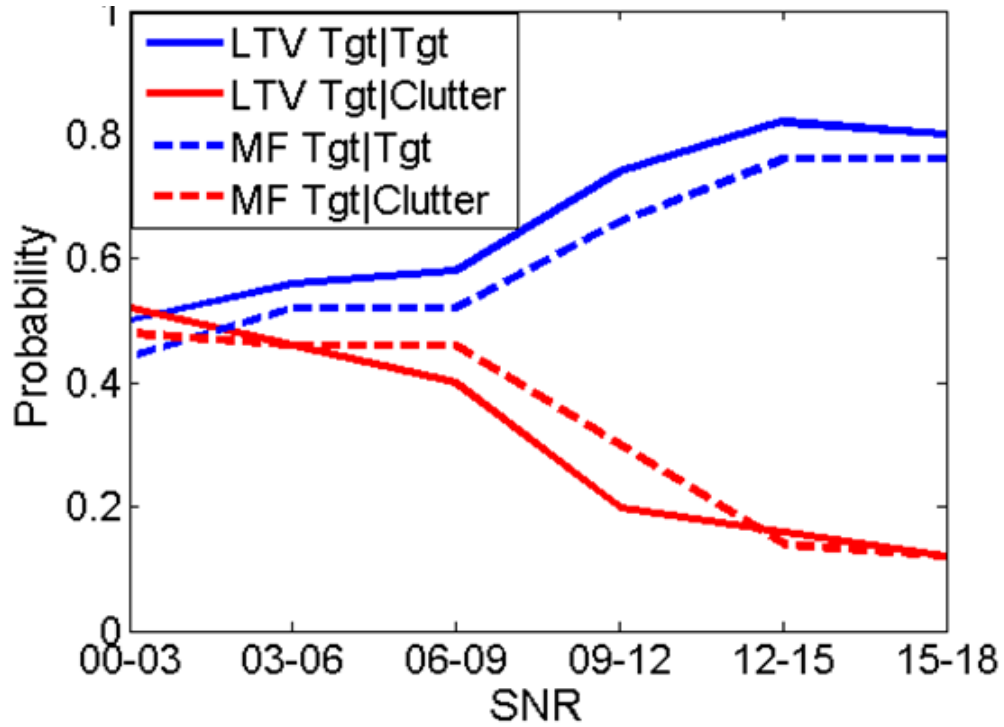
Figure 23: Correct detection and False alarm vs. SNR for MPE and Augmented MPE classifier

Table 11: Classification Results: LTV filter thresholded at 30dB

	Oilrig	Wellhead	Cylinder
Oilrig	0.383 (28/73)	0.287 (21/73)	0.328 (24/73)
Wellhead	0.232 (17/73)	0.438 (32/73)	0.328 (24/73)
Cylinder	0.301 (22/73)	0.315 (23/73)	0.383 (28/73)

Table 12: Classification Results: LTV filter thresholded at 20dB

	Oilrig	Wellhead	Cylinder
Oilrig	0.506 (37/73)	0.178 (13/73)	0.315 (23/73)
Wellhead	0.246 (18/73)	0.575 (42/73)	0.178 (13/73)
Cylinder	0.232 (17/73)	0.246 (18/73)	0.52 (38/73)

Table 13: Classification Results: LTV filter thresholded at 10dB

	Oilrig	Wellhead	Cylinder
Oilrig	0.397 (29/73)	0.301 (22/73)	0.301 (22/73)
Wellhead	0.301 (22/73)	0.369 (27/73)	0.328 (24/73)
Cylinder	0.315 (23/73)	0.356 (26/73)	0.328 (24/73)

Table 14: Classification Results: Classic MPE classifier

	Oilrig	Wellhead	Cylinder
Oilrig	0.369 (27/73)	0.315 (23/73)	0.315 (23/73)
Wellhead	0.246 (18/73)	0.452 (33/73)	0.328 (24/73)
Cylinder	0.274 (20/73)	0.356 (26/73)	0.369 (27/73)

7.0 CONCLUSIONS AND FUTURE WORK

7.1 CONCLUSIONS

In our work, several approaches of classification and detection of underwater targets in self-noise was discussed. We first extended the work of extracting invariant features to range dependent environments, we then saw the feasibility of applying the features derived for planar waves to cyilndrical waves. We concluded that while there is a definite degradation in the performance of the features, our range-dependent dispersion-invariant moments still provides performance benefits compared to other moments. While the rate of attenuation severely damages the features' performance, owing to the fact that the features were designed only to be dispersion invariant and not attenuation invariant. In addition to the normal mode model, we considered the feature extraction process for the parabolic model. This is especially useful as the parabolic model is applied to a wide variety of environments and attenuation scenarios. We also explored the possiblity of forumlating the Parabolic model using operators, enabling us to arrive at solutions previously considered infeasible when formulating in the time domain.

We considered the phase space approach to pulse propagation in a range dependent media, we considered a variety of propagating waves and boundaries and derived the approximate Wigner distributions. We also found that the results were analogus to the one derived for range-independent propagation. The dispersion relation and cylindrical/bounded spreading- as expected - increases by a square factor for the bilinear distribution.

We considered the approach for designing time-frequency kernels, to perform the classification of targets in the presence of clutter. We designed the optimal kernels for a stochastic reverberation model, and performed classification of targets in the presence of clutter with

increasing variance in the distance of the reverberations i.e. the targets are increasingly clutter-like. Expectedly as the targets get more clutter-like the classification performance deteriorates.

We also, consider performing classification of real-world data. The measurements was provided by the JRP (DRDC-Atlantic, NURC, ARL-PSU, NRL) and performed classification of targets and clutter. Two cases were performed: 1. Classifying the target class versus the clutter class and 2. Classification between three target classes. Our results show that designing time-frequency kernels at a certain energy threshold provides better performance than at different thresholds.

7.2   FUTURE WORK

Further explorations could be carried out in the area of Operator method to solve parabolic equation. Numerical methods to solve the parabolic equation would be a massive contribution to the field of ocean acoustics. Simulation and implementation of the feature extraction process described for the parabolic model would also be a leap forward in the area of invariant feature extractions.

Looking the oblique projection method where the operator is orthogonal to the undesired component would enhance the classification performance using the projection filtering to a great extent.

A closed form solution to the kernel design problem would also be highly desired as you wouldn't need any test signals to train the kernel to perform classification.

DERIVATIONS

A.1   RANGE-DEPENDENT PLANAR WAVES

The Wigner distribution of the propagated pulse from Eq. (3.96)

$$
\begin{aligned}
W(x_R, t, \omega) &= \frac{1}{2\pi} \int F(x_S, \omega - \frac{\lambda}{2}) F^*(x_S, \omega + \frac{\lambda}{2}) \frac{1}{\sqrt{k_x^*(x_R, \omega + \frac{\lambda}{2}) k_x(x_R, \omega - \frac{\lambda}{2})}} \\
&\quad e^{-j \int_{x_S}^{x_R} k_x^*(x', \omega + \frac{\lambda}{2}) dx'} e^{+j \int_{x_S}^{x_R} k_x(x', \omega - \frac{\lambda}{2}) dx'}
\end{aligned} \tag{.1}
$$

using the inverse Wigner identity

$$
\begin{aligned}
W(x_R, t, \omega) &= \int\int W(x_S, t', \omega) \times \\
&\quad \frac{e^{-j(K_x^*(x_R, \omega + \lambda/2) - K_x^*(x_S, \omega + \lambda/2))} e^{+j(K_x(x_R, \omega - \lambda/2) - K_x(x_S, \omega - \lambda/2))} e^{j\lambda(t - t')}}{\sqrt{k_x^*(x_R, \omega + \lambda/2) k_x(x_R, \omega - \lambda/2)}} d\lambda dt
\end{aligned} \tag{.2}
$$

Now, the dispersion relation can be split into real and imaginary parts.

$$
k_x(x, \omega) = k_x^{\Re}(x, \omega) + j k_x^{\Im}(x, \omega) \tag{.3}
$$

and

$$
K_x(x, \omega) = K_x^{\Re}(x, \omega) + j K_x^{\Im}(x, \omega) \tag{.4}
$$

where

$$\int_{x_S}^{x_R} k_x(x', \omega)dx' = K_x(x_R, \omega) - K_x(x_S, \omega) \tag{.5}$$

a given mode. (Since our analysis is per mode, without loss of generality).

The Taylor series expansion of a function around a certain value is given by

$$n\left(\omega - \frac{\lambda}{2}\right) = n\left(\omega\right) - \frac{\lambda}{2}n'\left(\omega\right) + \frac{1}{2!}\left(\frac{\lambda}{2}\right)^2 n''\left(\omega\right) \tag{.6}$$

$$n\left(\omega + \frac{\lambda}{2}\right) = n\left(\omega\right) + \frac{\lambda}{2}n'\left(\omega\right) + \frac{1}{2!}\left(\frac{\lambda}{2}\right)^2 n''\left(\omega\right) \tag{.7}$$

and the Taylor series expansion of the dispersion relation can be written as[45]

$$K_x^\Im(\omega - \frac{\lambda}{2}) + K_x^\Im(\omega + \frac{\lambda}{2}) = \sum_{n=0}^{\infty} \frac{K_x^{\Im(2n)}(\omega)}{2n!}\frac{\lambda^{2n}}{2^{2n-1}} \approx 2K_x^\Im(\omega) + \frac{1}{4}K_x^{\Im''}(\omega)\lambda^2 \tag{.8}$$

$$K_x^\Re(\omega - \frac{\lambda}{2}) - K_x^\Re(\omega + \frac{\lambda}{2}) = \sum_{n=0}^{\infty} \frac{K_x^{\Re(2n+1)}(\omega)}{2n+1!}\frac{\lambda^{2n+1}}{2^{2n}} \approx K_x^{\Re'}(\omega)\lambda + \frac{1}{24}K_x^{\Re'''}(\omega)\lambda^3 \tag{.9}$$

The product in the denominator of Eq. (.2) is written as

$$\left(k^\Re x(\omega + \frac{\lambda}{2}) - jk_x^\Im(\omega + \frac{\lambda}{2})\right)\left(k_x^\Re(\omega - \frac{\lambda}{2}) + jk_x^\Im(\omega - \frac{\lambda}{2})\right) =$$
$$k_x^\Re(\omega - \frac{\lambda}{2})k_x^\Re(\omega + \frac{\lambda}{2}) + k_x^\Im(\omega - \frac{\lambda}{2})k_x^\Im(\omega + \frac{\lambda}{2}) + jk_x^\Im(\omega - \frac{\lambda}{2})k_x^\Re(\omega + \frac{\lambda}{2})(-)$$
$$(-)jk_x^\Re(\omega - \frac{\lambda}{2})k_x^\Im(\omega + \frac{\lambda}{2}) \tag{.10}$$

expanding the terms into Taylor series of order 2:

$$k_x^\Re(\omega - \frac{\lambda}{2})k_x^\Re(\omega + \frac{\lambda}{2}) \approx (k_x^\Re(\omega))^2 + \left(k_x^{\Re'}(\omega)\frac{\lambda}{2}\right)^2 \tag{.11}$$

$$k_x^\Im(\omega - \frac{\lambda}{2})k_x^\Im(\omega + \frac{\lambda}{2}) \approx (k_x^\Im(\omega))^2 + \left(k_x^{\Im'}(\omega)\frac{\lambda}{2}\right)^2 \tag{.12}$$

$$jk_x^\Im(\omega - \frac{\lambda}{2})k_x^\Re(\omega + \frac{\lambda}{2}) \approx jk_x^\Im(\omega)k_x^\Re(\omega) - jk_x^{\Im'}(\omega)k_x^\Re(\omega)\frac{\lambda}{2}(+)$$
$$(+)jk_x^{\Im'}(\omega)k_x^\Re(\omega)\frac{\lambda}{2} - jk_x^{\Im'}(\omega)k_x^{\Re'}(\omega)\left(\frac{\lambda}{2}\right)^2 \tag{.13}$$

$$jk_x^{\Re}(\omega - \frac{\lambda}{2})k_x^{\Im}(\omega + \frac{\lambda}{2}) \approx jk_x^{\Re}(\omega)k_x^{\Im}(\omega) - jk_x^{\Re'}(\omega)k_x^{\Im}(\omega)\frac{\lambda}{2}(+)$$

$$(+)jk_x^{\Re'}(\omega)k_x^{\Im}(\omega)\frac{\lambda}{2} - jk_x^{\Re'}(\omega)k_x^{\Im'}(\omega)\left(\frac{\lambda}{2}\right)^2 \quad (.14)$$

Keeping only the first order terms we obtain:

$$\left(k_x^{\Re}(\omega + \frac{\lambda}{2}) - jk_x^{\Im}(\omega + \frac{\lambda}{2})\right)\left(k_x^{\Re}(\omega - \frac{\lambda}{2}) + jk_x^{\Im}(\omega - \frac{\lambda}{2})\right) \approx \left(k_x^{\Re}(\omega)\right)^2 + \left(k_x^{\Im}(\omega)\right)^2 \quad (.15)$$

splitting K and k into real and imaginary parts as mentioned before and using the Taylor Series approximation, we obtain the Wigner approximation

$$W(x_R, t, \omega) \approx e^{2(K_x^{\Im}(x_S,\omega) - K_x^{\Im}(x_R,\omega))} \int\int \frac{e^{-j\lambda(K_x^{\Re'}(x_R,\omega) - K_x^{\Re'}(x_S,\omega))}e^{j\lambda(t-t')}}{\sqrt{k_x^{\Re 2}(x_R,\omega) + k_x^{\Im 2}(x_R,\omega)}}W(x_S, t', \omega)d\lambda dt'$$

$$\approx \frac{e^{2(K_x^{\Im}(x_S,\omega) - K_x^{\Im}(x_R,\omega))}}{|k(x_R,\omega)|}W\left(x_S, t - \left(K_x^{\Re'}(x_R,\omega) - K_x^{\Re'}(x_S,\omega)\right), \omega\right) \quad (.16)$$

A.2   RANGE-DEPENDENT CIRCULAR WAVES

The Wigner distribution of the propagated pulse at r is written from Eq. (3.102)

$$W(r_R, t, \omega) = \frac{1}{2\pi}\int F(r_S, \omega - \frac{\lambda}{2})F^*(r_S, \omega + \frac{\lambda}{2})$$

$$\sqrt{\frac{2}{\pi\left(\frac{\omega}{c} - \frac{\lambda}{2c} + jk^{\Im}\left(\omega - \frac{\lambda}{2}\right)\right)(r_R - r_S)}}\sqrt{\frac{2}{\pi\left(\frac{\omega}{c} + \frac{\lambda}{2c} - jk^{\Im}\left(\omega + \frac{\lambda}{2}\right)\right)(r_R - r_S)}}$$

$$\exp\left(j\left(\left(\frac{\omega}{c} - \frac{\lambda}{2c} + jk^{\Im}\left(\omega - \frac{\lambda}{2}\right)\right)(r_R - r_S) - \frac{\pi}{4} - k_\theta\frac{\pi}{2}\right)\right)$$

$$\exp\left(-j\left(\left(\frac{\omega}{c} + \frac{\lambda}{2c} - jk^{\Im}\left(\omega + \frac{\lambda}{2}\right)\right)(r_R - r_S) - \frac{\pi}{4} - k_\theta\frac{\pi}{2}\right)\right)e^{jt\lambda}d\lambda \quad (.17)$$

using Wigner inversion

$$W(r_R, t, \omega) = \frac{1}{2\pi} \int \int W(r_S, t', \omega) \times$$

$$\sqrt{\frac{2}{\pi \left(\frac{\omega}{c} - \frac{\lambda}{2c} + jk^{\Im}\left(\omega - \frac{\lambda}{2}\right)\right)(r_R - r_S)}} \sqrt{\frac{2}{\pi \left(\frac{\omega}{c} + \frac{\lambda}{2c} - jk^{\Im}\left(\omega + \frac{\lambda}{2}\right)\right)(r_R - r_S)}}$$

$$\exp\left(j\left(\left(\frac{\omega}{c} - \frac{\lambda}{2c} + jk^{\Im}\left(\omega - \frac{\lambda}{2}\right)\right)(r_R - r_S) - \frac{\pi}{4} - k_\theta\frac{\pi}{2}\right)\right)$$

$$\exp\left(-j\left(\left(\frac{\omega}{c} + \frac{\lambda}{2c} - jk^{\Im}\left(\omega + \frac{\lambda}{2}\right)\right)(r_R - r_S) - \frac{\pi}{4} - k_\theta\frac{\pi}{2}\right)\right)$$

$$e^{j\lambda(t-t')}d\lambda dt' \tag{.18}$$

The dispersion relation can be split into real and imaginary parts.

$$k_x(\omega) = k_x^{\Re}(\omega) + jk_x^{\Im}(\omega) \tag{.19}$$

where $k_x^{\Re}(\omega) = \frac{\omega}{c}$.

The Taylor series expansion of a function around a certain value is given by

$$n\left(\omega - \frac{\lambda}{2}\right) = n\left(\omega\right) - \frac{\lambda}{2}n'\left(\omega\right) + \frac{1}{2!}\left(\frac{\lambda}{2}\right)^2 n''\left(\omega\right) \tag{.20}$$

$$n\left(\omega + \frac{\lambda}{2}\right) = n\left(\omega\right) + \frac{\lambda}{2}n'\left(\omega\right) + \frac{1}{2!}\left(\frac{\lambda}{2}\right)^2 n''\left(\omega\right) \tag{.21}$$

and the Taylor series expansion of the dispersion relation can be written as[45]

$$K_x^{\Im}(\omega - \frac{\lambda}{2}) + K_x^{\Im}(\omega + \frac{\lambda}{2}) = \sum_{n=0}^{\infty} \frac{K_x^{\Im(2n)}(\omega)}{2n!}\frac{\lambda^{2n}}{2^{2n-1}} \approx 2K_{Ix}(\omega) + \frac{1}{4}K_x^{\Im''}(\omega)\lambda^2 \tag{.22}$$

The product in the denominator of Eq. (.18) is written as

$$\left(\frac{\omega}{c} - \frac{\lambda}{2c} + jk_x^{\Im}(\omega - \frac{\lambda}{2})\right)\left(\frac{\omega}{c} + \frac{\lambda}{2c} - jk_x^{\Im}(\omega + \frac{\lambda}{2})\right) =$$

$$\left(\frac{\omega}{c}\right)^2 - \left(\frac{\lambda}{2c}\right)^2 + k_x^{\Im}(\omega - \frac{\lambda}{2})k_x^{\Im}(\omega + \frac{\lambda}{2}) + jk_x^{\Im}(\omega - \frac{\lambda}{2})(\frac{\omega}{c} + \frac{\lambda}{2c})(-)$$

$$(-)j(\frac{\omega}{c} - \frac{\lambda}{2c})k_x^{\Im}(\omega + \frac{\lambda}{2}) \tag{.23}$$

Expanding the terms into Taylor series upto order 2:

$$k_x^{\Im}(\omega - \frac{\lambda}{2})k_x^{\Im}(\omega + \frac{\lambda}{2}) \approx (k_x^{\Im}(\omega))^2 + \left(k_x^{\Im'}(\omega)\frac{\lambda}{2}\right)^2 \tag{.24}$$

$$
\begin{aligned}
jk_x^{\Im}(\omega - \frac{\lambda}{2})(\frac{\omega}{c} + \frac{\lambda}{2c}) &\approx jk_x^{\Im}(\omega)(\frac{\omega}{c}) - jk_x^{\Im'}(\omega)\,(\frac{\omega}{c})\,\frac{\lambda}{2}(-) \\
&\quad (-)\,jk_x^{\Im'}(\omega)\,(\frac{1}{c})\left(\frac{\lambda}{2}\right)^2
\end{aligned}
\tag{.25}
$$

$$
\begin{aligned}
j(\frac{\omega}{c} - \frac{\lambda}{2c})k_x^{\Im}(\omega + \frac{\lambda}{2}) &\approx j(\frac{\omega}{c})k_x^{\Im}(\omega) - j(\frac{\omega}{c})\,k_x^{\Im'}(\omega)\,\frac{\lambda}{2}(-) \\
&\quad (-)\,j(\frac{1}{c})\,k_x^{\Im'}(\omega)\left(\frac{\lambda}{2}\right)^2
\end{aligned}
\tag{.26}
$$

Simplification and discarding higher order terms gives

$$\left(k^{\Re}(\omega + \frac{\lambda}{2}) - jk^{\Im}(\omega + \frac{\lambda}{2})\right)\left(k^{\Re}(\omega - \frac{\lambda}{2}) + jk^{\Im}(\omega - \frac{\lambda}{2})\right) \approx \left(k^{\Re}(\omega)\right)^2 + \left(k^{\Im}(\omega)\right)^2 \tag{.27}$$

Plugging back the simplifications to Eq. (.18)

$$
\begin{aligned}
W(r_R, t, \omega) &= \frac{1}{\pi^2\,|k(\omega)|\,(r_R - r_S)}\int\int W(r_S, t', \omega) \times \\
&\qquad \exp\left(-j\left(\frac{\lambda}{c} + j2k^{\Im}(\omega)\right)(r_R - r_S)\right)e^{j\lambda(t-t')}d\lambda dt'
\end{aligned}
$$
$$\tag{.28}$$

Plugging back the terms into the equations yields

$$W(r_R, t, \omega) = \frac{2\exp\left(-2k^{\Im}(\omega)(r_R - r_S)\right)}{\pi(r_R - r_S)\,|k(\omega)|}W\left(r_S, t - \frac{1}{c}(r_R - r_S), \omega\right) \tag{.29}$$

89

A.3 RANGE-INDEPENDENT CYLINDRICAL WAVES

The Wigner distribution of the pulse at receiver r_R is written from Eq. (3.107) as

$$
W(r_R, t, \omega) = \frac{1}{2\pi} \int F(r_S, \omega - \frac{\lambda}{2}) F^*(r_S, \omega + \frac{\lambda}{2}) \frac{2}{\pi \, (r_R - r_S) \sqrt{k_r^*(\omega + \frac{\lambda}{2}) k_r(\omega - \frac{\lambda}{2})}} \tag{.30}
$$

$$
e^{-jk_r^*(\omega + \frac{\lambda}{2})(r_R - r_S)} e^{+jk_r(\omega - \frac{\lambda}{2})(r_R - r_S)} \tag{.31}
$$

using inverse Fourier identity for the Wigner distribution [6]

$$
W(x_R, t, \omega) = \int \int W(x_S, t', \omega) \times
$$

$$
\frac{e^{-j(k_r^*(\omega + \lambda/2))(r_R - r_S)} e^{+j(k_r(\omega - \lambda/2))(r_R - r_S)} e^{j\lambda(t - t')}}{\pi \, (r_R - r_S) \sqrt{k_r^*(\omega + \frac{\lambda}{2}) k_r(\omega - \frac{\lambda}{2})}} d\lambda dt' \tag{.32}
$$

The dispersion relation can be split into real and imaginary parts

$$
k_r(\omega) = k_r^{\Re}(\omega) + jk_r^{\Im}(\omega) \tag{.33}
$$

the Taylor series expansion of a function around a certain value is given by

$$
n\left(\omega - \frac{\lambda}{2}\right) = n(\omega) - \frac{\lambda}{2} n'(\omega) + \frac{1}{2!}\left(\frac{\lambda}{2}\right)^2 n''(\omega) \tag{.34}
$$

$$
n\left(\omega + \frac{\lambda}{2}\right) = n(\omega) + \frac{\lambda}{2} n'(\omega) + \frac{1}{2!}\left(\frac{\lambda}{2}\right)^2 n''(\omega) \tag{.35}
$$

and the Taylor series expansion of the dispersion relation can be written as[45]

$$
k_r^{\Im}(\omega - \frac{\lambda}{2}) + k_r^{\Im}(\omega + \frac{\lambda}{2}) = \sum_{n=0}^{\infty} \frac{k_r^{\Im(2n)}(\omega)}{2n!} \frac{\lambda^{2n}}{2^{2n-1}} \approx 2k_r^{\Im}(\omega) + \frac{1}{4} k_r^{\Im ''}(\omega)\lambda^2 \tag{.36}
$$

$$
k_r^{\Re}(\omega - \frac{\lambda}{2}) - k_r^{\Re}(\omega + \frac{\lambda}{2}) = \sum_{n=0}^{\infty} \frac{k_r^{\Re(2n+1)}(\omega)}{2n + 1!} \frac{\lambda^{2n+1}}{2^{2n}} \approx k_r^{\Re '}(\omega)\lambda + \frac{1}{24} k_r^{\Re '''}(\omega)\lambda^3 \tag{.37}
$$

90

The product in the denominator of Eq. (.32) is written as

$$\left(k^{\Re}r(\omega + \frac{\lambda}{2}) - jk_r^{\Im}(\omega + \frac{\lambda}{2})\right)\left(k_r^{\Re}(\omega - \frac{\lambda}{2}) + jk_r^{\Im}(\omega - \frac{\lambda}{2})\right) =$$
$$k_r^{\Re}(\omega - \frac{\lambda}{2})k_r^{\Re}(\omega + \frac{\lambda}{2}) + k_r^{\Im}(\omega - \frac{\lambda}{2})k_r^{\Im}(\omega + \frac{\lambda}{2}) + jk_r^{\Im}(\omega - \frac{\lambda}{2})k_r^{\Re}(\omega + \frac{\lambda}{2})(-)$$
$$(-)jk_r^{\Re}(\omega - \frac{\lambda}{2})k_r^{\Im}(\omega + \frac{\lambda}{2}) \tag{.38}$$

Expanding the terms into Taylor series of order 2:

$$k_r^{\Re}(\omega - \frac{\lambda}{2})k_r^{\Re}(\omega + \frac{\lambda}{2}) \approx (k_r^{\Re}(\omega))^2 + \left(k_r^{\Re'}(\omega)\frac{\lambda}{2}\right)^2 \tag{.39}$$

$$k_r^{\Im}(\omega - \frac{\lambda}{2})k_r^{\Im}(\omega + \frac{\lambda}{2}) \approx (k_r^{\Im}(\omega))^2 + \left(k_r^{\Im'}(\omega)\frac{\lambda}{2}\right)^2 \tag{.40}$$

$$jk_r^{\Im}(\omega - \frac{\lambda}{2})k_r^{\Re}(\omega + \frac{\lambda}{2}) \approx jk_r^{\Im}(\omega)k_r^{\Re}(\omega) - jk_r^{\Im'}(\omega)k_r^{\Re}(\omega)\frac{\lambda}{2}(+)$$
$$(+)jk_r^{\Im'}(\omega)k_r^{\Re}(\omega)\frac{\lambda}{2} - jk_r^{\Im'}(\omega)k_r^{\Re'}(\omega)\left(\frac{\lambda}{2}\right)^2 \tag{.41}$$

$$jk_r^{\Re}(\omega - \frac{\lambda}{2})k_r^{\Im}(\omega + \frac{\lambda}{2}) \approx jk_r^{\Re}(\omega)k_r^{\Im}(\omega) - jk_r^{\Re'}(\omega)k_r^{\Im}(\omega)\frac{\lambda}{2}(+)$$
$$(+)jk_r^{\Re'}(\omega)k_r^{\Im}(\omega)\frac{\lambda}{2} - jk_r^{\Re'}(\omega)k_r^{\Im'}(\omega)\left(\frac{\lambda}{2}\right)^2 \tag{.42}$$

Keeping only the first order terms we obtain:

$$\left(k_r^{\Re}(\omega + \frac{\lambda}{2}) - jk_r^{\Im}(\omega + \frac{\lambda}{2})\right)\left(k_r^{\Re}(\omega - \frac{\lambda}{2}) + jk_r^{\Im}(\omega - \frac{\lambda}{2})\right) \approx \left(k_r^{\Re}(\omega)\right)^2 + \left(k_r^{\Im}(\omega)\right)^2 \tag{.43}$$

Splitting k into real and imaginary parts as mentioned before and using the Taylor Series approximation, we obtain the Wigner approximation

$$W(r_R, t, \omega) \approx \frac{e^{-2k_r^{\Im}(\omega)}}{(r_R - r_S)}\int\int\frac{e^{-j\lambda(k_r^{\Re'}(\omega)(r_S - r_R))}e^{j\lambda(t-t')}}{\sqrt{k_r^{\Re 2}(\omega) + k_r^{\Im 2}(\omega)}}W(r_S, t', \omega)d\lambda dt'$$
$$\approx \frac{e^{-2k_r^{\Im}(\omega)}}{|k(\omega)|(r_R - r_S)}W\left(r_S, t - \left(k_r^{\Re'}(\omega)(r_R - r_S)\right), \omega\right) \tag{.44}$$

91

A.4   RANGE-DEPENDENT CYLINDRICAL WAVES

The Wigner distribution of the propagated pulse at r_R in terms of the Wigner distribution of the initial pulse at r_s is

$$
\begin{aligned}
W(r_R, t, \omega) &= \int\int W(r_S, t', \omega) \times \\
&\frac{e^{-j(K_r^*(r_R, \omega+\lambda/2) - K_r^*(r_S, \omega+\lambda/2))} e^{+j(K_r(r_R, \omega-\lambda/2) - K_r(r_S, \omega-\lambda/2))} e^{j\lambda(t-t')}}{\sqrt{k_r^*(r_R, \omega+\lambda/2) k_r(r_R, \omega-\lambda/2)}} d\lambda dt'
\end{aligned}
\tag{.45}
$$

The dispersion relation can be split into real and imaginary parts.

$$
k_r(r, \omega) = k_r^{\Re}(r, \omega) + j k_r^{\Im}(r, \omega)
\tag{.46}
$$

and

$$
K_r(r, \omega) = K_r^{\Re}(r, \omega) + j K_r^{\Im}(r, \omega)
\tag{.47}
$$

where

$$
K_r(r_R, \omega) - K_r(r_S, \omega) = \int_{r_S}^{r_R} k_r(r', \omega) dr'
\tag{.48}
$$

The Taylor series expansion of a function around a certain value is given by

$$
n\left(\omega - \frac{\lambda}{2}\right) = n(\omega) - \frac{\lambda}{2} n'(\omega) + \frac{1}{2!}\left(\frac{\lambda}{2}\right)^2 n''(\omega)
\tag{.49}
$$

$$
n\left(\omega + \frac{\lambda}{2}\right) = n(\omega) + \frac{\lambda}{2} n'(\omega) + \frac{1}{2!}\left(\frac{\lambda}{2}\right)^2 n''(\omega)
\tag{.50}
$$

and the Taylor series expansion of the dispersion relation can be written as[45]

$$
K_r^{\Im}(\omega - \frac{\lambda}{2}) + K_r^{\Im}(\omega + \frac{\lambda}{2}) = \sum_{n=0}^{\infty} \frac{K_r^{\Im(2n)}(\omega)}{2n!} \frac{\lambda^{2n}}{2^{2n-1}} \approx 2K_r^{\Im}(\omega) + \frac{1}{4} K_r^{\Im''}(\omega)\lambda^2
\tag{.51}
$$

$$
K_r^{\Re}(\omega - \frac{\lambda}{2}) - K_r^{\Re}(\omega + \frac{\lambda}{2}) = \sum_{n=0}^{\infty} \frac{K_r^{\Re(2n+1)}(\omega)}{2n+1!} \frac{\lambda^{2n+1}}{2^{2n}} \approx K_r^{\Re'}(\omega)\lambda + \frac{1}{24} K_r^{\Re'''}(\omega)\lambda^3
\tag{.52}
$$

The product in the denominator of Eq. (.45) is written as

$$\left(k^{\Re}r(\omega+\frac{\lambda}{2})-jk_r^{\Im}(\omega+\frac{\lambda}{2})\right)\left(k_r^{\Re}(\omega-\frac{\lambda}{2})+jk_r^{\Im}(\omega-\frac{\lambda}{2})\right)=$$

$$k_r^{\Re}(\omega-\frac{\lambda}{2})k_r^{\Re}(\omega+\frac{\lambda}{2})+k_r^{\Im}(\omega-\frac{\lambda}{2})k_r^{\Im}(\omega+\frac{\lambda}{2})+jk_r^{\Im}(\omega-\frac{\lambda}{2})k_r^{\Re}(\omega+\frac{\lambda}{2})(-)$$

$$(-)jk_r^{\Re}(\omega-\frac{\lambda}{2})k_r^{\Im}(\omega+\frac{\lambda}{2}) \tag{.53}$$

Expanding the terms into Taylor series of order 2:

$$k_r^{\Re}(\omega-\frac{\lambda}{2})k_r^{\Re}(\omega+\frac{\lambda}{2}) \approx (k_r^{\Re}(\omega))^2+\left(k_r^{\Re'}(\omega)\frac{\lambda}{2}\right)^2 \tag{.54}$$

$$k_r^{\Im}(\omega-\frac{\lambda}{2})k_r^{\Im}(\omega+\frac{\lambda}{2}) \approx (k_r^{\Im}(\omega))^2+\left(k_r^{\Im'}(\omega)\frac{\lambda}{2}\right)^2 \tag{.55}$$

$$jk_r^{\Im}(\omega-\frac{\lambda}{2})k_r^{\Re}(\omega+\frac{\lambda}{2}) \approx jk_r^{\Im}(\omega)k_r^{\Re}(\omega)-jk_r^{\Im'}(\omega)k_r^{\Re}(\omega)\frac{\lambda}{2}(+)$$

$$(+)jk_r^{\Im'}(\omega)k_r^{\Re}(\omega)\frac{\lambda}{2}-jk_r^{\Im'}(\omega)k_r^{\Re'}(\omega)\left(\frac{\lambda}{2}\right)^2 \tag{.56}$$

$$jk_r^{\Re}(\omega-\frac{\lambda}{2})k_r^{\Im}(\omega+\frac{\lambda}{2}) \approx jk_r^{\Re}(\omega)k_r^{\Im}(\omega)-jk_r^{\Re'}(\omega)k_r^{\Im}(\omega)\frac{\lambda}{2}(+)$$

$$(+)jk_r^{\Re'}(\omega)k_r^{\Im}(\omega)\frac{\lambda}{2}-jk_r^{\Re'}(\omega)k_r^{\Im'}(\omega)\left(\frac{\lambda}{2}\right)^2 \tag{.57}$$

Keeping only the first order terms we obtain:

$$\left(k_r^{\Re}(\omega+\frac{\lambda}{2})-jk_r^{\Im}(\omega+\frac{\lambda}{2})\right)\left(k_r^{\Re}(\omega-\frac{\lambda}{2})+jk_r^{\Im}(\omega-\frac{\lambda}{2})\right) \approx (k_r^{\Re}(\omega))^2+(k_r^{\Im}(\omega))^2 \tag{.58}$$

Splitting K and k into real and imaginary parts as mentioned before and using the Taylor Series approximation, we obtain the Wigner approximation

$$W(r_R,t,\omega) \approx e^{2(K_r^{\Im}(r_S,\omega)-K_r^{\Im}(r_R,\omega))}\int\int\frac{e^{-j\lambda(K_r^{\Re'}(r_R,\omega)-K_r^{\Re'}(r_S,\omega))}e^{j\lambda(t-t')}}{\sqrt{k_r^{\Re 2}(r_R,\omega)+k_r^{\Im 2}(r_R,\omega)}}W(r_S,t',\omega)d\lambda dt'$$

$$\approx \frac{e^{2(K_r^{\Im}(r_S,\omega)-K_r^{\Im}(r_R,\omega))}}{|k(r_R,\omega)|}W\left(r_S,t-\left(K_r^{\Re'}(r_R,\omega)-K_r^{\Re'}(r_S,\omega)\right),\omega\right) \tag{.59}$$

BIBLIOGRAPHY

[1] Richard A Altes. Detection, estimation, and classification with spectrograms. *The Journal of the Acoustical Society of America*, 67(4):1232–1246, 1980.

[2] L. Atlas, J. Droppo, and J. McLaughlin. Optimizing time-frequency distributions for automatic classification. In *Proc. SPIE*, volume 3162, pages 161–171. Citeseer, 1997.

[3] Arthur B Baggeroer, William A Kuperman, and Peter N Mikhalevsky. An overview of matched field methods in ocean acoustics. *Oceanic Engineering, IEEE Journal of*, 18(4):401–424, 1993.

[4] William S Burdic. *Underwater acoustic system analysis*, volume 2. Prentice-Hall Englewood Cliffs, 1984.

[5] P Chevret, N Gache, and V Zimpfer. Time-frequency filters for target classification. *The Journal of the Acoustical Society of America*, 106(4):1829–1837, 1999.

[6] L. Cohen. *Time Frequency Analysis : Theory and Applications (Prentice-Hall Signal Processing)*. Prentice Hall PTR, December 1994.

[7] L. Cohen. The wigner distribution and pulse propagation. In *SPIE proceedings series*, pages 20–24. Society of Photo-Optical Instrumentation Engineers, 2001.

[8] L. Cohen, P. Loughlin, and G. Okopal. Exact and approximate moments of a propagating pulse. *Journal of Modern Optics*, 55(19):3349–3358, 2008.

[9] Leon Cohen. Reverberation noise in phase-space. *Journal of Modern Optics*, 57(19):1949–1953, 2010.

[10] Pierre Faure. Theoretical model of reverberation noise. *The Journal of the Acoustical Society of America*, 36(2):259–266, 1964.

[11] L. B. Felsen and N. Marcuvitz. Radiation and scattering of waves. 1973.

[12] L. B. Felsen and N. Marcuvitz. Radiation and scattering of waves. 1973.

[13] L. Galleani and L. Cohen. Dynamics using the wigner distribution. In *Pattern Recognition, 2000. Proceedings. 15th International Conference on*, volume 3, pages 250–253. IEEE, 2000.

[14] L. Galleani and L. Cohen. The wigner distribution for ordinary linear differential equations and wave equations. In *Statistical Signal and Array Processing, 2000. Proceedings of the Tenth IEEE Workshop on*, pages 589–593. IEEE, 2000.

[15] L. Galleani and L. Cohen. Wigner equations of motion for classical systems. In *SPIE's 45th Annual Meeting*, 2000.

[16] L. Galleani and L. Cohen. Time frequency wigner distribution approach to differential equations. *Nonlinear Signal and Image Processing: Theory, Methods, and Applications*, 2003.

[17] L. Galleani and L. Cohen. The phase space of non-stationary noise. *Journal of Modern Optics*, 51(16-18):2731–2740, 2004.

[18] GC Gaunaurd and D. Brill. Acoustic spectrogram and complex-frequency poles of a resonantly excited elastic tube. *The Journal of the Acoustical Society of America*, 75:1680, 1984.

[19] G.C. Gaunaurd and H.C. Strifors. Frequency-and time-domain analysis of the transient resonance scattering resulting from the interaction of a sound pulse with submerged elastic shells. *Ultrasonics, Ferroelectrics and Frequency Control, IEEE Transactions on*, 40(4):313–324, 1993.

[20] G.C. Gaunaurd and H.C. Strifors. Signal analysis by means of time-frequency (wigner-type) distributions-applications to sonar and radar echoes. *Proceedings of the IEEE*, 84(9):1231–1248, 1996.

[21] G.C. Gaunaurd and H.C. Strifors. Applications of time-frequency signature analysis to target identification. In *Proceedings of SPIE*, volume 3723, page 78, 1999.

[22] Bradford W Gillespie and Les E Atlas. Optimizing time-frequency kernels for classification. *Signal Processing, IEEE Transactions on*, 49(3):485–496, 2001.

[23] V. T. Gomatam and P. Loughlin. A wigner phase space approximation for range-dependent propagation,. *Proc. European Conf. on Underwater Acoustics (ECUA), Edinburgh, Scotland,*, July, 2012.

[24] Vikram Gomatam and Patrick Loughlin. Dispersion-invariant features for classification of objects from their acoustic backscatter in a range-dependent channel. In *SPIE Defense, Security, and Sensing*, pages 83910D–83910D. International Society for Optics and Photonics, 2012.

[25] Vikram Thiruneermalai Gomatam and Patrick Loughlin. Impact of range dependent propagation on classification of underwater objects by their sonar backscatter. In *SPIE*

Defense, Security, and Sensing, pages 80490E–80490E. International Society for Optics and Photonics, 2011.

[26] Brandon Hamschin and Patrick Loughlin. Application of a minimum probability of error classifier with linear time-varying pre-filters for buried target recognition. In *OCEANS 2010*, pages 1–7. IEEE, 2010.

[27] RH Hardin and FD Tappert. Applications of the split-step fourier method to the numerical solution of nonlinear and variable coefficient wave equations. *Siam Rev*, 15(423):0–021, 1973.

[28] RH Hardin and FD Tappert. Applications of the split-step fourier method to the numerical solution of nonlinear and variable coefficient wave equations. *Siam Rev*, 15:423, 1973.

[29] Franz Hlawatsch. *Time-frequency analysis and synthesis of linear signal spaces: time-frequency filters, signal detection and estimation, and Range-Doppler estimation.* Springer, 1998.

[30] Franz Hlawatsch and Werner Kozek. Time-frequency projection filters and time-frequency signal expansions. *Signal Processing, IEEE Transactions on*, 42(12):3321–3334, 1994.

[31] Franz Hlawatsch, Gerald Matz, Heinrich Kirchauer, and Werner Kozek. Time-frequency formulation, design, and implementation of time-varying optimal filters for signal estimation. *Signal Processing, IEEE Transactions on*, 48(5):1417–1432, 2000.

[32] Jens M Hovem. Deconvolution for removing the effects of the bubble pulses of explosive charges. *The Journal of the Acoustical Society of America*, 47(1B):281–284, 1970.

[33] DH Hughes and PL Marston. Local temporal variance of wigners distribution function as a spectroscopic observable: Lamb wave resonances of a spherical shell. *The Journal of the Acoustical Society of America*, 94:499, 1993.

[34] F. B. Jensen, W. A. Kuperman, M. B. Portor, and H. Schmidt. *Computational Ocean Acoustics (Modern Acoustics and Signal Processing)*. American Institute of Physics.

[35] Steven M Kay. Fundamentals of statistical signal processing: detection theory. 1998.

[36] JH Leclere and RL Field. A comparison of time-domain parabolic equation and measured ocean impulse responses. Technical report, DTIC Document, 1990.

[37] P Loughlin. Time-varying spectral approximation of filtered signals. *IEEE Signal Processing Letters*, 13:604–607, 2006.

[38] P. Loughlin and L. Cohen. A wigner approximation method for wave propagation. *The Journal of the Acoustical Society of America*, 118(3):1268–1271, 2005.

[39] W.D. Mark. Spectral analysis of the convolution and filtering of non-stationary stochastic processes. *Journal of Sound and Vibration*, 11(1):19–63, 1970.

[40] David Middleton. A statistical theory of reverberation and similar first-order scattered fields–i: Waveforms and the general process. *Information Theory, IEEE Transactions on*, 13(3):372–392, 1967.

[41] David Middleton. A statistical theory of reverberation and similar first-order scattered fields–ii: Moments, spectra and special distributions. *Information Theory, IEEE Transactions on*, 13(3):393–414, 1967.

[42] David Middleton. A statistical theory of reverberation and similar first-order scattered fields–iii: Waveforms and fields. *Information Theory, IEEE Transactions on*, 18(1):35–67, 1972.

[43] S.F. Morse and P.L. Marston. Backscattering of transients by tilted truncated cylindrical shells: Time-frequency identification of ray contributions from measurements. *The Journal of the Acoustical Society of America*, 111:1289, 2002.

[44] G. Okopal. Implementation and evaluation of dispersion-invariant features for signal classification. Master's thesis, University of Pittsburgh, 2007.

[45] G. Okopal. *Phase space analysis and classification of sonar echoes in shallow-water channels*. PhD thesis, University of Pittsburgh, 2009.

[46] G. Okopal and P. Loughlin. Feature extraction for classification of signals propagating in channels with dispersion and dissipation. volume 6566, pages 65660G+. SPIE, 2007.

[47] G. Okopal, P. Loughlin, and L. Cohen. Dispersion-invariant features for classification. *The Journal of the Acoustical Society of America*, 123(2):832–841, 2008.

[48] Greg Okopal, Patrick Loughlin, and Leon Cohen. Recognition of propagating vibrations and invariant features for classification. In *Defense and Security Symposium*, pages 623415–623415. International Society for Optics and Photonics, 2006.

[49] Greg Okopal and Patrick J Loughlin. Propagation-invariant classification of sounds in channels with dispersion and absorption. *The Journal of the Acoustical Society of America*, 128(5):2888–2897, 2010.

[50] WH Prosser, M.D. Seale, and B.T. Smith. Time-frequency analysis of the dispersion of lamb modes. *The Journal of the Acoustical Society of America*, 105:2669, 1999.

[51] Akbar M Sayeed and Douglas L Jones. Optimal detection using bilinear time-frequency and time-scale representations. *Signal Processing, IEEE Transactions on*, 43(12):2872–2883, 1995.

[52] L. Sevgi, F. Akleman, and L.B. Felsen. Visualizations of wave dynamics in a wedge waveguide with non-penetrable boundaries: Normal-, adiabatic-, and intrinsic-mode representations. *Antennas and Propagation Magazine, IEEE*, 49(3):76 –94, june 2007.

[53] F. Tappert. The parabolic approximation method. *Wave propagation and underwater acoustics*, pages 224–287, 1977.

[54] I. Tolstoy and C. S. Clay. *Ocean Acoustics : Theory and Experiment in Underwater Sound*. Acoustical Society of America, 1987.

[55] G. B. Whitham. *Linear and Nonlinear Waves (Pure and Applied Mathematics)*. Wiley-Interscience.

[56] N. Yen, L.R. Dragonette, and S.K. Numrich. Time–frequency analysis of acoustic scattering from elastic objects. *The Journal of the Acoustical Society of America*, 87(6):2359–2370, 1990.